Batch separation of tetrafluoroethylene, hexafluoropropylene and octafluorocyclobutane

Francois Conradie

BATCH SEPARATION OF TETRAFLUOROETHYLENE, HEXAFLUOROPROPYLENE AND OCTAFLUOROCYCLOBUTANE

by

Francois JacobusConradie

Submitted in fulfilment of the requirements for the degree of
MASTER OF ENGINEERING (CHEMICAL ENGINEERING)

in the

FACULTY OF ENGINEERING, BUILT ENVIRONMENT AND INFORMATION TECHNOLOGY

Department of Chemical Engineering
University of Pretoria
South Africa

December 2011

Synopsis

BATCH SEPARATION OF TETRAFLUOROETHYLENE, HEXAFLUOROPROPYLENE AND OCTAFLUOROCYCLOBUTANE

by

Francois Jacobus Conradie

Supervisor: Phillipus L. Crouse
Department: Department of Chemical Engineering
Degree: Master of Engineering (Chemical Engineering)

This dissertation details research aimed at designing a small batch distillation column to purify tetrafluoroethylene and hexafluoropropylene from a mixture containing tetrafluoroethylene, hexafluoropropylene and octafluorocyclobutane.

As no vapour-liquid equilibrium data are available for these chemicals in this mixture, new vapour-liquid equilibrium data were experimentally generated and modelled for use in the design of the batch distillation column. The data were fitted to the Peng-Robinson equation of state, utilizing the Mathias-Copeman alpha function. The model was used with the Wong-Sandler mixing rules alongside the NRTL alpha function.

The model was fitted with mean relative deviations lower than 1.2 %, indicating an acceptably accurate description of the VLE data gathered by the model. The experimental data and the model also passed the thermodynamic consistency test for all the systems and isotherms.

The design simulations were completed by means of the Aspen Batch Distillation, a module of the Aspen Technologies package. The results show that the optimum design for recovering high-purity products requires six equilibrium stages in the column. The batch column should consist of a still pot, also functioning as a reboiler, a packed column section and a total condenser. The total condenser and the reboiler both count as equilibrium stages. Using this design, a TFE product purity of 99.999 % is predicted with a recovery of 96 %. An HFP

product purity of 99 % is predicted at a recovery of 68 %. The recovery of the HFP product can be increased, but entails a significant loss of product purity.

The minimum column diameter required to achieve the flow rates suggested in the simulation is 29 mm. The column diameter was selectedas 1¼ ″ (or 31.75 mm) on the basis of the standard pipe diameters available in the industry. Pall ring packing is suggested for use in the column, with an estimated maximum HETP of 0.5 m. As there are five equilibrium stages in the column itself, the column has to be at least 2.5 m high.

Keywords: Vapour-Liquid Equilibrium, Tetrafluoroethylene, Hexafluoropropylene, Octafluorocyclobutane, Batch Distillation, Fluoropolymers

Declaration

I, Francois Jacobus Conradie, hereby declare that:

- This dissertation has not been submitted, in full or in part, for any degree or examination at any other university;
- That this dissertation, along with the research reported therein, is my own work and is expressed in my own words. All the sources that I have used, or partly used, of other authors in any form (e.g. ideas, equations, figures, text, tables, programmes) have been indicated and acknowledged at the point of their use as full references.

Francois Conradie Date

Acknowledgements

I wish to express my appreciation and gratitude to the following organisations and persons who made this project and dissertation possible:

- First and foremost I wish to thank my Heavenly Father who gave me this opportunity and the capabilities to complete my studies.
- I wish to thank my supervisor, Prof Philip Crouse, for his supervision, wisdom and commitment to making this project a success. I sincerely appreciate his efforts and input into the completion of this dissertation.
- Prof Deresh Ramjugernath from the Thermodynamic Research Unit at the University of KwaZulu-Natal for making the unit's equipment and expertise available for my experimental work.
- Kelly Robertson, Lindinkosi Mkize and Ayanda Khanyile from the School of Chemical Engineering at the University of KwaZulu-Natal for their technical expertise and support.
- The Applied Chemistry Division at Necsa that funded the experimental work, through funding received from the Department of Science and Technology for the FEI project.
- Jaco van der Walt, from the Applied Chemistry Division at Necsa, for the resources and materials he supplied from his department.
- Cliff Thompson at the Applied Chemistry Division of Necsa for his work in preparing the materials as well as the TFE loading system.
- Xavier Courtial, my friend and colleague, for his help and supervision during the experimental work in the laboratory. I thank him for his motivation and willingness to support me.
- Lastly, I want to thank my mother, Seran Conradie, and my brother, David Conradie, for their support and encouragement throughout all my studies.

Dedication

I want to dedicate this dissertation to my late father, who always supported and encouraged my studies. He was always willing to help and to sacrifice his valuable time whenever I needed help or advice throughout my school career and my undergraduate and postgraduate studies.

Contents

List of Tables

List of Figures

Nomenclature

Definitions and Abbreviations

CAP	-	Capacity Factor
EoS	-	Equation of State
ETFE	-	Ethylene Tetrafluoroethylene
FEI	-	Fluoro-Chemical Expansion Initiative
FEP	-	Perfluorinated Ethylene Propylene
FUG	-	Fenske-Underwood-Gilliland
GC	-	Gas Chromatograph
HETP	-	HeightEquivalent to a Theoretical Plate
HF	-	Hydrogenfluoride
HFP	-	Hexafluoropropylene
HPVLE	-	High Pressure Vapour-Liquid equilibrium
HTU	-	Height of a Transfer Unit
LHS	-	Left Hand Side
LPVLE	-	Low Pressure Vapour-Liquid Equilibrium
MC	-	Mathias-Copemann alpha function
MS	-	Mass Spectrometry
MW	-	Molecular Weight
Necsa	-	South African Nuclear Energy Corporation
NRTL	-	Non-Random Two-Liquid local composition model
OFCB	-	Octafluorocyclobutane
PFIB	-	Perfluoroisobutylene
PR	-	Peng-Robinson
RK	-	Redlich-Kwong
SRK	-	Soave-Redlich-Kwong
TFE	-	Tetrafluoroethylene
UKZN	-	University of KwaZulu-Natal
UP	-	University of Pretoria
VLE	-	Vapour-Liquid Equilibrium
VLLE	-	Vapour-Liquid-Liquid Equilibrium
WS	-	Wong Sandler mixing rule

Description of symbols

Symbol	Units	Description
A^E	kJ/mol	Excess Helmholtz energy
a	-	Parameter for the cubic equation of state
B	-	Second virial coefficient
$B^{(0)}$	-	Functions of the generalized second virial coefficient correlation
$B^{(1)}$	-	Functions of the generalized second virial coefficient correlation
B_{ij}	-	Binary interaction of the second virial coefficient
b		Parameter for the cubic equation of state
D	kmol/hour	Distillate rate
f_i	kPa	Fugacity of pure species *i*
$\hat{f}_i$	kPa	Fugacity of species *i* in solution
G	kJ/mol	Specific Gibbs energy
G	m^3	Constant volume holdup
G_i^R	kJ/mol	Residual Gibbs Energy of species *i*
$\bar{G}_i^E$	kJ/mol	Excess Partial Gibbs Energy of species *i* in solution
$\bar{G}_i^R$	kJ/mol	Residual Partial Gibbs Energy of species *i* in solution
G^C	kJ/mol	Combinatorial Excess Gibbs energy
G^E	kJ/mol	Excess Gibbs energy
$\mathcal{H}_i$	-	Henry's Constant of species *i* in solution
h_L	kJ/kmol	Liquid enthalpy
H_V	kJ/kmol	Vapour enthalpy
Ki	-	Vapour-Liquid equilibrium ration of species *i*
L	kmol/hour	Liquid rate in the column
M	kmol	Molar liquid hold up
N	-	Number of plates in a column
N_{min}	-	Minimum number of plates required for separation
n_i	Mole	Number of Moles of species *i*
P	kPa	Absolute pressure
P_c	kPa	Critical Pressure
P_r	-	Reduced Pressure
P_i^{sat}	kPa	Saturation vapour pressure of species *i*
Q	kJ/hour	Heat duty the column, either stages or the condenser or reboiler
R	J/mol.K	Universal gas constant
R	-	Reflux ratio

R_{min}	-	Minimum reflux ratio
T	K	Absolute Temperature
T_c	K	Critical Temperature
T_r	-	Reduced Temperature
t	hour	Time span of distillation
V	kmol/hour	Vapour boilup rate
V	Kmol/m^3	Molar Volume
W	kmol	Moles in the still pot
W_0	kmol	Initial load in still pot
$x_{D_{ave}}$	-	Average mole fraction in the distillate
x_i	-	Mole fraction of species *i* in the liquid phase
x_0	-	Initial mole fraction in still pot
x_w	-	Mole fraction in the liquid phase in the sill pot
y_i	-	Mole fraction of species *i* in the vapour phase
y_d	-	Mole fraction in the vapour distillate
Z	-	Compressibility factor
Z_c	-	Critical compression factor

Greek letters

α	-	Function of the cubic equation of state or the relative volatility
β	-	Parameter of the cubic equation of state
Γ_i	-	Integration constant
γ_i	-	Activity coefficient of species *i* in solution
ε	-	Constant of the cubic equation of state
μ_i	kJ/mole	Chemical potential of species *i* in solution
μ_r	Debye	Reduced Dipole Moment
μ_i^{ig}	kJ/mole	Ideal gas chemical potential of species *i* in solution
ρ_0	kmol/m^3	Liquid molar density
ρ_L, ρ_v	kg/m^3	Liquid and vapour density
σ	-	Constant of the cubic equation of state
Φ_i		Ratio of fugacity coefficients
$\emptyset_i$	-	Fugacity coefficient of pure species *i*
$\hat{\emptyset}_i$	-	Fugacity coefficient of species *i* in solution
Ω	-	Constant of the cubic equation of state
ω	-	Acentric factor

Chapter 1

Introduction

1. Introduction

The separation of chemicals is an integral part of most chemical processes. The most common form of separation in the industry is the use of distillation columns. Separation processes are made possible by the fact that the equilibrium compositions of chemical species in mixtures are not equal in coexisting phases (Doherty & Malone, 2001: 21). A description of the behaviour in the equilibrium phases is needed for the design of separation processes. For distillation columns, a description of the vapour-liquid equilibrium (VLE) behaviour is needed and in some cases where there is more than one liquid phase, a description of the vapour-liquid-liquid equilibrium (VLLE) behaviour is needed for the design purposes as well.

The VLE of a mixture occurs when the rate of evaporation from the liquid phase is equal to the rate of condensation from the vapour phase. At a macroscopic level, conditions appear static, as the temperature, pressure and phase compositions will remain constant. However, at molecular level, the species close to the interface surface move between the two phases (Smith, Van Ness & Abbott, 2001: 330).

Thermodynamic principles state that the composition of the liquid phase and the vapour phase are related directly to a specific pressure and temperature. The description and prediction of this phase equilibrium is helpful in chemical engineering (Seader & Henley, 2006: 119). Highly accurate descriptions and predictions of the VLE phase behaviour lead to accurate and effective designs for separation processes, which in turn reduce the capital costs as well as the operating costs in a plant (Doherty & Malone, 2001: 21).

Methods for predicting VLE behaviour might not be accurate, as several assumptions are made during the calculations, such as assuming an ideal mixing, ideal gas phase behaviour and ideal liquid phase behaviour. Another challenge for the prediction of VLE data is that the physical properties used in the calculations are not accurate under operating conditions. To

solve this problem, VLE data can be measured experimentally and then be fitted to various models to describe the VLE behaviour more accurately for various operating conditions.

1.1. Background to the Fluoro-chemical Expansion Initiative (FEI)

The South African government started the Fluoro-chemical Expansion Initiative (FEI) in 2007. This initiative strives to expand the South African fluoro-chemical production market. South Africa has the second-largest base reserves of fluorspar in the world (as can be seen in Figure 1.1). South Africa has an estimated base reserve of 88 million tons of fluorspar. Base reserves refer to the total quantity of fluorspar reserves, including the reserves that are not economically viable for mining. Approximately 340 000 tons of fluorspar are produced annually (Miller, 2009). The Chamber of Mines of South Africa estimated the total exports at 218 000 tons of fluorspar in 2006, making South Africa the third-largest exporter of fluorspar in that year (Chamber of Mines, 2007).

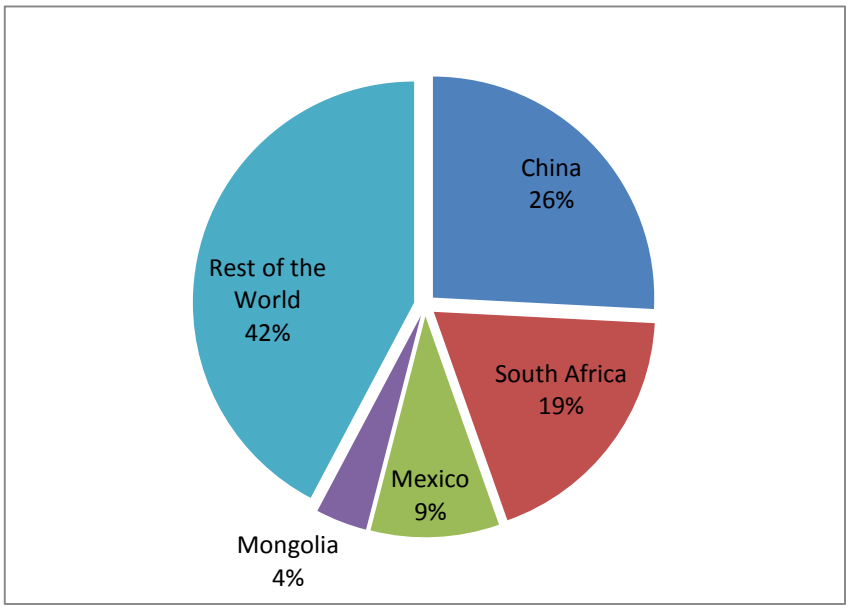

Figure 1.1: Fluorspar base reserves worldwide (Miller, 2009).

At the current rate of production, the fluorspar reserves will last another 300 years in South Africa. At present, only about 15 % of the produced fluorspar is converted into high-end products. Most of the fluorspar is converted into hydrogenfluoride (HF) and fluorine (F_2). Fluorspar can be exported for about 10 US cents per kg, HF for about US$1 per kg and F_2 for about US$15 per kg. Therefore the beneficiation of fluorspar could become an important base of the South African economy, especially if some of the downstream products could be

sold for up to US$5 000 per kg (Chamber of Mines of South Africa, 2007). The aim of FEI is to increase the beneficiation of fluorspar to above the 25 % mark.

The Department of Science and Technology has awarded several grants to the South African Nuclear Energy Corporation (Necsa), the University of Pretoria (UP) and the University of KwaZulu-Natal (UKZN) to perform research on FEI. One such project under the supervision of Necsa is the production of a high-end commodity, polytetrafluoroethylene (PTFE) and several other fluoropolymers.

1.2. Fluoropolymer production

The Applied Chemistry Division at Necsa is building a laboratory-scale demonstration plant to produce several fluoropolymers, including PTFE, perfluorinated ethylene-propylene (FEP) and ethylene tetrafluoroethylene (ETFE). The monomers for these polymers are tetrafluoroethylene, hexafluoropropylene and ethylene. The process will use scrap PTFE as raw material to produce some of the monomers by pyrolysis. The operating pressure of the pyrolysis process will determine which compounds form from the decomposition reaction (Hunadi & Baum, 1982). Hunadi and Baum (1982) state that pyrolysis at pressures higher than 20 kPa will produce tetrafluoroethylene (TFE), hexafluoropropylene (HFP) and octafluorocyclobutane (OFCB). Withthe current configuration used at Necsa, the following gases are formed: TFE, HFP, OFCB and perfluoro-isobutylene (PFIB) (Van der Walt & Bruinsma, 2006). A radiofrequency induction generator is used as the heat source for the reactor which operates under vacuum. The composition of the mixture may vary, but the average composition of the mixture is 60 % TFE, 30 % HFP, 10 % OFCB and less than 1 % of PFIB.

This gas is currently distilled by a small batch distillation column, with no control over flow rates, heat duties or purity. The gas mixture is frozen in a still pot and allowed to reach room temperature, where the heat transfer from the environment acts as a reboiler. This column must produce pure TFE (purity greater than 99.999 %), for the PTFE polymerization reaction, and pure HFP to serve as monomer for other fluoropolymers. The current column was not designed by chemical engineering methods and is operated by estimating the operating temperatures and flow rates. The purity of each run varies and this causes additional problems with studying the polymerization reactions. A very high purity TFE is required to produce a high quality PTFE product.

1.3. Project Objectives

To ensure that high purity TFE is produced during each run, a detailed batch column design must be developed. The column must be able to deliver high purity TFE and high purity HFP while operating within specific time boundaries. VLE data are required to produce an accurate column design. A literature study revealed that no experimental VLE data are available for these chemicals and that they would have to be determined. The objectives for the project are therefore:

- Finding suitable apparatus to measure the VLE data
- Using the measurements of a known system to compare with published data the accuracy of the experimental results obtained on the apparatus
- Measuring the data for the binary systems of TFE + HFP, TFE + OFCB and HFP + OFCB
- Correlating the VLE data with thermodynamic models
- Designing a preliminary batch distillation column

PFIB is an extremely toxic gas, even at very low concentrations. Patocka and Bajgar (1998) state that the lethal concentration (LC50) for single exposures in rats is 0.5 ppm. The two-hour LC50 for mice is reported to be between 0.98 ppm and 1.6 ppm. PFIB exposure in humans leads to “polymer fume fever”, with symptoms similar to those of a flu virus (Patocka & Bajgar, 1998). Due to the high boiling temperature relative to the other components, no PFIB is currently found in the distillate. Working with PFIB makes it difficult to operate the available equipment safely. Owing to the negligible influence that the small amount of PFIB would have on the system, a decision was made against including it in the study.

The safety standards at Necsa, are intended to prevent any possible self-decomposition or auto-polymerization, provide that pure TFE may only be stored at pressures lower than 0.18 MPa (absolute). The column must also be operated at pressures lower than 0.2 MPa. This pressure specification limit means the operating temperature of the condenser has to be lower than 223 K. It is important to note that the melting temperature of OFCB is 232.96K (Daubert, Danner, Sibul & Stebbins, 1998) which is slightly higher than the minimum suggested operation temperature range. Problems might arise as the OFCB might start crystallizing.

The Experimental setupwas available at the Thermodynamic Research Unit at the University of KwaZulu-Natal. The research unit is well-established with several pieces of apparatus for

measuring various systems. Due to the limitations of the apparatus for taking liquid and vapour phase samples below pressures of 0.25 MPa and the fairly low vapour-pressures of OFCB and HFP at the targeted temperatures, the temperature ranges for sampling had to be adapted. Low pressure data could not be measured on a different set of equipment as the available equipment could not operate at such a low temperature. The possibility of auto-polymerization or self-decomposition also prevented work on low-pressure glass apparatus.

The measurements for each isotherm were taken at the following temperatures:

- TFE and OFCB: 248, 263 and 283 K
- TFE and HFP: 248, 263 and 283 K
- HFP and OFCB: 293, 323 and 353 K

1.4. The Materials

1.4.1. Tetrafluoroethylene (TFE)

Figure 1.2 shows the molecular structure of TFE (C_2F_4). TFE is also commonly known as perfluoroethylene or R-1114. The TFE used in this project was purified by a distillation column at Necsa. It has an estimated purity greater than 99.8 %. Table 1.1 gives a summary of the physical properties of TFE. As mentioned above, TFE is not stable under pressure and can undergo auto-polymerization. This auto-polymerization creates an exponential increase in temperature and pressure, resulting in the possibility of an explosion if the vessel is incapable of containing the higher pressure.

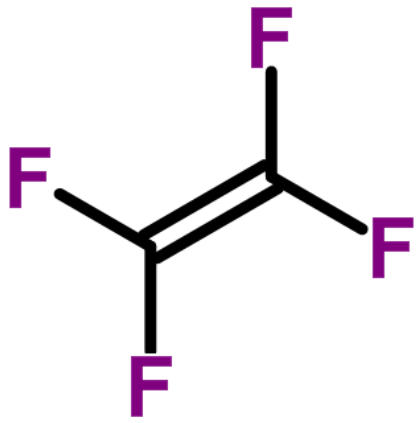

Figure 1.2: Molecular structure of tetrafluoroethylene (CAS number: 116-14-3) (The Royal Society of Chemistry, 2009).

TFE also poses the risk of self-decomposition into CF_4 and C. This is similar to the decomposition reactions for ethylene and acetylene, where all of the reactions result in violent explosions. As a result of these possible risks, legislation was enacted in the European Community that forbids the transportation of TFE in any state (Espech, Goldmann, Killich, Löhr & Stautd, 2002). Even though TFE is a common material in the industry, no explosion has been reported in the industry for applications below 0.6 MPa (Lisochkin & Poznyak, 2006). Lisochkin and Poznyak (2006) also state that the probability of an explosion is very high when TFE is operated above 1 MPa.

Table 1.1: Physical Properties of TFE, HFP and OFCB.

	Molecular Weight	Normal Boiling Point (K)	Critical Pressure (MPa)	Critical Temperature (K)
TFE[a]	100.016	197.51	3.944	306.5
HFP[b]	150.023	243.55	3.136	358.9
OFCB[c]	200.031	267.17	2.7775	388.4

[a] – Reid, Prausnitz& Poling,1987. [b] – Coquelet, Ramjugernath, Valtz, Naidoo & Meniai (2010). [c] – Daubert*et al.*, 1998.

1.4.2. Hexafluoropropylene (HFP)

Figure 1.3 shows the molecular structure of HFP (C_3F_6). The HFP used in this project was produced by Pelchem, the chemical division of Necsa. It had an estimated purity greater than 99.7 %. Table 1.1 includes a brief summary of the physical properties of HFP.

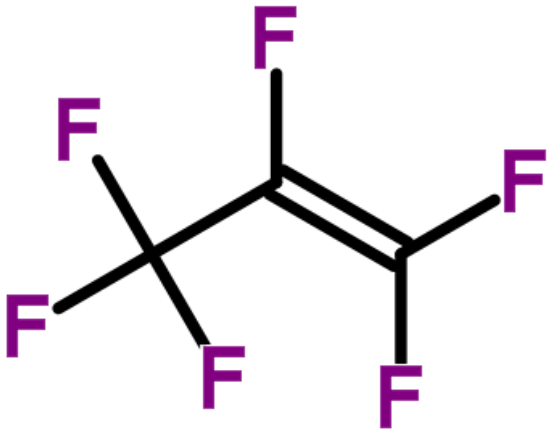

Figure 1.3: Molecular structure of hexafluoropropylene (CAS number: 116-15-4) (The Royal Society of Chemistry, 2009).

1.4.3. Octafluorocyclobutane (OFCB)

Figure 1.4 shows the molecular structure of OFCB (c-C_4F_8), also referred to as R-c318. The OFCB used in this project was produced in-house at the Research and Development Department at Necsa. It had an estimated purity greater than 99.8 %. Table 1.1 gives a summary of the physical properties of OFCB.

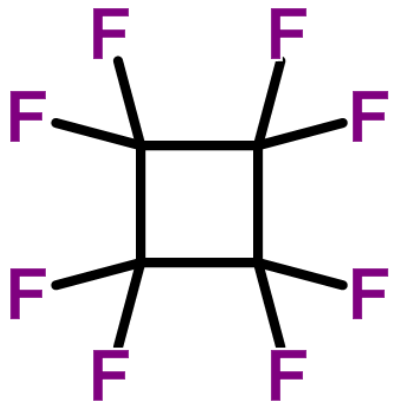

Figure 1.4: Molecular structure of octafluorocyclobutane (CAS number: 115-25-3) (The Royal Society of Chemistry, 2009).

Chapter 2

Thermodynamic Principles

2. Thermodynamic Principles

A familiar sight in industry is the thermodynamic phenomenon of coexisting phases, with unique properties attributed to the interacting phases. The most common phases occurring in industry are vapour-liquid phases, but vapour-liquid-liquid, liquid-liquid, vapour-solid and liquid-solid phase coexistence is also found in the industry (Smith *et al.*, 2001: 329). Several models have been developed to describe these phases as well as the interaction between the phases. This chapter focuses on the thermodynamic principles of vapour-liquid phase behaviour. Systems exist where the components react with one another to a certain extent, but this was omitted from this study as the fluorocarbons are characterized by low dipole moments and have a low intermolecular attraction. The chapter will start by looking at the pure component behaviour of materials then look at the thermodynamic behaviour of the components in the mixtures.

2.1. Fundamentals of Equilibrium

The VLE of a mixture occurs when the rate of evaporation from the liquid phase is equal to the rate of condensation from the vapour phase. At a macroscopic level, it will seem as if conditions are static, because the temperature, pressure and phase compositions will remain constant. However, at a sub-microscopic level, the molecules close to the interface surface move between the two phases (Smith *et al.*, 2001: 330).

The phase rule can be used to explain the above definition. The phase rule states that if any system is at equilibrium, the number of independent variables that must be fixed to selected values to establish its intensive state is restricted. The following equation describes the phase rule for non-reactive systems (Smith *et al.*, 2001: 29 – 30):

$$F = 2 - \pi + N \tag{2.1}$$

Here π is the number of phases, N is the number of chemical species present and F is the number of degrees of freedom.

The variables that can be fixed are the temperature, pressure and the composition of the phases. To illustrate the phase rule, consider a system of two chemical species both appearing in two coexisting phases. Then the equation yields two degrees of freedom. So if the temperature and pressure are fixed for the system, it can only be in equilibrium for a specific set of compositions in the two phases. This principle allows for the experimental determination of VLE data for various sets of experimental conditions in different laboratory setups. If the same two variables can be controlled, the same equilibrium conditions should be obtained.

Several thermodynamic models have been developed to describe or predict the VLE behaviour. Some of the models assume ideal phase behaviour but the more complex models compensate for the non-ideal behaviour in the phases. These models include theories of molecular physics and statistical mechanics (Smith *et al.*, 2001: 338). Firstly themodels to describe the behaviour of a pure component need to be defined and then adjusted for the behaviour in mixtures. The next section looks at models for pure components.

2.2. Equations of State

The relation between pressure, temperature and volume for pure components are important values for the use in engineering calculations and simulations. Models should be able to predict the behaviour of pure components in the liquid and vapour phase. A well-knownmethod used to predict these behaviours are the Virial Equation of State. The Equations of State investigated in this section can be expanded for mixtures, this will be shown later in the chapter. Included in this chapter are variations on the equations of state as well as some correlations that can be used with the equation of state.

2.2.1. Virial Equation of State

The general form of the Virial EoS can be written as (Smith *et al.*, :2001:70):

$$Z \equiv \frac{PV}{RT} = 1 + \frac{B}{V} + \frac{C}{V^2} + \frac{C}{V^3} + \cdots \tag{2.2}$$

Z is known as the compressibility factor of a species and is dimensionless. The second virial coefficient, *B*, is a function of temperature and composition. The equation shown next is a truncated form of the original Virial equation useful in calculating the number of moles for a non-ideal gas:

$$Z = 1 + \frac{BP}{RT} \tag{2.3}$$

This equation is applicable to low to moderate pressures and the relation to the composition is based on statistical mechanics.

2.2.2. Pitzer and Curl Correlation

Pitzer and Curl (1957) suggested a correlation to predict this second-order virial coefficient by first rewriting the virial equation of state:

$$Z = 1 + \frac{BP}{RT} = 1 + \left(\frac{BP_c}{RT_c}\right)\frac{P_r}{T_r} \tag{2.4}$$

The Pitzer and Curl correlation yields a solution for BP_c/RT_c:

$$\frac{BP_c}{RT_c} = B^{(0)} + \omega B^{(1)} \tag{2.5}$$

Here $B^{(0)}$ and $B^{(1)}$ are both functions of the reduced temperature and ω is the acentric factor. The acentric factor is calculated from the following equation:

$$\omega = -\log P_r - 1 \tag{26}$$

P_r is the reduced vapour pressure (P^*/P_c) with the reduced temperature (T_r) at 0.7.

The $B^{(0)}$ and $B^{(1)}$equations are related to the critical properties of the species and are modified to give improved fits at low temperature with the addition of small T^{-3} and smaller terms:

$$B^{(0)} = 0.1445 - \frac{0.330}{T_r} - \frac{0.1385}{T_r^2} - \frac{0.0121}{T_r^3} \tag{2.7}$$

$$B^{(1)} = 0.073 - \frac{0.460}{T_r} - \frac{0.50}{T_r^2} - \frac{0.097}{T_r^3} - \frac{0.073}{T_r^8} \tag{2.8}$$

The Pitzer and Curl correlation fits well for low to moderate pressures of non-polar compounds.

2.2.3. Tsonopoulos Correlation

Tsonopoulos (1974) suggests a modification of the Pitzer and Curl correlation to adjust for polar compounds. This correlation can be used for hydrogen-carbon mixtures at low pressures. To adjust for the polarity of the compounds, a parameter dependent on the dipole moment is added to the Pitzer and Curl correlation:

$$\frac{BP_c}{RT_c} = \frac{B^{(0)}P_c}{RT_c} + \omega\frac{B^{(1)}P_c}{RT_c} + \frac{B^{(2)}P_c}{RT_c} \tag{2.9}$$

The functions $B^{(0)}$ and $B^{(1)}$ are the same as those used in the Pitzer and Curl correlation and $B^{(2)}$ is defined as:

$$B^{(2)} = \frac{a}{T_r^6} \tag{2.10}$$

where a is defined by:

$$a = -2.188 \times 10^{-11}\mu_r^4 - 7.831 \times 10^{-21}\mu_r^8 \tag{2.11}$$

$$\mu_r = \frac{\mu^2 P_c}{1.01325T_c^2} \tag{2.12}$$

The parameter *a* is written in terms of the reduced dipole moment (μ_r), which in turn is dependent on the dipole moment (Debye), critical pressure (Pa) and critical temperature (K). Equation 2.41 can be expanded to include a term to describe the associated behaviour in the components in a mixture (Tsnopoulos, 1974).

2.2.4 Cubic Equation of States

The cubic equation of state is used to describe the behaviour of pressure, volume and temperature of liquids and vapours. There are many different forms of the equation though they all originate from the following generic cubic equation of state (Smith *et al.*, 2001: 91 – 93):

$$P = \frac{RT}{(V-b)} - \frac{a(T)}{(V+\varepsilon b)(V+\sigma b)} \tag{2.13}$$

ε and σ in this equation are pure numbers that are the same for all substances and will determine the form of the equation of state. The parameters *a(T)* and *b* are dependent on the species used in the equation. The rest of the section discusses several popular variations in the generic cubic equation of state. All of the equations discussed can also be expanded for fluid mixtures. This introduces the need for mixing rules to estimate the properties of the mixture.

2.2.5. Van der Waals Equation

The Van der Waals equation is the most basic form of the cubic equation of state. For this equation ε = 0 and σ = 0 and the *a(T)* parameter has no temperature dependence:

$$P = \frac{RT}{(V-b)} - \frac{a}{V^2} \tag{2.14}$$

This equation becomes the ideal gas law when *a* and *b* are zero. These parameters are calculated from the critical properties of the species. This equation was proposed by Johannes Diderik van der Waals in 1873. The *a*-parameter compensates for the attraction forces between the molecules and the *b*-parameter is the effective molar volume. The parameters can be fitted to experimental data or estimated from the critical temperatures and pressures. Smith *et al.* (2001) show that the following conditions apply to the equation of state at the critical point because of a horizontal inflection point:

$$\left(\frac{\partial P}{\partial V}\right)_{T\ @\ \text{critical point}} = \left(\frac{\partial^2 P}{\partial V^2}\right)_{T\ @\text{critical point}} = 0 \tag{2.15}$$

Along with the differentiation of Equation 2.14, the parameters for the Van der Waals equation can be calculated from the critical properties:

$$a = \frac{27}{64}\frac{R^2 T_c^2}{P_c^2} \tag{2.16}$$

$$b = \frac{1}{8}\frac{RT_c}{P_c} \tag{2.17}$$

$$Z_c = \frac{P_c V_c}{RT_c} = \frac{3}{8} \tag{2.18}$$

This equation serves as the basis for other expansions on the cubic equation of state. A problem with the Van der Waals equation is that it predicts the compressibility of all fluids as 0.375, which is not accurate as this varies among compounds. Other expansions of the cubic equation of states try to take greater non-ideal behaviour into account. A very common expansion on this equation is the Redlich-Kwong equation of state.

2.2.6. Redlich-Kwong Equation of State

Redlich and Kwong (1949) proposed one of the first expansions to the Van der Waals equation to try and accommodate predictions at higher pressures:

$$P = \frac{RT}{(V-b)} - \frac{aT^{-\frac{1}{2}}}{V(V-b)} \tag{2.19}$$

The *a*-parameter from the Van der Waals EoS is divided by the square root of the temperature for the Redlich-Kwong (RK) EoS. The denominator in the second term is also expanded to include the b-parameter. Similarly to the Van der Waals EoS, the *a* and *b* parameters can be calculated from the critical properties (Prausnitz, 1969: 152 – 153):

$$a = \frac{\Omega_a R^2 T_c^{2.5}}{P_c} \tag{2.20}$$

$$b = \frac{\Omega_b R T_c}{P_c} \tag{2.21}$$

where $\Omega_a = 0.4278$ and $\Omega_b = 0.0867$.

The RK EoS allows for the examination of ideal gases at moderate pressures but cannot be used for liquids. This equation is still not fully capable of predicting the properties of the components accurately.

2.2.7. Soave-Redlich-Kwong Equation of State

The equations described so far are only two-parameter equations and give poor results in VLE calculations (Soave, 1972). Soave (1972) suggests a modification to the RK EoS to expand it

to a three-parameter equation. Soave (1972) modified the $a/T^{½}$ term to take a temperature dependency into account:

$$P = \frac{RT}{(V-b)} - \frac{a(T)}{V(V-b)} \tag{2.22}$$

Again, the pure component properties can be calculated at the critical point:

$$a(T_c) = a_c = 0.42747\ \frac{R^2T_c^2}{P_c} \tag{2.23}$$

$$b = 0.8664\frac{RT_c}{P_c} \tag{2.24}$$

At temperatures other than the critical point, the following temperature-dependent expansion is used:

$$a(T) = a_c\alpha(T_r, \omega) \tag{2.25}$$

with:

$$\alpha(T_r, \omega) = \left[1 + (0.480 + 1.574\omega - 0.176\omega^2)\left(1 - T_r^{\frac{1}{2}}\right)\right]^2 \tag{2.26}$$

where T_r is the reduced temperature and ω is the acentric factor of the species involved.

2.2.8. Peng-Robinson Equation of State

The equations of state mentioned so far still have problems with calculating accurate liquid density values (Peng and Robinson, 1976). Peng and Robinson (1976) suggest their eponymous equation of state to predict liquid density values more accurately, as well as more accurate vapour pressure values and equilibrium ratios than previously suggested models:

$$P = \frac{RT}{(V-b)} - \frac{a(T)}{V(V+b)+b(V+b)} \tag{2.27}$$

Similar to the Soave-Redlich-Kwong (SRK) EoS, the *a*-parameter is also dependent on the temperature. The denominator in the second term is also expanded for better dependency on the *b*-parameter. The parameters can also be evaluated at the critical temperature:

$$a_c = 0.45724\ \frac{R^2 T_c^2}{P_c} \tag{2.28}$$

$$b = 0.8664\ \frac{RT_c}{P_c} \tag{2.29}$$

$$Z_c = 0.307 \tag{2.30}$$

For temperatures other than the critical temperature, the a-parameter function has the same form as that of the SRK equation, which is also dependent on the acentric factor and the reduced temperature. The alpha-function for the Peng-Robinson (PR) EoS differs slightly from the form used by the SRK EoS:

$$a(T) = a_c \alpha(T_r, \omega) \tag{2.31}$$

$$\alpha(T_r, \omega) = \left[1 + (0.37464 + 1.54226\omega - 0.26992\omega^2)\left(1 - T_r^{\frac{1}{2}}\right)\right]^2 \tag{2.32}$$

Peng and Robinson (1976) noted that this equation is similar to the one suggested by Soave (1972) even though the equation is derived from the vapour pressure data between the normal boiling point and the critical point, unlike the Soave equation that calculates the vapour pressure at $T_r = 0.7$, based on the acentric value.

Only the calculations for pure substances have been mentioned so far. All of the EoS can be expanded for mixtures. Firstly, the equation of state can be written in terms of the compressibility of the components, as shown here in its polynomial form (Peng & Robinson, 1976):

$$Z^3 - (1 - B)Z^2 + (A - 3B^2 - 2B)Z - (AB - B^3 - B^2) = 0 \tag{2.33}$$

where *A* and *B* are:

$$A = \frac{a\alpha P}{R^2 T^2} \tag{2.34}$$

$$B = \frac{bP}{RT} \tag{2.35}$$

2.2.9. Mathias-Copeman Alpha Function

Mathias and Copeman (1983) suggest using an alpha-function (this function is noted as a β in the original reference document) that can correlate the vapour pressures of highly polar substances, as the current alpha functions mentioned so far fall short of such components. The alpha-function is similar to the functions determined by Soave (1972) and Peng and Robinson (1976), but has three parameters to fit to vapour pressure data:

$$\alpha(T_r) = \left[1 + c_1(1 - \sqrt{T_r}) + c_2(1 - \sqrt{T_r})^2 + c_3(1 - \sqrt{T_r})^3\right] \tag{2.36}$$

c_1, c_2 and c_3 are adjustable parameters that can be fitted to experimental vapour pressure data. T_r is the reduced temperature. This alpha function expands the use of the PR EoS to high pressure as well.

2.3 Simple Thermodynamic Models

Simple thermodynamic models use several different assumptions to predict system behaviour. These assumptions are only valid under certain conditions or with specific components.

2.3.1 Raoult's Law

The most basic models used to describe the VLE behaviour of systems are Raoult's law and Henry's law.

Raoult's law assumes that the vapour phase is an ideal gas and the liquid phase is an ideal solution. To keep the assumption of gas ideality valid, the pressure in the system should be low to moderate. To keep the assumption of liquid ideality valid, the species should be chemically similar. Raoult's law is described by the following equation:

$$y_i P = x_i P_i^{sat} \tag{2.37}$$

Here x_i is the liquid phase mole fraction, y_i is the vapour phase mole fraction and P_i^{sat} is the vapour pressure of the pure species i at the system temperature (Smith *et al.*, 2001: 341:342).

The left side of the equation gives the *partial pressure* of species *i*. This law gives a description of a few systems, as only a very few systems actually comply with these assumptions. Another limitation of this law is that the species cannot be in its supercritical state as the vapour pressure for the species will not be available.

Raoult's law can be modified to compensate for non-ideal behaviour in the solutions of liquid mixtures. The modified equation is:

$$y_i P = x_i \gamma_i P_i^{sat} \tag{2.38}$$

where γ_i is the activity coefficient.

This activity coefficient is a function of temperature and liquid phase composition and is usually correlated from experimental VLE data (Smith *et al.*, 2001: 349 – 350).

2.3.2. Henry's Law

Another simple law to describe the VLE behaviour in a system that operates above the critical temperature of a component, is Henry's law. Henry's law states that if a species is present in a very small amount in the liquid phase, the partial pressure of the species in the vapour phase is directly proportional to its liquid-phase mole fraction. The following equation shows this relationship:

$$y_i P = x_i \mathcal{H}_i \tag{2.39}$$

where $\mathcal{H}_i$ is Henry's constant. Henry's constant is also determined experimentally.

These models can be used to do bubble point and dew point calculations by solving iteratively. The following criteria are used in solving the models:

$$\sum_i x_i = 1 \text{ and} \sum_i y_i = 1 \tag{2.40) and (2.41}$$

$$P = \sum_i x_i P_i^{sat} \tag{2.42}$$

These simple models can be expanded further by taking into consideration the non-ideal behaviour of the liquid and vapour phases. Fugacity is used to describe this non-ideal behaviour. Changes in composition in the phases are addressed via the chemical potential.

2.3.3. K-value correlations

The K-value correlation is a convenient way of describing how a species will partition itself preferentially between the liquid and the vapour phases. The K-value (K_i) or the equilibrium ratio is defined by the following equation:

$$K_i = \frac{y_i}{x_i} \tag{2.43}$$

This K-value gives a measurement of how light a component is in a mixture. The greater the K-value, the lighter the component, i.e. there will be more of the component in the vapour phase than in the liquid phase. A heavy component that is more present in the liquid phase than the vapour phase, will have a K-value lower than unity. The K-value simplifies the calculations of the bubble point and the dew point (Smith *et al.*, 2001: 354 – 355).

2.4. Chemical Potential and Phase Equilibria

The chemical potential, μ_i, describes the effect of changing composition on thermodynamic properties:

$$\mu_i = \left[\frac{\delta(nG)}{\delta n_i}\right]_{P,T,n_j} \tag{2.44}$$

where *nG* is the Gibbs energy (Smith *et al.*, 2001: 369; Kyle, 1999:201 - 202).

Smith *et al.* (2001: 370 – 371) show that a closed system with more than one phase at equilibrium, where each phase is an open system free to transfer mass to one another, will result in each species having the same chemical potential in all phases:

$$\mu_i^{\alpha} = \mu_i^{\beta} = \cdots = \mu_i^{\pi} \tag{2.45}$$

π is the number of phases present.

This is only valid if all the phases have the same temperature and pressure. The chemical potential for a gas in an ideal gas mixture can also be derived, as shown by Smith *et al.* (2001: 348):

$$\mu_i^{ig} = \Gamma_i(T) + RT \ln y_i P \tag{2.46}$$

where Γ_i is an integration constant ata constant temperature.

2.5. Fugacity and Fugacity Coefficient

There is no absolute value for the chemical potential because the chemical potential and the Gibbs energy are related to the internal energy and entropy of the species. As the chemical potential provides fundamental criteria for phase equilibrium and there are no absolute values, fugacity (f_i) is defined as relating the chemical potential to the phase equilibrium. For any real fluid, the fugacity can be related to the Gibbs energy in the following equation:

$$G_i = \Gamma_i(T) + RT \ln f_i \tag{2.47}$$

Equation 2.47 provides a partial definition for fugacity (Smith *et al.*, 2001:384).
From the definition of the residual Gibbs energy, G_i^R, which quantifies the deviation from the ideal gas propertiesa new property namely the fugacity coefficient (ϕ_i) is now defined:

$$G_i^R = RT \ln \emptyset_i \tag{2.48}$$

where

$$\emptyset_i = \frac{f_i}{P} \tag{2.49}$$

The definition of fugacity is now complete and the ideal gas value for fugacity of a pure species is equal to its pressure.

It can also be shown for a pure species present in a liquid phase and a gas phase that it will be in equilibrium when they have the same temperature, pressure and fugacity:

$$f_i^l = f_i^v = f_i^{sat} \tag{2.50}$$

The same can be shown for the fugacity coefficient.

Until now the fugacity was defined for a pure species in an equilibrium situation. The definition for the fugacity of a species in a solution is similar to that of a single species. $\hat{f}_i$ is used for the *fugacity of species i in the solution*. Equations 2.51 to 2.53 show the definition of the fugacity of a species in solution:

$$\hat{f}_i^{\alpha} = \hat{f}_i^{\beta} = \cdots = \hat{f}_i^{\pi} \tag{2.51}$$

$$\bar{G}_i^{\,R} = RT \ln \hat{\emptyset}_i \tag{2.52}$$

where

$$\hat{\emptyset}_i = \frac{\hat{f}_i}{y_i P} \tag{2.53}$$

$\bar{G}_i^R$ is the partial residual Gibbs energy and $\hat{\emptyset}_i$ is the fugacity coefficient of species *i* in solution. Several correlations for the calculation of the fugacity coefficient exist and are discussed later in this chapter.

An ideal solution model is set up to put forward a standard to which real-solution behaviour can be compared. This also gives rise to excess properties. The fugacity of a species in an ideal solution can be calculated by the following equation; Smith *et al.* (2001:401) show the derivation of the equation:

$$\hat{f}_i^{id} = x_i f_i \tag{2.54}$$

This is the Lewis-Randall rule and is valid for each species in the ideal solution at all temperatures, pressures and compositions. The Lewis-Randall rule states that the fugacity of each species in the ideal solution is proportional to its mole fraction, multiplied by the fugacity of the pure component in the same physical state as the solution and at the same temperature and pressure. Dividing both sides of Equation 2.54 by Px_i an alternative form can be written with the fugacity coefficients:

$$\hat{\emptyset}_i^{id} = x_i \emptyset_i \tag{2.55}$$

The fugacity for both the gas phase and liquid phase can be calculated from the equations of state mentioned earlier in the chapter. This section focuses on methods to calculate the

fugacity, including the fugacity coefficient, in the gas phase. The Lewis-Randall law mentioned above is a popular and simple way of calculating the fugacity and fugacity coefficient of the species in the solution. Various forms of the equations of state are used to calculate the fugacity coefficient of a species in a solution.

The second virial coefficient from the Virial EoS can be used to calculate the fugacity. The following equation shows the dependence on the composition (Smith *et al.*, 2001: 393 – 394):

$$B = \sum_i \sum_j y_i y_j B_{ij} \tag{2.56}$$

B_{ij} describes the bi-molecular interaction between molecule i and j. This equation can be manipulated to express the fugacity coefficient (Smith *et al.*, 2001: 395):

$$\ln \hat{\emptyset}_k = \frac{P}{RT}\left[B_{kk} + \frac{1}{2}\sum_i \sum_j y_i y_j (2\delta_{ik} - \delta_{ij})\right] \tag{2.57}$$

The following equations are used in conjunction with the above derivation from the virial EoS:

$$\delta_{ik} = 2B_{ik} - B_{ii} - B_{kk} \tag{2.58a}$$

$$\delta_{ij} = 2B_{ij} - B_{ii} - B_{jj} \tag{2.58b}$$

$$\delta_{ii} = 0\,, \delta_{kk} = 0 \tag{2.58c}$$

$$\delta_{ki} = \delta_{ik} \tag{2.58d}$$

The second virial coefficient can be determined by the regression of experimental data, but these data are not always available. Several correlations exist that can predict this second virial coefficient from theory. Different correlations can fit better to specific conditions, such as low to moderate pressures, non-polar mixtures or polar mixtures. Some of the more common correlations are discussed in the next sections.

2.6. Activity Coefficients

The activity coefficient, described earlier in relation to Raoult's law, is defined from the excess Gibbs energy:

$$\bar{G}_i^E = RT \ln \frac{\hat{f}_i}{x_i f_i} \tag{2.59}$$

The activity coefficient is defined as the dimensionless ratio on the right-hand side of the equation; i.e. the activity coefficient of species *i* in solution is:

$$\gamma_i = \frac{\hat{f}_i}{x_i f_i} \tag{2.60}$$

This equation relates the non-ideal behaviour in liquids to thermodynamic principles. A similarity in the way Equation 2.52 relates $\bar{G}_i^R$ to the fugacity coefficient is shown in Equation 2.59 in the way that $\bar{G}_i^E$ is related to the activity coefficient (Smith *et al.*, 2001: 405 – 406). Since *ln* γi is a partial property with respect to $\frac{G^E}{RT}$ the following important phase-equilibrium thermodynamic equations can be set up:

$$\frac{G^E}{RT} = \sum_i x_i \ln \gamma_i \tag{2.61}$$

$$\sum_i x_i \, d\ln \gamma_i = 0 \tag{2.62}$$

Equation 2.62 is only valid under constant temperatures and pressures. The excess Gibbs energy is used to quantify the deviation of the actual values from the ideal solution values. Several models have been proposed to estimate the activity coefficients of species in solution and are discussed later in the chapter.

2.7. Activity Coefficient Models

The activity coefficients are mostly used in combination with the equations of state to give a full description of the fluid behaviour in equilibrium. Simple activity coefficient models can be used, such as the Margules models or the Van Laar model or more complex, temperature-dependent models such as the NRTL or UNIQUAC models. The activity coefficient models

are discussed in this section. Equation 2.59 discussed earlier in the chapter shows the relationship between the excess Gibbs free energy and the activity coefficient for a species in solution:

$$\frac{G^E}{RT} = \sum_i x_i \ln \gamma_i \tag{2.59}$$

It is clear from this equation that the excess Gibbs energy depends more on the mixture composition than on the pressure of the system. At low to moderate pressure, far from the critical point, pressure has a very small influence on the excess Gibbs energy (Prausnitz, Lichtenthaler & de Azevedo, 1999: 225). A binary system is analysed to describe the first models. As the excess Gibbs energy describes the deviation from an ideal solution, the excess Gibbs energy will be zero when only one component is present (pure component).

2.7.1. Margules Equation

The first model proposed was by Margules and is a simple two-suffix model at a constant temperature (Prausnitz*et al.*, 1999: 226):

$$G^E = RTAx_1x_2 \tag{2.63}$$

where A is an empirical constant, dependent on temperature and units of energy. Substituting Equation 2.63 for Equation 2.59 gives a direct solution for the two activity coefficients:

$$\ln \gamma_1 = \frac{A}{RT}x_2^2 \tag{2.64}$$

$$\ln \gamma_2 = \frac{A}{RT}x_1^2 \tag{2.65}$$

This model shows a good representation for simple liquid mixtures. The two-suffix model was expanded to a three-suffix model for better accuracy (Smith *et al.*, 2001: 424):

$$\frac{G^E}{RT} = (A_{21}x_1 + A_{12}x_2)x_1x_2 \tag{2.66}$$

Again, substitution for Equation 2.59 gives solutions for the activity coefficients:

$$\ln \gamma_1 = x_2^2[A_{12} + 2(A_{21} - A_{12})x_1] \tag{2.67}$$

$$\ln \gamma_2 = x_1^2[A_{21} + 2(A_{12} - A_{21})x_2] \tag{2.68}$$

This model should be appropriate for mixtures with components which have molecules of the same size, shape and chemical nature. The lack of temperature dependency in the constants also limits the accuracy of the model. The constants of the equation can be fitted to experimental data.

2.7.2. Van Laar Equations

Van Laar proposed a model to take the molecular size of the components in the mixture into consideration. Van Laar truncated an expression of the excess Gibbs energy by Wohl (Prausnitz *et al.*, 1999: 250 – 252; Smith *et al.*, 2001: 433):

$$\frac{G^E}{RT} = \frac{2a_{12}x_1x_2q_1q_2}{x_1q_1+x_2q_2} \tag{2.69}$$

where *q* and *a* are parameters for the equation. Next the activity coefficients can be calculated for the system:

$$\ln \gamma_1 = \frac{A'}{\left(1+\frac{A'x_1}{B'x_2}\right)^2} \tag{2.70}$$

$$\ln \gamma_2 = \frac{B'}{\left(1+\frac{B'x_2}{A'x_1}\right)^2} \tag{2.71}$$

with $A' = 2q_1a_{12}$ and $B' = 2q_2a_{12}$. By taking the limit for the activity coefficient at the infinite dilution of the components, it can be shown that $ln\ \gamma_1^{\infty} = A'_{12}$ at $x_1 = 0$ and the same for $ln\ \gamma_2^{\infty} = A'_{21}$ at $x_2 = 0$. Again this equation fall short of an accurate description of more complex systems, as there is no temperature dependency in the model. Nor is there a theory to justify the model as it is merely used to fit the parameters to experimental data, so it cannot be used for the prediction of complex systems over a wide range of temperatures.

Local composition models were developed so as to alleviate the problems arising from these models. The local composition models account for the short range order and non-random molecular orientations that result from differences in molecular size and the intermolecular forces (Smith *et al.*, 2001: 434).

2.7.3. Wilson Equation

The Wilson equation was the first local composition model available and, due to the success of this model with fitting experimental VLE data, several modifications and alternative models have been proposed such as the Non-Random-Two-Liquid model and the Universal Quasi-Chemical equation. The Wilson equation contains two parameters similar to those of the Margules and van Laar equations (Wilson, 1964; Smith *et al.*, 2001: 434):

$$\frac{G^E}{RT} = -x_1 \ln(x_1 + x_2\Lambda_{12}) - x_2 \ln(x_2 + x_1\Lambda_{21}) \tag{2.72}$$

and the following equations can then be set up for the activity coefficients:

$$\ln \gamma_1 = -\ln(x_1 + x_2\Lambda_{12}) + x_2\left(\frac{\Lambda_{12}}{x_1 + x_2\Lambda_{12}} - \frac{\Lambda_{21}}{x_2 + x_1\Lambda_{21}}\right) \tag{2.73}$$

$$\ln \gamma_2 = -\ln(x_2 + x_1\Lambda_{21}) - x_1\left(\frac{\Lambda_{12}}{x_1 + x_2\Lambda_{12}} - \frac{\Lambda_{21}}{x_2 + x_1\Lambda_{21}}\right) \tag{2.74}$$

When the equations are evaluated at infinite dilution they become:

$$\ln \gamma_1^{\infty} = -\ln \Lambda_{12} + 1 - \Lambda_{21} \tag{2.75}$$

$$\ln \gamma_2^{\infty} = -\ln \Lambda_{21} + 1 - \Lambda_{12} \tag{2.76}$$

2.7.4. Non-Random-Two-Liquid (NRTL) Equation

Renon and Prausnitz (1968) used the Scott's two-liquid theory for binary mixtures but added an extra parameter to their equation to compensate for the non-randomness of mixing in the liquid phases. The following three-parameter equations were set up by Renon and Prausnitz (1968) (Renon & Prausnitz, 1968; Smith *et al.*, 2001: 434 – 435):

$$\frac{G^E}{x_1 x_2 RT} = \frac{G_{21}\tau_{21}}{(x_1 + x_2 G_{21})} + \frac{G_{12}\tau_{12}}{(x_2 + x_1 G_{12})} \tag{2.77}$$

$$\ln \gamma_1 = x_2^2\left[\tau_{21}\left(\frac{G_{21}}{(x_1 + x_2 G_{21})}\right)^2 + \frac{G_{12}\tau_{12}}{(x_2 + x_1 G_{12})^2}\right] \tag{2.78}$$

$$\ln \gamma_2 = x_1^2\left[\tau_{12}\left(\frac{G_{12}}{(x_2 + x_1 G_{12})}\right)^2 + \frac{G_{21}\tau_{21}}{(x_1 + x_2 G_{21})^2}\right] \tag{2.79}$$

where

$$G_{12} = e^{-\alpha_{12}\tau_{12}} \tag{2.80}$$

$$G_{21} = e^{-\alpha_{21}\tau_{21}} \tag{2.81}$$

with

$$\tau_{ij} = \frac{g_{ij} - g_{jj}}{RT} \tag{2.82}$$

Here $\alpha_{12} = \alpha_{21}$. The parameters α, τ_{12} and τ_{21} are specific to the compounds in the mixture and are independent of the composition and the temperature. The α parameter was added to compensate for the non-randomness in the mixture and it is usually set to 0.2, 0.3 or 0.47 depending on the kind of mixture (Renon & Prausnitz, 1968). The most commonly used non-randomness parameter is 0.3 but it can also be fitted to experimental data with the other parameters. τ_{12} and τ_{21} are dimensionless adjustable interaction parameters or can be calculated by the energy parameters shown in Equation 2.69.

The NRTL model can be used to describe non-ideal mixtures and is more effective than the Wilson model, as this model can predict partially and completely miscible systems. The NRTL function is dependent on temperature as well.

2.7.5. UNIQUAC Equations

Abrams and Prausnitz (1975) derived a new equation that extends the quasi-chemical theory of Guggenheim to include and compensate for mixtures that contain different size molecules (Prausnitz *et al.*, 1999: 263). This new set of equations is called the universal quasi-chemical theory (UNIQUAC) and is of greater complexity than the other models mentioned so far (Smith *et al.*, 2001: 435). It is assumed for the UNIQUAC model that the excess Gibbs energy consists of two parts (Prausnitz *et al.*, 1999: 263):

- The combinatorial part (G^C) which describes the dominant entropic contribution, accounting for molecular size and shape differences
- The residual part (G^R) which tries to compensate for the intermolecular forces that give rise to the enthalpy of mixing.

The combinatorial excess Gibbs energy is only described by pure component parameters whereas the residual excess Gibbs energy part contains two binary parameters for each pair of

molecules. The UNIQUAC equations for a multicomponent system are (Smith *et al.*, 2001: 763 – 764):

$$G^C = \sum_i x_i \ln\frac{\phi_i}{x_i} + 5\sum_i q_i x_i \ln\frac{\theta_i}{\phi_i} \tag{2.83}$$

$$G^R = -\sum_i q_i x_i \ln\left(\sum_j \theta_i \tau_{ij}\right) \tag{2.84}$$

where

$$\phi_i \equiv \frac{x_i r_i}{\sum_j x_j r_j} \tag{2.85}$$

$$\theta_i \equiv \frac{x_i q_i}{\sum_j x_j q_j} \tag{2.86}$$

It should be noted that $\tau_{ji} \neq \tau_{ij}$ and $\tau_{ii} = \tau_{jj} = 1$. In Equations 2.85 and 2.86 r_i is the relative volume and q_i is the relative molecular surface area, both for the pure component. The τ_{ij} parameter introduces a temperature dependency to the model:

$$\tau_{ij} = e^{\frac{-(u_{ji}-u_{ii})}{RT}} \tag{2.87}$$

The parameters for the UNIQUAC equation are therefore ($u_{ji} - u_{ii}$) and are fitted to experimental data. Similar to the other models mentioned above, expressions for the activity coefficients can be set up as shown in Smith *et al*. (2001: 764) and Prausnitz *et al*. (1999: 264).

A similar method, UNIFAC, used to estimate the activity coefficients for system, was proposed. A group contribution method is used to estimate the activity coefficients. This model assumes that a liquid mixture consists of a solution of structural units instead of molecules. Such a unit is referred to as a subgroup. So the interactions between the subgroups have an effect on the activity coefficients as well as on the properties of such a subgroup.

Now that non-ideal behaviour can be estimated or correlated to experimental data, VLE data can be generated by the combination of the models discussed here, and these models are further available in the literature.

2.8. Mixing Rules

Mixing rules are used to predict the behaviour of a mixture, based on the way the pure component behaves at a certain temperature and pressure. The better the calculation of the mixture behaviour, the better the calculation of the equation of state of the VLE behaviour of the system. These rules include a simple linear mixing rule or more complex rules such as the Wong-Sandler mixing rule.

Other simple mixing rules include the quadratic mixing ruleand the combining rule (Smith et al., 2001: 540 – 541):

$$a_{ij} = (a_i a_j)^{\frac{1}{2}} \tag{2.88}$$

Another basic rule known as Kay's Rule assumes a pseudo-critical temperature and pressure for the gas mixture.

2.8.1. Kay's Rule

W.B. Kay suggests treating the gas mixture as a pseudo-pure substance (Annamalai &Puri, 2002: 423; Rathakrishnan, 2006: 209). The linear mixing rule is applied to find the pseudo-critical temperatures and pressures of the system:

$$T_{c,mix} = \sum_i y_i T_{c_1} \tag{2.89}$$

$$P_{c,mix} = \sum_i y_i P_{c_1} \tag{2.90}$$

If these mixtures are applied to the RK EoS the following mixture parameters for the equation of state are set up:

$$a = \frac{0.4275\ R^2 T_{c,mix}^{2.5}}{P_{c,mix}} \tag{2.91}$$

$$b = \frac{0.08664\ RT_{c,mix}}{P_{c,mix}} \tag{2.92}$$

This is a very basic approach to taking the behaviour of a mixture into consideration, as components tend to behave differently at temperatures other that the critical temperature.

The following two mixing rules combine the equation of state with activity coefficients to predict the mixing in the system.

2.8.2. The Huron-Vidal Model

As the mixing rules mentioned up to this point does not apply to polar compounds, Huron and Vidal (1979) examine the relationship between the Gibbs free energy, from the equation of state, and mixing rules to take the interaction between polar compounds into consideration. The relationship between an equation of state, activity coefficient and the excess Gibbs free energy is shown by the following equation (Orbey & Sandler, 1998: 44 – 47):

$$\frac{G^{E}_{EoS}}{RT} = Z - \sum_i x_i Z_i - \sum_i x_i \ln\left(\frac{Z}{Z_i}\right) - \sum_i x_i \ln\left(\frac{1-\frac{b}{V}}{1-\frac{b_i}{V_i}}\right) + \left(\frac{a}{bRT}\right) C - \sum_i x_i \left(\frac{a_i}{b_i RT}\right) C \qquad (2.93)$$

Similarly it can be equated with the Helmholtz free energy:

$$\frac{A^{E}_{EoS}}{RT} = -\sum_i x_i \ln\left(\frac{Z}{Z_i}\right) - \sum_i x_i \ln\left(\frac{1-\frac{b}{V}}{1-\frac{b_i}{V_i}}\right) + \left(\frac{a}{bRT}\right) C - \sum_i x_i \left(\frac{a_i}{b_i RT}\right) C \qquad (2.94)$$

where C is a molar-volume-dependent function specific to the EoS that is selected. When pressure is at infinity, Equations 2.93 and 2.94 become:

$$\frac{A^{E}_{EOS}(T,P=\infty,x_i)}{C^{*}RT} = \frac{1}{RT}\left(\frac{a}{b} - \sum_i x_i \frac{a_i}{b_i}\right) \qquad (2.95)$$

and

$$\frac{G^{E}_{EOS}(T,P=\infty,x_i)}{C^{*}RT} = \frac{1}{RT}\left(\frac{a}{b} - \sum_i x_i \frac{a_i}{b_i}\right) + \frac{P}{RT}\sum_I x_i (b - b_i) \qquad (2.96)$$

where C^{*} is now a constant value as $V_i \rightarrow b_i$ and $V_{mix} \rightarrow b_{mix}$ at infinite pressure thus $C(V_{mix} = b_{mix}) = C(V_i = b_i) = C^{*}$. Huron and Vidal (1979) now equated the Gibbs free energy calculated by the EoS and from the activity coefficient model at infinite pressures:

$$G^{E}_{\gamma}(T, P = \infty, x) = G^{E}_{EoS}(T, P = \infty, x) \qquad (2.97)$$

A condition is now set up because $G^E = A^E + PV^E$ and since A^E in the liquid phase is independent of pressure:

$$V^E = V - \sum_i x_i V_i = b - \sum_i x_i b_i = 0 \tag{2.98}$$

To ensure that Equation 2.95 remains finite, Equation 2.98 can be used and the Huron and Vidal mixing rule for parameter *a* is now:

$$a = b\left[\sum_i x_i \left(\frac{a_i}{b_i}\right) + \frac{G^E}{C^*}\right] \tag{2.99}$$

b is calculated from the Van der Waals mixing rule (Equation 2.114).

2.8.3. Wong-Sandler Mixing Rule

Due to the shortcomings of the mixing rule by Huron and Vidal, Wong, Orbey and Sandler (1992) suggest a new cubic equation of state mixing model that can be used to predict the behaviour of non-ideal systems and which allows for extrapolation over wide temperatures and pressures to predict VLE behaviour (Orbey & Sandler, 1998: 50 – 51). Wong *et al.* set up a second virial coefficient binary interaction, by placing constraints on the two functions of *a* and *b* for a single relation and applying it to the combining rule (Orbey and Sandler, 1998: 51 – 53):

$$B(x,T) = \sum_i \sum_j x_i x_j \left(b_{ij} - \frac{a_{ij}}{RT}\right) = b - \frac{a}{RT} \tag{2.100}$$

$$\left(b - \frac{a}{RT}\right)_{ij} = \frac{1}{2}\left[\left(b_i - \frac{a_i}{RT}\right) + \left(b_j - \frac{a_j}{RT}\right)\right]\left(1 - k_{ij}\right) \tag{2.101}$$

Equation 2.100 does not give separate solutions for *a* and *b*, so one more equation is still required to solve these two parameters.

Similar to the Huron-Vidal mixing rule, excess properties are used to determine one of the parameters. Wong and Sandler suggest that the Helmholtz free energy along with a cubic equation of state should rather be used. In the study released by *Wong et al.* (1992), they show that the Helmholtz free energy is almost independent of pressure whereas the Gibbs free energy depends far more on the pressure, so that the following approximation can be made:

$$G^E(T, P = 1\text{bar}, x) = A^E(T, P = 1\text{bar}, x) = A^E(T, \text{high pressure}, x) \tag{2.102}$$

Another equality that can be set up is due to the fact that A^E is independent of pressure at liquid densities:

$$A^E_{EoS}(T, P = \infty, x) = A^E_\gamma(T, P = \infty, x) = A^E_\gamma(T, P = low, x) = G^E_\gamma(T, P = low, x) \quad (2.103)$$

The following mixing rules follow if Equations 2.91, 2.92 and 2.114 are combined:

$$b_m = \frac{\sum_i \sum_j x_i x_j \left(b - \frac{a}{RT}\right)}{1 + \frac{A^E_\infty(x)}{RT} - \sum_i \left(\frac{a_i}{b_i RT}\right)} \quad (2.104)$$

$$a_m = b_m \left[\sum_i x_i \frac{a_i}{b_i} - \frac{A^E_\infty(x)}{C^*}\right] \quad (2.105)$$

This rule is effective as it can predict high-pressure VLE behaviour even though any Gibbs excess free energy model, effective at low pressure, can be used. The models have so far almost explicitly described the behaviour of the gas phase of the fluid in equilibrium.

2.8.4. Mixing Rules for Pitzer and Curl Correlation

When this correlation is applied to mixtures, cross-coefficient parameters are required and can be found by adjustments to the form of the correlation (Prausnitz, 1969: 128 – 1929):

$$B_{ij} = \frac{RT_{c\,ij}}{P_{c\,ij}} \left(B^{(0)}_{ij} + \omega B^{(1)}_{ij}\right) \quad (2.106)$$

The following mixture rules are used along with the equation:

$$T_{c_{ij}} = \left(T_{c_i} T_{c_j}\right)^{1/2} \quad (2.107)$$

$$P_{c_{ij}} = \frac{Z_{c_{ij}} R T_{c_{ij}}}{\frac{1}{8}\left(v_{c_i}^{1/3} + v_{c_j}^{1/3}\right)^3} \quad (2.108)$$

$$v_c = Z_c \frac{RT_c}{P_c} \quad (2.109)$$

where Z_c is the compressibility factor at the critical point, which can be calculated by the Pitzer correlation for normal fluids:

$$Z_c = 0.291 - 0.08\omega \tag{2.110}$$

To calculate the acentric factor of the mixture, the following assumption is made when using a binary mixture:

$$\omega_{12} = \frac{1}{2}(\omega_1 + \omega_2) \tag{2.111}$$

Therefore

$$z_{c_{12}} = \frac{1}{2}(z_{c_1} + z_{c_2}) \tag{2.112}$$

These mixing rules can also be applied to the Tsonopoulos correlation from section 2.2.3, except that the mixture rule for the pressurewill be:

$$P_{c_{ij}} = \frac{4T_{c_{ij}}\left(P_{c_i}\nu_{c_i}/T_{c_i} + P_{c_j}\nu_{c_j}/T_{c_j}\right)}{\left(\nu_{c_i}^{1/3} + \nu_{c_j}^{1/3}\right)^3} \tag{2.113}$$

2.8.5. Mixing rules for the Peng-Robinson Equation of State

When this equation is used to predict values in mixtures, parameters *a* and *b* become mixture parameters defined by the following mixture rules (Peng & Robinson, 1976):

$$a = \sum_i \sum_j x_i x_j a_{ij} \tag{2.114}$$

$$b = \sum_i x_i b_i \tag{2.115}$$

with

$$a_{ij} = (1 - \delta_{ij}) a_i^{\frac{1}{2}} a_j^{\frac{1}{2}} \tag{2.116}$$

δ_{ij} is a binary interaction coefficient that characterizes the binary mixture formed by component *i* and *j*. This binary interaction coefficient can be determined from experimental VLE data. This binary interaction coefficient gives more accurate liquid densities and better VLE calculations than the other methods mentioned thus far.

Equation 2.89 is also known as the Van der Waals one-fluid mixing rule (Orbey and Sandler, 1998:25). Orbey and Sandler (1998: 27 – 34) state that this method cannot predict VLE for highly non-ideal systems. Systems such as alkanes and alcohols, alkanes and water and acetone and water, have difficulty with predicting the liquid split in the VLE behaviour. All these rules work with a single binary interaction parameter. The Van der Waals mixing rules can also be expanded to include additional composition dependence and an extra parameter for the combining rule (Orbey & Sandler, 1998: 34).

2.9. Correlation of VLE Data

Earlier in the chapter it is shown that when a mixture is at equilibrium, the fugacity of the liquid phase will be equal to the fugacity of the vapour phase (Equation 2.50). This is used as the basis for most calculations of VLE data. There are two main methods to calculate or regress VLE data:

- Gamma-Phi method
- Direct method (or the equation of state method)

The methods are based on the fact that the liquid fugacity of a species is equal to the vapour fugacity of a species when the mixture is at equilibrium:

$$\hat{f}_i^l = \hat{f}_i^v = \hat{f}_i^{sat} \tag{2.50}$$

2.9.1. Gamma/Phi Method

The gamma-phi method, also known as the combined method, uses an equation of state to describe the non-idealities of the vapour phase, and an activity coefficient model to describe the non-ideal behaviour of the liquid phase. This method can be used for low to moderate pressure systems and for complex systems (Perry and Green, 1997: 4-25). The limitations of this method can be expanded if rules and models are used which allow for specific conditions, such as high-pressure models. Using Equation 2.50 the following equation can be set up that describes the gamma-phi method:

$$\gamma_i^l x_i f_i^l = \hat{\phi}_i^v y_i P \tag{2.117}$$

f_i^l can be replaced by:

$$\int_i^l = \phi_i^{sat} P_i^{sat} e^{\left(\frac{v_i^l (P - P_i^{sat})}{RT}\right)} \tag{2.118}$$

The exponential in this equation is known as the Poynting correction factor. This correction accounts for the difference between the existing pressure and the saturated pressure, with a significant influence at high pressures. The relation in Equation 2.118 nowreduces Equation 2.117 to:

$$y_i \Phi_i P = x_i \gamma_i P_i^{sat} \tag{2.119}$$

The vapour pressure can be calculated by correlation, and Φ_i is calculated from any equation of state and will reduce to a function containing the binary interaction parameters. γ_i can be calculated or fitted to any activity coefficient model that is suitable to the system (Smith *et al.*, 2001: 526 – 527; Perry & Green, 1997: 4-25 – 4-26).

Bubble point and dew point pressure calculations can be done using these equations, depending on the data that are available. For bubble point calculations, the temperature and the liquid composition must be given; and for dew point calculations, the temperature and the vapour phase composition must be known. Bubble point and dew point temperature calculations can also be done if the pressure is known, instead of the temperature. Figure 2.1 shows a diagram for solving a bubble point pressure calculation iteratively (Smith *et al.*, 2001: 529). The fact that the compositions of the liquid phase and vapour phase must both add up to one, along with Equation 2.94, gives the following solutions for the pressure of the system:

$$P = \sum_i \frac{x_i \gamma_i P_i^{sat}}{\Phi_i} \tag{2.120}$$

$$P = \frac{1}{\sum_i \frac{y_i \Phi_i}{\gamma_i P_i^{sat}}} \tag{2.121}$$

These equations can also be used to reduce experimental data so as to correlate the parameters.

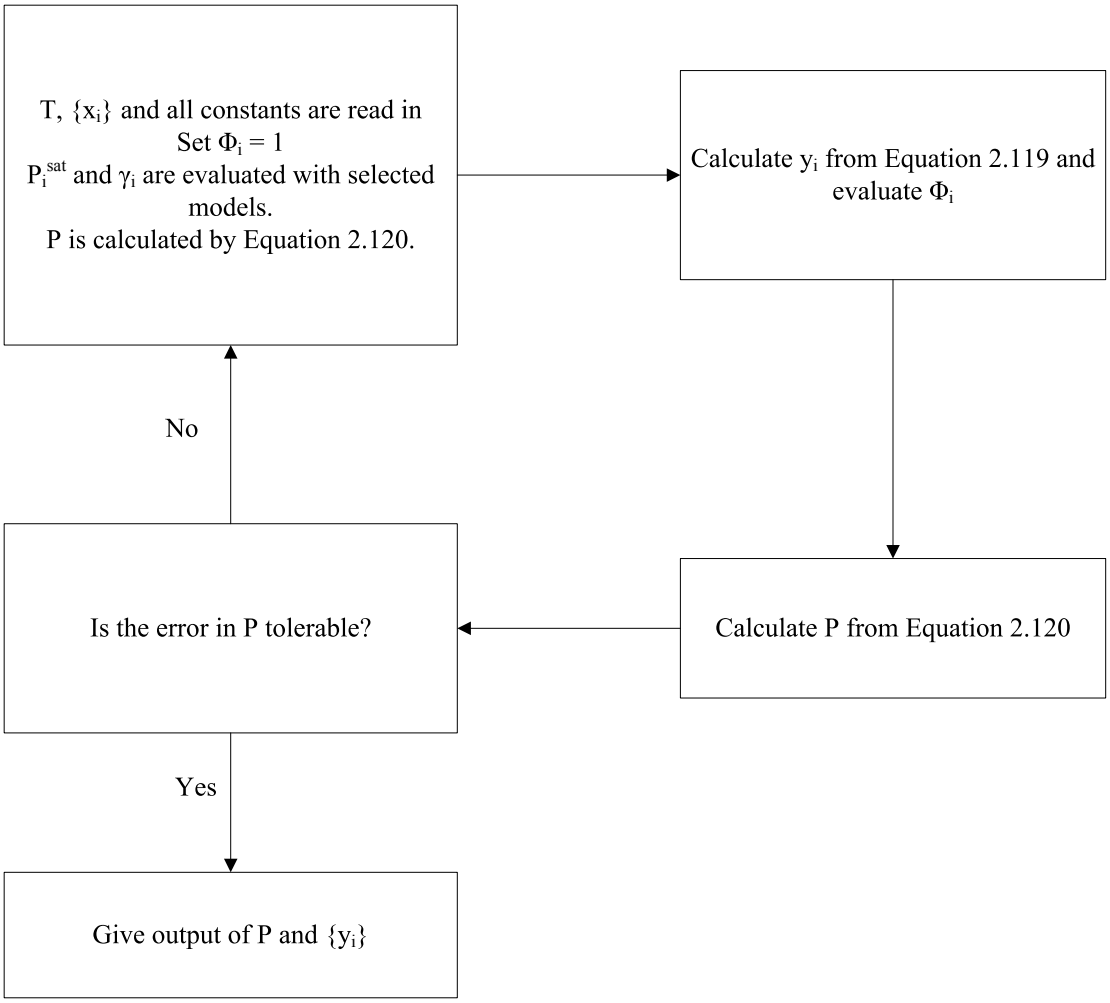

Figure 2.1: Block diagram for a bubble point pressure calculation using the gamma-phi method.

2.9.2. Direct Method

The direct method, also known as the phi-phi method, uses an equation of state to describe both phases in the vapour-liquid equilibrium mixture. Equation 2.117 can be modified for the fugacity coefficients of the species in the mixture and be simplified to:

$$y_i \hat{\phi}_i^v = x_i \hat{\phi}_i^l \tag{2.122}$$

This equation serves as the backbone for solving VLE calculations by the phi-phi method. The fugacity coefficient for a pure component can be calculated from the equation of state (Smith *et al.*, 2001: 539):

$$\ln \phi_i = Z_i - 1 - \ln(Z_i - \beta_i) - q_i I_i \tag{2.123}$$

where I_i is a function based on the equation of state that is selected, and q_i is solved by:

$$q_i = \frac{Z_i^v - Z_i^l + \ln \frac{Z_i^l - \beta_i}{Z_i^v - \beta_i}}{I_i^v - I_i^l} \tag{2.124}$$

β_i is solved by:

$$\beta_i \equiv \frac{b_i P}{RT} \tag{2.125}$$

The fugacity coefficient for a species in solution can also be derived from an equation of state, as shown by Smith *et al.* (2001:540 – 543):

$$\ln \hat{\phi}_i = \frac{\bar{b}_i}{b}(Z - 1) - \ln(Z - \beta) - \bar{q}_i I \tag{2.126}$$

Again I is a function based on the equation of state that is applied. I is a function of ε, β, σ and Z found andis calculated by:

$$I = \frac{1}{\sigma - \varepsilon} \ln\left(\frac{Z + \sigma\beta}{Z + \varepsilon\beta}\right) \text{ when } \varepsilon \neq \sigma \tag{2.127a}$$

Or

$$I = \frac{\beta}{Z + \varepsilon\beta} \text{ when } \varepsilon = \sigma \tag{2.127b}$$

$\bar{q}_i$ is solved by the following partial derivative:

$$nq = \frac{n(na)}{RT(nb)} \tag{2.128}$$

$$\bar{q}_i \equiv \left[\frac{\partial(nq)}{\partial n_i}\right]_{T,\, n_j} = q\left(1 + \frac{\bar{a}_i}{a} - \frac{\bar{b}_i}{b}\right) \tag{2.129}$$

where $\bar{a}_i$ and $\bar{b}_i$ are found with derivatives of the mixing rules used, similar to thatof $\bar{q}_i$.

When mixing rules that are linked to the activity coefficient of the species are used, Equation 2.129 must be expanded to include this coefficient. Using Equations 2.49 and 2.60, the activity coefficient can be related to the fugacity coefficients (this is for the liquid phase calculations) (Smith *et al.*, 2001: 547 -549):

$$\gamma_i = \frac{\hat{f}_i}{x_i f_i} = \frac{\hat{f}_i P}{x_i f_i P} = \frac{\hat{\phi}_i}{\phi_i} \tag{2.130}$$

$$\ln \gamma_i = \ln \hat{\phi}_i - \ln \phi_i \tag{2.131}$$

Now Equation 2.123 is subtracted from Equation 2.126 and a new equation for $\bar{q}_i$ can be derived:

$$\bar{q}_i = \frac{1}{l}\left[1 - Z_i + \frac{b_i}{b}(Z-1) - \ln\frac{(Z-\beta)}{(Z_i-\beta_i)} + q_i I_i - \ln \gamma_i\right] \tag{2.132}$$

$\bar{q}_i$is a partial property, therefore the following summability applies:

$$q = \sum_i x_i \bar{q}_i \tag{2.133}$$

Smith *et al.* (2001) expanded Equation 2.43 to give a K-value by using the fugacity coefficients of the species in the solution:

$$K_i = \frac{\hat{\phi}_i^l}{\hat{\phi}_i^v} \tag{2.134}$$

This equation can be used because the summation of the product of $x_i K_i$ must add up to one.

Now that all the equations have been set up, VLE calculations similar to those of the gamma-phi method can be done. Figure 2.2 shows a diagram for the bubble point pressure calculations. This method can also be used to fit the parameters in the EoS and the different rules used for experimental data.

2.10. Selection of Thermodynamic Model

Selecting the right thermodynamic model for a specific system is crucial as some models only apply under certain conditions for certain compounds. Sinnot (2006: 341 – 352) states that

the best method for fitting experimental data to a thermodynamic model is strongly dependent on these two factors:

- Class of the system (determined by the system investigated)
- System conditions, such as pressure

Several methods have been proposed to choose the model and method for fitting parameters to experimental data. The model used for the work discussed in this document has been successfully used on fluorocarbons before. Table 2.1 gives a summary of recent studies done on fluorocarbons and the systems used in modelling the experimental data. The authors in the table all successfully applied the Peng-Robinson equation of state to their systems. The NRTL activity coefficient model was also used in most of the studies. Most systems used the Wong-Sandler mixing rules. A few systems incorporated different mixing rules, also with great success in modelling the experimental work. The Thermodynamic Research Unit at UKZN has a preference for the Peng-Robinson equation of state with the Mathias-Copeman alpha function, incorporating the Wong-Sandler mixing rules. The NRTL activity coefficient is utilized with this mixing rule (Ramjugernath, 2010b). Based on this information and the personal communication with Ramjugernath (2010b) the Peng-Robinson equation of state with the Mathias-Copeman alpha function, incorporating the Wong-Sandler mixing rules and utilizing the NRTL activity coefficient was used in the modelling of the experimental data shown in this work.

Table 2.1: A summary of models used with fluorocarbon systems

System	Model	Source
Hexafluoroethane and propane	Peng-Robinson - Mathias Copeman – Wong Sander with NRTL	Ramjugernath, Valtz, Coquelet and Richon (2009)
Propane, hexafluoroethane, octafluoropropane and ethane	Peng-Robinson - Mathias Copeman – Wong Sander utilizing NRTL	Thsibangu (2010)
Tetrafluoroethane and fluoroethane	Peng-Robinson – Huron-Vidal utilizing NRTL	Dong, Gong, Lui and Wu (2010)
Carbon dioxide and decafluorobutane	Peng-Robinson - Mathias Copeman – Wong Sander utilizing NRTL	Valtz, Courtial, Johansson and Ramjugernath (2011)
Perfluorobutane and ethane	Peng-Robinson - Mathias Copeman – Wong Sander utilizing NRTL	Ahmar, Valtz, Naidoo, Couquelet and Ramjugernath (2011)
Tetrafluoroethane and propane	Peng-Robinson – Huron-Vidal utilizing NRTL	Dong, Gong, Lui and Wu (2011)

System	Model	Source
Carbon dioxide and trifluoroethane	Peng-Robinson – Wong Sandler utilizing NRTL	Kim, Yoo and Lim (2010)
Difluoromethane, pentafluoroethane and propane	Peng-Robinson with various Mixing Rules	Hou and Duan (2010)
Carbon dioxide and heptafluoropropane	Peng-Robinson – Wong Sandler utilizing NRTL	Kim, Lim and Kang (2010)

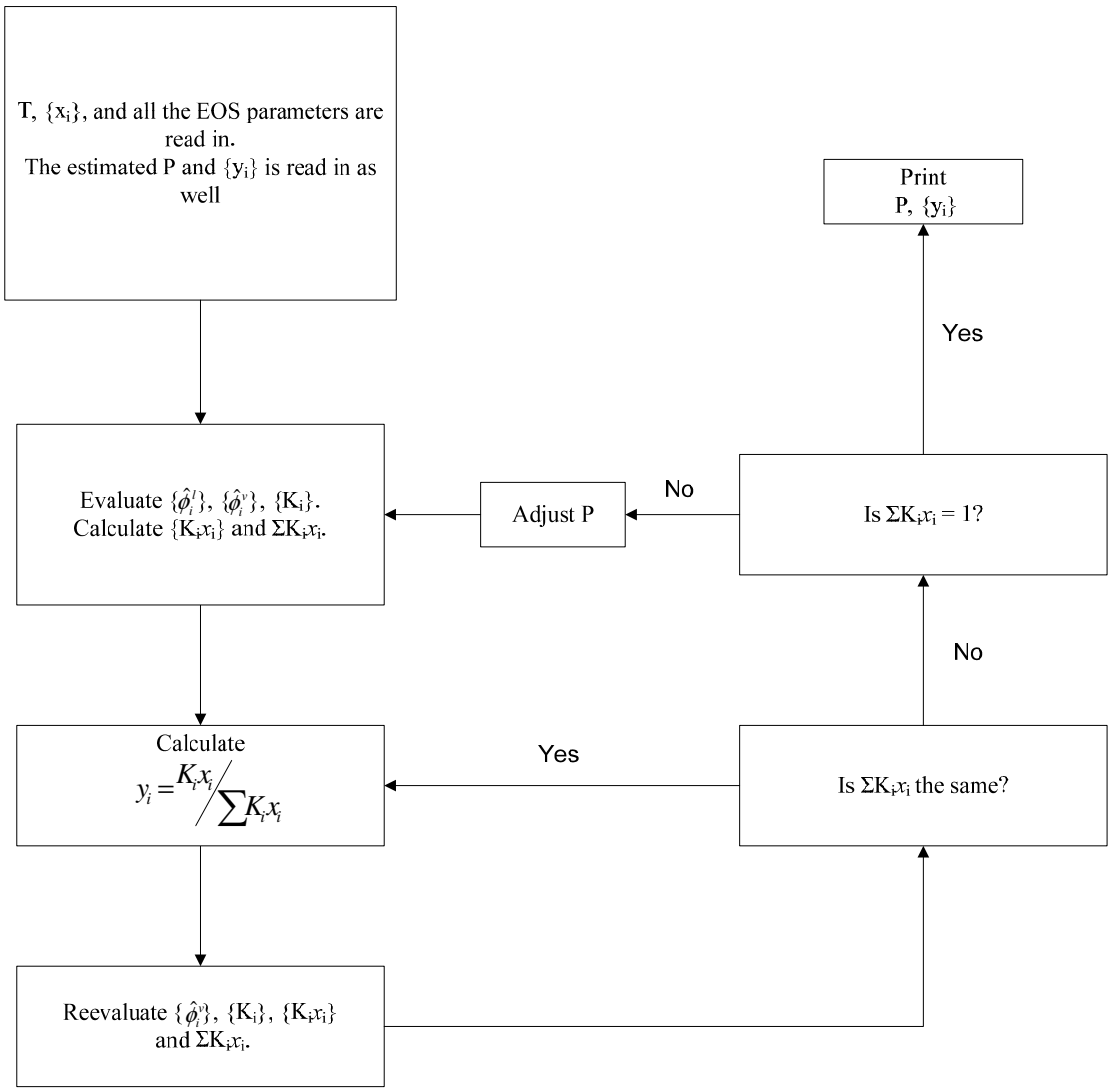

Figure 2.2: Block diagram for the VLE calculations of a bubble point pressure calculation for the direct method (Smith *et al.*, 2001: 546)

2.11. Thermodynamic Consistency

Any experimental data that are fitted to sets of equations should be tested to see whether the data and the calculated parameters are valid and can indeed be used. Thermodynamic consistency tests serve to indicate if a data set and calculated parameter are valid. The Gibbs-Duhem equation forms the basis for thermodynamic consistency tests and this equation is as follows for a binary system (Kyle, 1999: 332 – 333; Prausnitz *et al.*, 1999: 245):

$$x_1 \frac{d \ln \gamma_1}{dx_1} + x_2 \frac{d \ln \gamma_2}{dx_1} = 0 \tag{2.135}$$

The equation can easily be manipulated in various forms. One of the first indications that a set of data is inconsistent is if the activity coefficients do not fit reasonably well to any activity coefficient model or equation. A more definitive test would be to test the system at several liquid compositions in the data set, using Equation 2.135. It is more accurate to test all the data together instead of using a point-by-point analysis.

2.11.1. Area Test

Redlich and Kister (1948) define the following function that is related to the excess Gibbs energy:

$$Q = x_1 \ln \gamma_1 + x_2 \ln \gamma_2 \tag{2.136}$$

This equation can now be differentiated with respect to x_1 at a constant temperature and pressure, and with $dx_1 = -dx_2$ the Gibbs-Duhem equation will simplify to:

$$\frac{dQ}{dx_1} = \ln \frac{\gamma_1}{\gamma_2} \tag{2.137}$$

With integration between the limits of $x_1 = 0$ and $x_1 = 1$, with the knowledge that Q is zero at each limit (since it is a state function) the following is true:

$$0 = \int_0^1 \ln \frac{\gamma_1}{\gamma_2} dx_1 \tag{2.138}$$

The area under the function $\ln\frac{\gamma_1}{\gamma_2}$ must be zero or close to zero, to have thermodynamically consistent data. Since there is no dependency on pressure, the test has shortcomings even though it is very popular (Kyle, 1999: 336).

2.11.2. Point Test

Van Ness (Tshibangu, 2010) suggests using the Point Test to check data for thermodynamic consistency. In this test the vapour phase composition is determined from the experimental temperature and liquid phase composition. The error is then calculated between the experimental value and the calculated value.

These residuals should scatter randomly about the zero axes over the full data set (Danner and Gess, 1990). Danner and Gess (1990) suggest that the absolute average deviation should be less than 0.01 to ensure that the data are in fact thermodynamically consistent.

Chapter 3

Equipment for the Measurement of VLE Data

3. Equipment for the Measurement of VLE Data

Accurate experimental data are required to regress the parameters of the models described in the previous chapter. To ensure accurate data, the experimental equipment and apparatus must be selected to fit the system of interest. Selecting the right apparatus for a system can greatly increase the accuracy of the data gathered and is important, as systemsmay vary greatly in temperature, pressure and physical propertyranges (Weir and de Loos, 2005: 90). Several methods, with several different types of equipment, have been developed and are used in the industry. Equipment for the measurement of VLE data can be split into three main groups (Kyle, 1999: 244; Weir & de Loos, 2005: 72 – 73):

- Static apparatus
- Dynamic apparatus
- Methods for measuring infinite dilution activity coefficients

Another significantdifference in VLE measurements is apparent in low to moderate pressure, and in high-pressure measurements. High-pressure measurements increase the difficulty of the experimental methods, as high pressure poses a danger and most of the compounds investigated at these pressures are above their critical point. Sampling and accuracy in the sampling of supercritical phases and components present a huge difficulty. Raal and Mühlbauer (1998: 40) divided the low-pressure VLE (LPVLE) measurement method into five categories, a few which are similar to the categories proposed byWeir and de Loos (2005):

- Dynamic methods
- Static VLE methods
- Semi-micro techniques
- Measurement of infinite dilution activity coefficients
- Dew point and/or bubble point methods

The system investigated in this project can be classified as a high-pressure system, so the focus will be on high-pressure VLE equipment. Dohrn and Brunner (1995) split the high-pressure VLE measurements into two main groups, based on the method of analysing the phase composition: analytical methods and synthetic methods. Analytical methods examine the composition of all the coexisting phases and can be evaluated inside or outside the equilibrium cell. Synthetic methods are those where a known mixture composition is made up and entered into the equilibrium cell and the phase behaviour is then observed. The problem with synthetic methods is the difficulty of creating the mixtures and loading them into the equilibrium cell. Raal and Mühlbauer (1998: 39 – 40) differentiate between methods by referring to dynamic methods and static methods. They also refer to an experimental method as dynamic when one or both of the phases are circulated to obtain proper mixing in the equilibrium cell, whereas static methods have no phases circulating and use mechanical methods to create agitation in the equilibrium cell.

This section gives a brief survey of the different experimental methods, but focuses largely on the static-analytical methods as this equipment was assigned to the experimental work. A more detailed description of the equipment used in the experimental work for this work appears in Chapter 5.

3.1. Dynamic Methods

Several dynamic experimental methods for the measurement of VLE data have been developed and are in use in several VLE research laboratories in the world. Raal and Mühlbauer (1998: 40 – 55) give a detailed description and review of the literature of low-pressure VLE dynamic methods. Weir and de Loos (2005: 99 – 100; 117 – 118) give an overview of several literature sources for high-pressure measurements using dynamic methods. Most pieces of apparatus are similar in design, as all the equipment must perform the same basic function, viz. reaching equilibrium in a cell with the circulation of phases. The differences are the way that the phases are circulated and the method of sampling the different phases. A wide variety of different designs is available in the industry and is cited in several literature sources. The right dynamic method should be selected according to the project at hand and the possible problems that might arise from the materials used.

3.2. Static Methods

As mentioned earlier there are different categories of static methods. There are various methods to reach the equilibrium in the cells and to determine the phase composition inside them. The same method and equipment can be used for the analytical methods and the synthetic methods.

3.2.1. Synthetic Methods

Synthetic methods describe equipment and methods that use mixtures of known (and accurately measured) compositions. The mixture is introduced into an equilibrium cell where the temperature and pressure are adjusted until phase separation takes place. The mixture composition, temperature and pressure at this equilibrium point are now known. The pressure and temperature are changed until phase separation occurs again, and this is repeated for various pressures, temperatures and mixture compositions.

Pressure isopleths, as a function of temperature, are created by keeping the pressure constant and varying the temperature. Temperature isopleths, as a function of pressure, can be created by keeping the temperature constant and varying the temperature. By cross-plotting these isopleths, the equilibrium curves (temperature vs. mole fraction and pressure vs. mole fraction) can be completed for the system (Raal and Mühlbauer, 1994).

This method is very attractive if the mixture can be synthesized accurately, as no equipment is needed to circulate the phases and to analyse the phases. The systems can also be investigated near the supercritical point.

3.2.2. Analytical Methods

The advantage of the analytical method over the synthetic method is that the composition of the mixture added to the equilibrium cell does not need to be known beforehand. The VLE data generated by the analytical method can be highly accurate at high precision if the system is well calibrated. Vigorous internal agitation is used to reach equilibrium inside the enclosed equilibrium cell. Once equilibrium has been reached, each phase is sampled separately and analysed by a gas chromatograph (GC) or by mass spectrometry (MS) (Tshibangu, 2010: 13). Figure 3.1 shows a diagram illustrating the main functions of a static analytical apparatus.

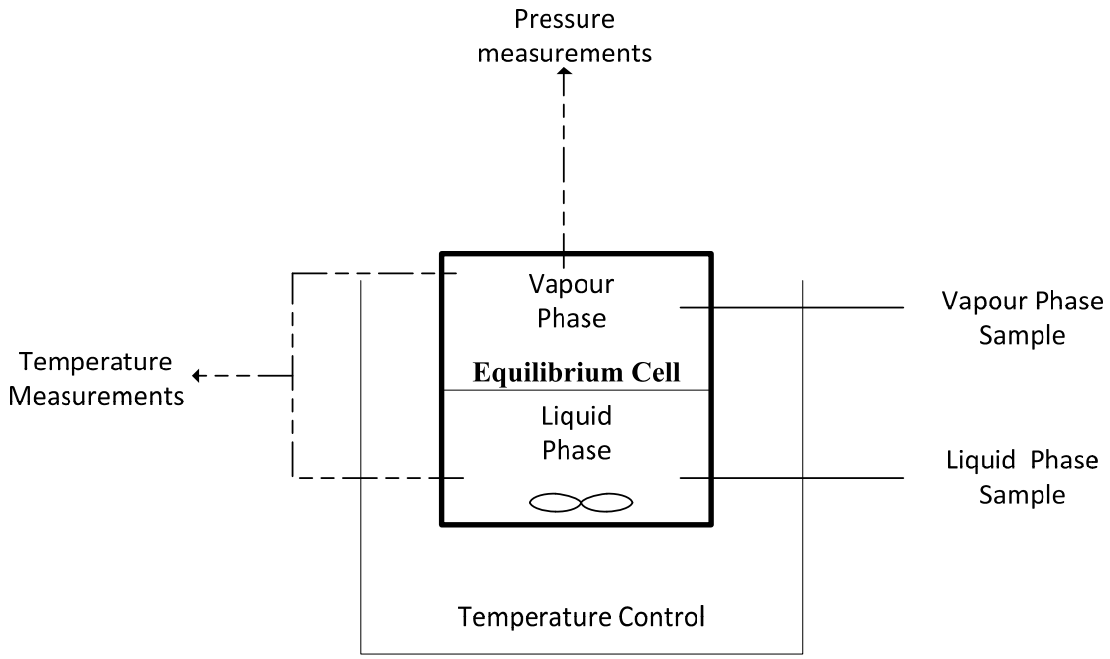

Figure 3.1: The required functions for static analytical apparatus (Raal and Mühlbauer, 1998: 165)

The equilibrium cells are used either as constant volume or as variable volume cells. To ensure accurate data are gathered from the cell, methods must be used for withdrawing the samples from the cell, without influencing the equilibrium. Partial condensation during sampling must be avoided.

The volume in a Variable Volume Cell can be controlled by a movable piston or by injecting a liquid which is immiscible with the materials being investigated. Richon (1996) describes a variable volume apparatus that does not require sampling and can be classified as a synthetic variable volume apparatus. Naidoo, Ramjugernath and Raal (2008) used a similar setup for the apparatus they designed but adapted it to be an analytical variable volume apparatus. Figure 3.2 shows a schematic diagram of the apparatus designed by Naidoo *et al.* (2008). The piston used for controlling the volume in the cell is clearly visible. The lines used for sampling are also visible in the schematic diagram.

One disadvantage of using a variable volume is that a bigger volume cell is required than for a constant volume cell. A bigger volume requires a greater quantity of material for construction and for filling the cell with the materials for the system analysis. A big volume is required in the equilibrium cell so that any samples taken from the cell will not affect the equilibrium inside. After the arrival of the ROLSI™ sampler (Guilbot *et al.*, 2000), big equilibrium cell volumes became redundant as the sampler can take very small samples that will not influence

the equilibrium in the cell. The pressure drop in the equilibrium cell from a sampling with the ROLSI^{TM} is negligible as it is usually smaller than the uncertaintyof the pressure transducer calibrations.

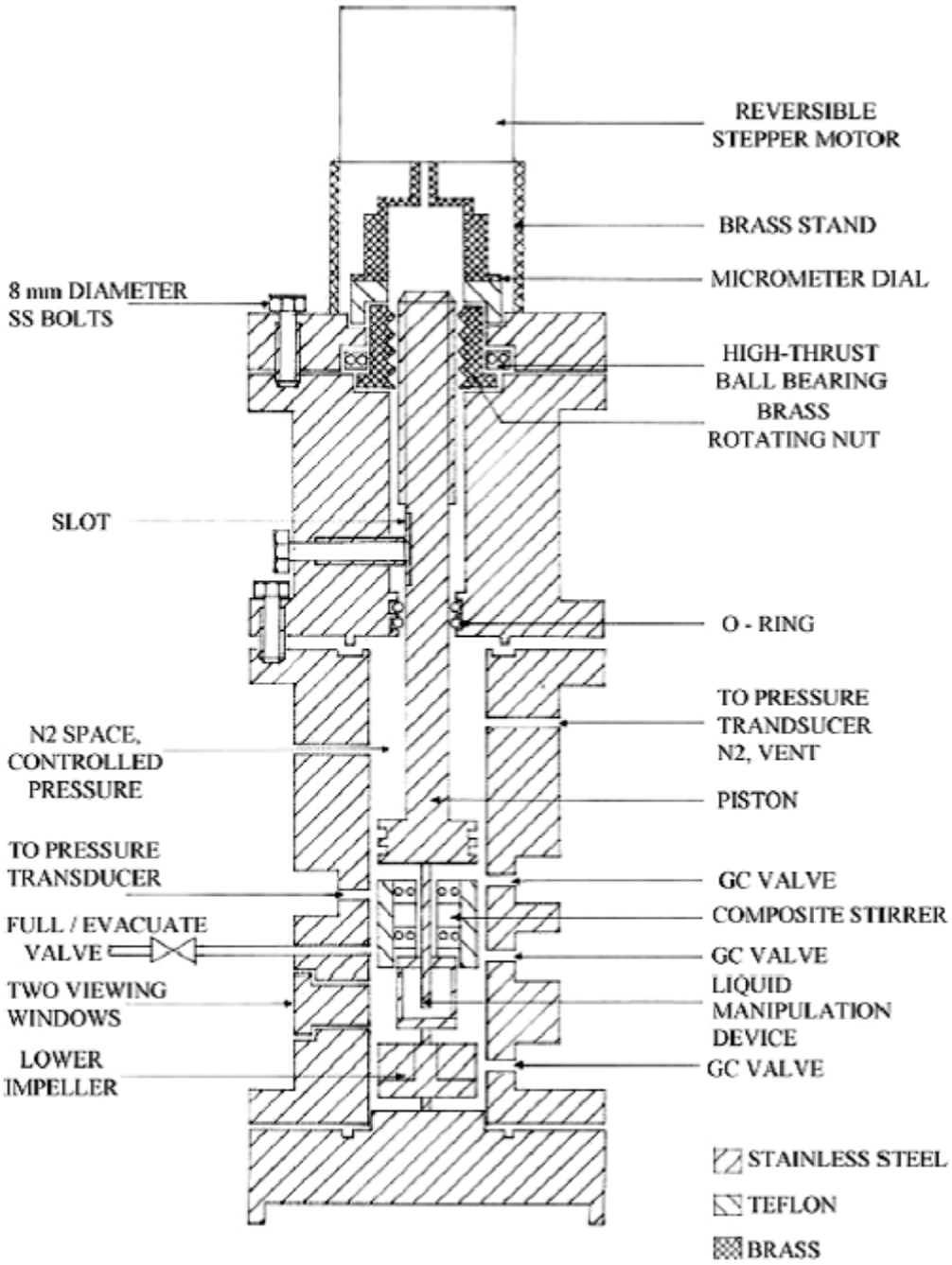

Figure 3.2: A schematic diagram of a variable volume static analytical apparatus (Naidoo *et al.*, 2008).

Using a constant volume cell, the pressure in the equilibrium cell is increased by adding more of the pure component to the cell. The sampling occurs in a way similar to that of a variable volume cell. Valtz, Coquelet, Baba-Ahmed and Richon (2002) describe an apparatus designed and used to measure fluorocarbon vapour pressure data. The apparatus used in their experiments is shown in Figure 3.3. The vapour and liquid phase samples are taken by separate ROLSI™ capillary samplers and then analysed by a GC. The temperature of the cell is controlled by a liquid bath surrounding the equilibrium cell. Equipment similar to this was designed by Tshibangu (2010) and tested on several fluorochemical systems. The equipment used by Tshibangu (2010) measured both the liquid and vapour phases using the same ROLSI™ capillary sampler. This equipment is described in detail in Chapter 5. The equipment described by Valtz (2002) and Tshibangu (2010) can measure VLE data over a wide range of temperature and pressure. Other literature sources describe similar apparatus that can make accurate measurements. The equipment by Thsibangu (2010) could analyse the fluorocarbon system in Chapter 1 and was available for the experimental work.

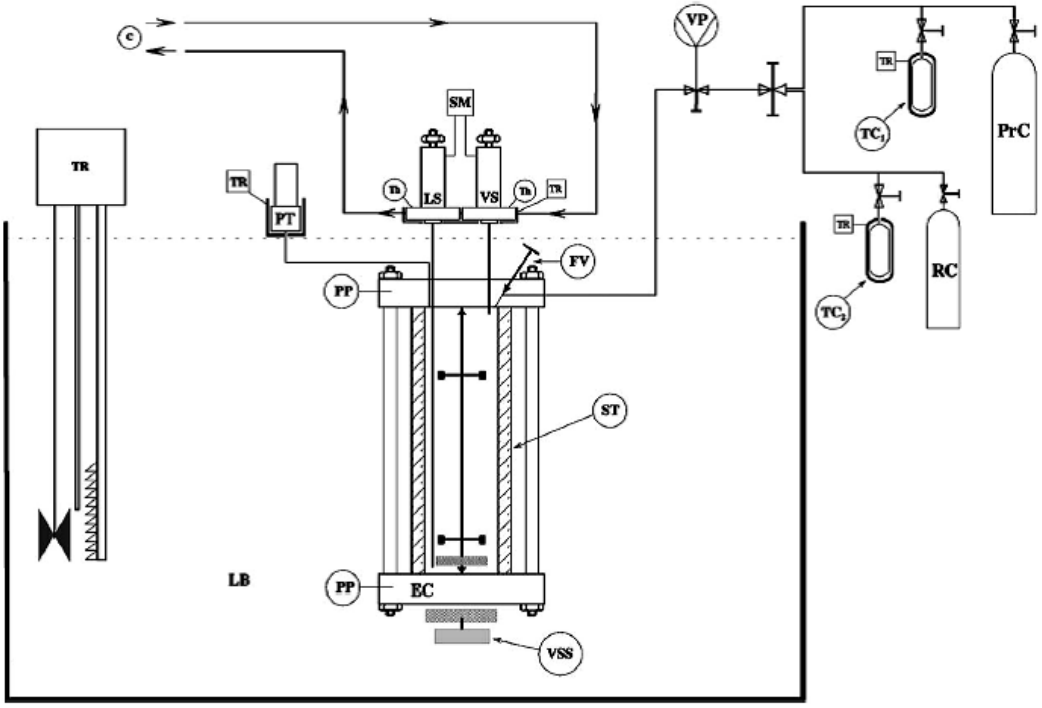

Figure 3.3: The apparatus used by Valtz *et al.* (2002) to measure the VLE data for propane and R227ea.

Chapter 4

Batch Distillation Models

4. Batch Distillation Models

The user requirements from Necsa are to design a distillation column for the separation of the three fluorocarbon gases mentioned in Chapter 1. Currently, as mentioned earlier, a batch distillation column is used for the system, i.e. a feed mixture is loaded into the distillation column and purified from the still pot and then a new feed mixture can be loaded and purified. This is in comparison to a continuous distillation process where the feed is continually added to a column on a specific feed plate at a constant rate. As this project requires the use of very small quantities for the distillation process, several literature sources suggest that a batch distillation column would be most appropriate (Seader & Henley, 2006: 681, Sinnot, 2005: 546). Other benefits of using a batch distillation process for this project are that changes in the feed mixture can be handled by the column. The process upstream of the separation column also operates as batch operations (Seader & Henley, 2006: 681).

Batch distillation requires a unique approach to designing and simulating the equipment compared to that for a continuous distillation column. A continuous process will have a constant composition feed entering the column. As soon as equilibrium is reached in the column, the conditions and compositions inside the column will remain constant throughout the operation if the temperature and the heat duties are kept constant. A batch distillation column differs as the feed in the still pot will change as the product is drawn off the column. So it may seem as if a new equilibrium will be found in the column with each change in the composition in the still pot. This fact increases the difficulty of describing mathematically what is occurring inside the column. Various models found in the literature predict behaviour inside the column. The models range from simple to detailed, rigorous methods. The simplest method used to describe batch distillation was attributed to Lord Rayleigh.

4.1. Simple Batch Distillation

The most basic still used through the ages is shown in Figure 4.1. There is no reflux in the column and it is assumed that the vapour leaving the still pot (y_d) is in equilibrium with the liquid in the pot. If all of the product is condensed (total condenser), the liquid product will have the same composition as that of the vapour leaving the pot ($y_d = x_d$). W will be the amount of liquid left in the pot and x_W is then the liquid composition of the still pot at that time. D is the distillate rate at which the product is drawn off in kmol/h.

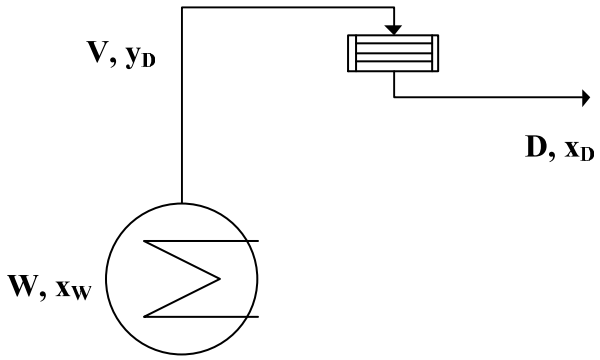

Figure 4.1: A simple batch still setup with no reflux.

The following mass balance can be set up for the still at any time:

$$-\frac{d(Wx_W)}{dt} = Dy_D \tag{4.1}$$

Differentiation of the left-hand side and multiplication by dt gives:

$$Wdx_W + x_W dW = y_D(-Ddt) = y_D dW \tag{4.2}$$

Next Equation 4.2 can be integrated from the initial conditions. Since there is no reflux, it can be simplified as y_d and x_W are in equilibrium:

$$\int_{x_{W_0}}^{x_W} \frac{dx_W}{y_D - x_W} = \ln\left(\frac{W}{W_0}\right) \tag{4.3}$$

Equation 4.3 is known as the Rayleigh equation and can easily be integrated if the pressure remains constant, the temperature in the still pot stays relatively constant, and the K-values (describing the equilibrium behaviour) are independent of the composition.

This case assumes that the distillate that is drawn of directly from the still pot, without an actual column. The equilibriumphase that is created in this instance can be referred to an equilibrium stage, with the liquid phase in equilibrium with the vapour phase. For a distillation column several of these equilibrium stages can be created with either trays or by the use of packing inside the column. A different equilibrium between the liquid and vapour phase will be found on each tray, creating an equilibrium stage. In the design of a distillation column a theoretical number of equilibrium stages are calculated and then depending on the efficiency of the trays to be used an actual number of stages can be calculated. For a packed column a height of the theoretical transfer stage is calculated and based on the type of packing the total height of the packing in the column can be determined.

This is a very simple example of a batch distillation process. Realistically, there will be several equilibrium stages on top of the still pot as well as a way of introducing reflux into the column. Two main groups of batch distillation columns, with a reflux ratio, are widely described (Seader & Henley: 2006: 685 – 689):

- A constant reflux and a variable distillate composition
- A constant distillate composition and a variable reflux

4.2. Binary Batch Distillation with Constant Reflux and Variable Distillate Composition

Figure 4.2 shows a batch rectification column, i.e. a column that has a reflux flowing back into the column. If the reflux is kept constant during operation, the distillate composition will have to vary with time. McCabe-Thiele describes a graphical method for solving such a column when a binary mixture is used. This method is similar to that used in the solving of a continuous distillation column. To apply the McCabe-Thiele method, the following assumptions must be made:

- The holdup of vapour and liquid in the column is negligible
- Phase equilibrium is reached on each stage
- Constant molar overflow (CMO) applies to the column

After making these assumptions, Equation 4.3 can be applied to and used in the McCabe-Thiele graphical solution.

Following the McCabe-Thiele method for a string of values for x_D (which is equal to y_D if a total condenser is in use), pairs can be set up for y_D and x_W. Integrating Equation 4.3

graphically with these pairs and assuming a constant boil-up rate (V), the following equation can be set up for the time required to complete the distillation:

$$t = \frac{W_o - W_t}{V\left(1 - \frac{L}{V}\right)} = \frac{R+1}{V}(W_0 - W_t) \tag{4.4}$$

Here R is the reflux ratio, which is constant in this scenario. As the distillate composition varies through the distillation, the average mole fraction of the most volatile component can be calculated:

$$x_{D_{ave}} = \frac{W_0 x_0 - W_t x_{W_t}}{W_0 - W_t} \tag{4.5}$$

The McCabe-Thiele graphical solution method is shown in Figure 4.3 for a binary system with a continuous distillation column. From this diagram the calculated number of theoretical equilibrium stages are eight. A stage is formed each time a step is made up from the operational line with a slope of L/V to the equilibrium line.

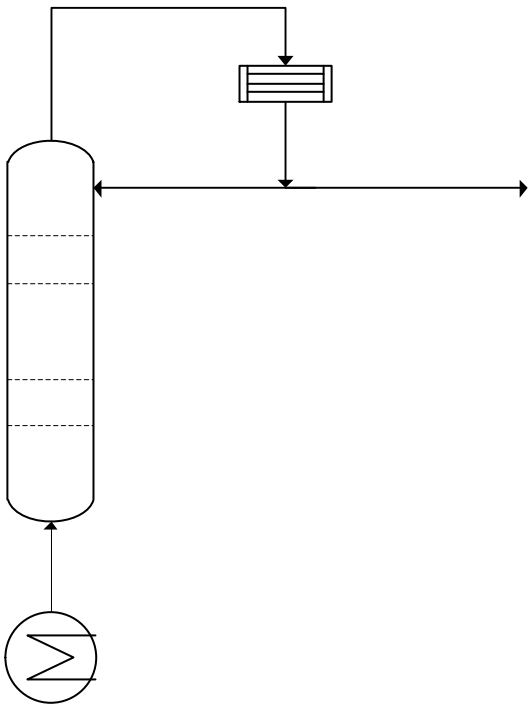

Figure 4.2: A batch rectification column.

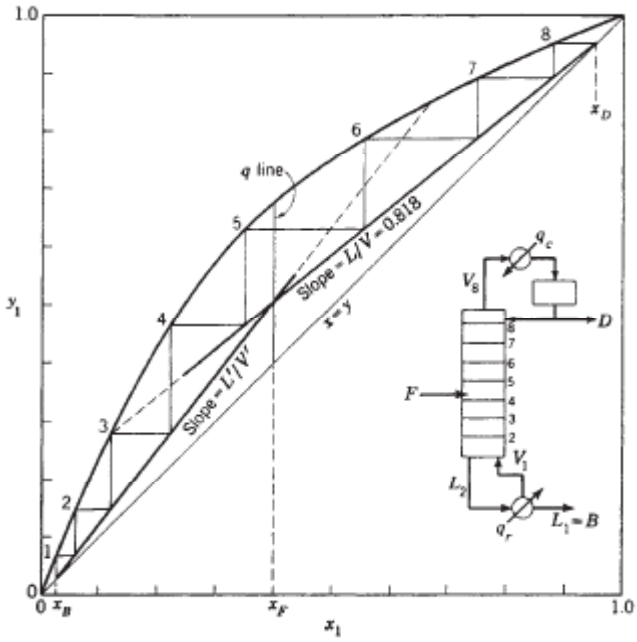

Figure 4.3: An example of the McCabe-Thiele graphical solution method (Perry & Green, 1997: 13-31).

4.3. Binary Batch Distillation with Constant Distillate Composition and Variable Reflux

Another option for designing a batch distillation column is by varying the reflux and keeping the distillate composition constant. For this purpose, a complex control systems will be required as well as online composition analysis equipment. Seader and Henley (2006: 688 – 689) show a method using the McCabe-Thiele diagram to solve this scenario when it is assumed that the liquid holdup is negligible and constant molar overflow is valid. Equation 4.5 can be rearranged for W as a function of x_W, when x_D is constant:

$$W = W_0 \left(\frac{x_D - x_0}{x_D - x_W}\right) \tag{4.6}$$

As W and x_W will vary over time, it can be differentiated in respect of time (t):

$$\frac{dW}{dt} = W_0 \frac{(x_D - x_0)}{(x_D - x_0)^2} \frac{dx_W}{dt} \tag{4.7}$$

Because constant molar overflow is assumed to be valid, the rate of distillation is given by the rate at which the feed mixture is lost from the still pot:

$$-\frac{dW}{dt} = (V - L) = \frac{dD}{dt} \tag{4.8}$$

D refers to the total accumulated distillate, not to the distillate rate. L is the liquid rate in the column. Equation 4.8 can now be substituted into Equation 4.7 and be integrated:

$$t = \frac{W_0(x_D - x_0)}{V} \int_{x_{W_t}}^{x_0} \int \frac{dx_W}{\left(1 - \frac{L}{V}\right)(x_D - x_W)^2} \tag{4.9}$$

L/V is the reflux ratio. This equation, with known, or selected, values for W_0, x_0, x_D and *V* can now be solved by graphical integration to determine the time required for the distillation or for estimating the number of theoretical stages.

The McCabe-Thiele method used in these solutions can only be used with binary systems. A different approach must be used for multicomponent scenarios in order to design or simulate the operation of a column.

4.4. Multicomponent Batch Distillation with a Constant Reflux

Several authors (Diwekar &Mudhaven, 1991; Sundaram &Evans, 1993) have developed shortcut methods based on the Fenske-Underwood-Gilliland (FUG) method used for continuous distillation. The solution methods these authors use break down the batch distillation into time segments, solving each segment as a continuous distillation column. Other developed models take an in-depth look at the batch distillation. These models perform stage-by-stage calculations, taking the energy balance into consideration as well. The distillation time is also split up into time segments and solved as continuous distillation columns. Temperature and composition profiles are calculated throughout the column for each time segment.

4.4.1. Shortcut Method

Sundaram and Evans (1993) developed their model to describe the behaviour of a column with a constant reflux. Starting their model with an overall mole balance:

$$-\frac{dW}{dt} = D \tag{4.10}$$

Therefore

$$-\frac{dW}{dt} = \frac{V}{1+R} \tag{4.11}$$

An instantaneous mole balance for any component, *i*, can be completed next:

$$\frac{d(x_{W_i} W)}{dt} = x_{D_i} \frac{dW}{dt} \tag{4.12}$$

The left-hand side (LHS) of Equation 4.12 can now be expanded and solved for dx_{Wi}:

$$dx_{W_i} = (x_{D_i} - x_{W_i}) \frac{dW}{W} \tag{4.13}$$

Equations 4.11 to 4.13 can now be solved by numerical integration methods if the value of x_{D_i} is known for each time step used in the integration. Using total reflux as a starting condition for the column, the values for $x_{D_i}^{\ 0}$ can be calculated for the known values of $x_{W_i}^{\ 0}$ with the Fenske equation, solved here for x_{D_i}:

$$x_{D_i} = x_{W_i} \frac{x_{D_r}}{x_{W_r}} \alpha_{i,r}^{N} \tag{4.14}$$

where *r* is an arbitrary reference component of the mixture, α is the relative volatility of the components and N is the number of plates. The constraint that x_{D_i} should add up to 1 can be incorporated into Equation 4.14:

$$x_{D_r} = \frac{x_{W_r}}{\sum_i x_{W_i} \alpha_{i,r}^{N}} \tag{4.15}$$

The next time-step calculations require a new value of x_{D_i} since the column is no longer running at total reflux. The FUG method can be applied to find these values for x_{D_i} at each time step. Seader and Henley (2006: 693) show an approximate equation for the Gilliland correlation:

$$\frac{N-N_{min}}{N+1} = 0.75\left[1 - \left(\frac{R-R_{min}}{R+1}\right)^{0.5668}\right] \tag{4.16}$$

The Class I Underwood equation can be used for the estimation of the reflux ratio. This Class I equation assumes that all of the components will be found in the distillate as well as the bottom product:

$$R_{min} = \frac{\left(\frac{x_{D_1}}{x_{W_1}}\right) - \alpha_{1,c}\left(\frac{x_{D_c}}{x_{W_c}}\right)}{\alpha_{1,c} - 1} \tag{4.17}$$

where subscript *1* refers to the lightest component and subscript *c* to the heaviest component. Equation 4.14 and Equation 4.15 can now be substituted into Equation 4.15:

$$R_{min} = \frac{\alpha_{1,c}^{N_{min}} - \alpha_{1,c}}{(\alpha_{1,c} - 1)\sum_i x_{W_i} \alpha_{1,c}^{N_{min}}} \tag{4.18}$$

For the selected values of N and R, N_{min} and R_{min} can be solved simultaneously by iteration. From these values x_{D_c} is solved with Equation 4.15, assuming $N_{min} = N$, followed by the solving Equation 4.14 to collect the values of x_{D_i}.

This method is not sufficient if a full temperature and composition profile throughout the column is needed. A rigorous model that assumes equilibrium stages inside the column can give a better description of the behaviour in the column.

4.4.2. Rigorous Model

Several rigorous models have been developed for multicomponent batch distillation. Distefano (1968), Boston, Britt, Jirapongphan and Shah (1981) and Galindez and Fredenslund (1988) all based their solutions and expansions on a rigorous model described by Meadows (1963). These models are described in detail by Mujtaba (2004: 74 - 84). Boston *et al.* (1981) suggest a more efficient way of solving the rigorous model; Galindez and Fredenslund (1988) suggest a rapid solution method that utilizes a quasi-steady-state solution procedure. The following assumptions are used in the rigorous model:

- The column contains theoretical equilibrium stages
- Perfect mixing between the liquid and vapour phases occurs at each stage
- The vapour holdup in the column is negligible
- There is a constant molar liquid holdup (M) at each stage and in the condenser
- There is negligible heat loss from the column
- The stages are adiabatic

Figure 4.3 shows the equipment used in the model suggested by Distefano. The column has a partial reboiler and a total condenser with a reflux drum. The model is based on a column that is started at full reflux. Due to the liquid holdup at the stages, the condenser and the

reflux drum, the composition of the liquid leaving the condenser will differ from the original content of the feed mixture.

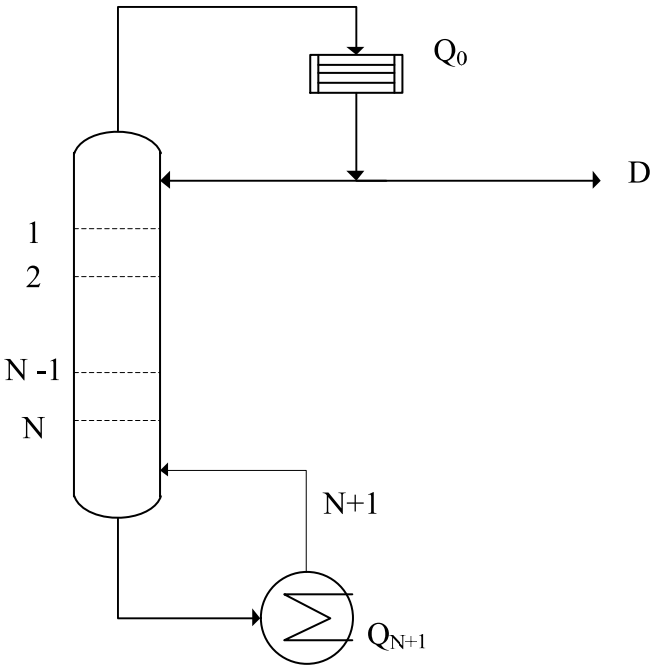

Figure 4.4: Batch rectification column with a total condenser.

Distefano changed the heat duty to the reboiler to maintain a constant reflux ratio and constant distillate rate. The model is broken down into three sections. Section I is the condensing system, Section II is the column stages and Section III is the reboiler system. All three systems and their boundaries are indicated in Figure 4.3. A component balance, overall material balance and an energy balance is set up across Section I:

$$V_1 y_{i,1} - L_0 x_{i,0} - D x_{i,D} = \frac{d(M_0 x_{i,0})}{dt} \tag{4.19}$$

$$V_1 - L_0 - D = \frac{dM_0}{dt} \tag{4.20}$$

$$V_1 h_{V_1} - (L_0 + D) h_{L_0} = Q_0 + \frac{d(M_0 h_{L_0})}{dt} \tag{4.21}$$

Due to the liquid holdup in the equipment, derivative terms appear in these balances. Phase equilibrium is also valid for Stage 1 of the column:

$$y_{i,1} = K_{i,1} x_{i,1} \tag{4.22}$$

These equations are now reworked to simplify the calculations by making sure the component balance is in terms of the liquid-phase compositions and by trying to eliminate the derivative term (dM_0/dt) from the equations. The model for all three sections can be completed by simplifying and eliminating the terms from the equations. Subscript i refers to the component and subscript j to the stage, so that $i = 1$ to C and $j = 1$ to N and M is the molar liquid holdup.

Component balances for the condensing section, column stages and reboiler, are respectively:

$$\frac{dx_{i,0}}{dt} = -\left[\frac{L_0+D+\frac{dM_0}{dt}}{M_0}\right]x_{i,0} + \left[\frac{V_1 K_{i,1}}{M_0}\right]x_{i,1} \tag{4.23}$$

$$\frac{dx_{i,j}}{dt} = \left[\frac{L_{j-1}}{M_j}\right]x_{i,j-1} - \left[\frac{L_j+K_{i,j}V_j+\frac{dM_j}{dt}}{M_j}\right]x_{i,j} + \left[\frac{V_{j+1}K_{i,j+1}}{M_j}\right]x_{i,j+1} \tag{4.24}$$

$$\frac{dx_{i,N+1}}{dt} = \left[\frac{L_N}{M_{N+1}}\right]x_{i,N} - \left[\frac{K_{i,N+1}V_{N+1}+\frac{dM_{N+1}}{dt}}{M_{N+1}}\right]x_{i,N+1} \tag{4.25}$$

where$L_0 = R/D$.

The total mole balances for the condensing section and column stages are respectively:

$$V_1 = D(R+1) + \frac{dM_0}{dt} \tag{4.26}$$

$$L_j = V_{j+1} + L_{j-1} + V_j - \frac{dM_j}{dt} \tag{4.27}$$

The enthalpy balances around the condensing section, adiabatic column stages and the reboiler are respectively:

$$Q_0 = V_1(h_{V_1} - h_{L_0}) - M_0\frac{dh_{L_0}}{dt} \tag{4.28}$$

$$V_{j+1} = \frac{1}{\left(h_{V_{j+1}}-h_{L_j}\right)}\left[V_j\left(h_{V_j}-h_{L_j}\right) - L_{j-1}\left(h_{L_{j-1}}-h_{L_j}\right) + M_j\frac{dh_{L_j}}{dt}\right] \tag{4.29}$$

$$Q_{N+1} = V_{N+1}(h_{V_{N+1}} - h_{L_{N+1}}) - L_N\left(h_{L_N} - h_{L_{N+1}}\right) + M_{N+1}\frac{dh_{L_{N+1}}}{dt} \tag{4.30}$$

Phase equilibrium at the column stages and the reboiler is given by:

$$y_{i,j} = K_{i,j}x_{i,j} \tag{4.31}$$

Mole fraction constraints on the column stages and the reboiler:

$$\sum_i y_{i,j} = \sum_i K_{i,j}x_{i,j} = 1 \tag{4.32}$$

Molar holdups in the condenser and the column stages are respectively:

$$M_0 = G_0\rho_0 \tag{4.33}$$

$$M_j = G_j\rho_j \tag{4.34}$$

where ρ is the liquid molar density (kmol/m^3) and G_j is the constant volume holdup.

The changing molar holdup in the reboiler is given by:

$$M_{N+1} = M_{N+1}^0 - \sum_j M_j - \int_0^t D dt = 1 \tag{4.35}$$

This model, Equations 4.23 to 4.35, forms an initial-value problem for a system of ordinary differential and algebraic equations. With the properties, G_j, liquid densities, vapour and liquid enthalpies and the K-values (either by prediction with property packages or by experimental data), a system with the number of equations equal to that of the unknown variables is described.

This model can easily be adapted to other system configuration by applying the same method of component balances, overall material balances and energy balances.

4.5. Column Sizing

The column can be sized once the required boilup rate and heat duties of the reboiler and condenser are known as well as the required number of equilibrium stages. Several ways of estimating a column diameter have been suggested, mostly based on methods used for continuous columns and absorption columns (Seader & Henley, 2006: 325 – 334). Al-

Tuwaim and Luyben (1991) suggest a method for sizing the column diameter during the process of optimizing the column. Firstly, the capacity factor (CAP) is defined by Al-Tuwaim and Luyben (1991) as the total on-specification product produced per unit of time. The CAP is calculated by using the following equation and 0.5 hour (t_E) is added for the start-up and equilibration time:

$$\mathrm{CAP} = \frac{H_{B_0} - S_1 - S_2}{t_E + t_F} \tag{4.36}$$

where H_{B_0} is the initial charge to the still pot, S_1 and S_2 are the number of moles in each cut (more cuts can be added) and t_F is the total time required for the distillation. With the production rate (D) known and the boilup rate (V) known from the simulation of the model, the vapour flow rate required (V') can be calculated:

$$V' = \frac{VD}{\mathrm{CAP}} \tag{4.37}$$

The maximum allowable superficial vapour velocity (V_m) can be calculated with:

$$V_m = K_v \left[\frac{\rho_L - \rho_v}{\rho_v}\right]^{0.5} \tag{4.38}$$

where ρ_L is the liquid density,$\rho_v$is the vapour density in kg/m^{3}and K_v (m/s) is an empirical constant related to the velocity of the vapour and the tray spacing. Next the minimum column diameter can be estimated with the following equation:

$$D_{min} = 2\left[\frac{(MW)V'}{\rho_v \pi V_m}\right]^{0.5} \tag{4.39}$$

where MW is the molecular weight of the vapour phase. A diameter larger than this should be selected for the column design.

The column height must be specified next. The height of an equilibrium stage will depend on the type of column being used, either a packed column or a plate column. Height equivalent estimations can be made for each type of column. Columns consisting of trays use a Height Equivalent to Theoretical Plate (HETP) value to calculate the height of the column. The HETP value is dependent on the type of tray as well as on the tray spacing used in the column. Tray spacing is the distance between to trays. The tray spacing can affect both the height of spray that may be generated on the tray deck and also the allowable head of liquid in

the downcomers. See Figure 4.5 below for an illustration of a tray. Packed columns use a Height of Transfer Unit (HTU) to calculate the column height. This value is dependent on the type of column packing as well as on the spacing between the packing. The HTU is a value based on the hydrodynamics of the fluid moving through the specific value and is usually supplied by the supplierbased on experimental work. This is multiplied by the theoretical number of plates required according to the thermodynamic model used to predict the separation in the column. The final column height takes both hydrodynamic and thermodynamic behaviour into consideration for a design.

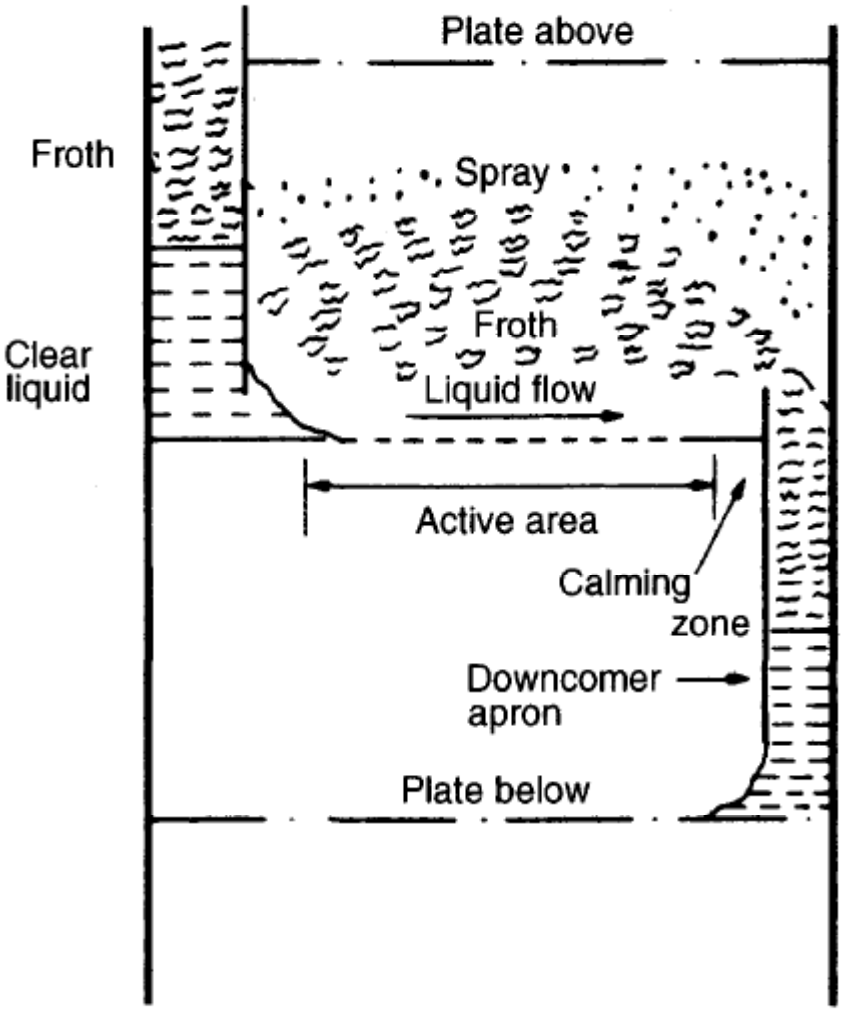

Figure 4.5: Illustration of a column plate (Sinnott: 2005:558).

Chapter 5

Experimental Apparatus and Methods

5. Experimental Apparatus and Methods

The experimental VLE measurements were taken on a static-analytical steel apparatus capable of operating at temperatures up to 473 K and pressures up to 10 MPa. The apparatus used was designed and constructed by Malumba Tshibangu (Tshibangu, 2010). Tshibangu (2010) gives a detailed description of the apparatus and associated equipment. Figure 5.1 shows a schematic diagram of the apparatus and all the equipment needed. The apparatus consists of the following elements and is discussed in this chapter:

- 316 stainless-steel equilibrium cell
- Movable ROLSI™ sampler
- 2 Pt-100 temperature probes
- P-10WIKA pressure transducer
- Heidolph Model RZR 2021 mechanical stirrer with a chain drive system connected to a magnet
- Shimadzu 17-A gas chromatograph
- Series of lines and valves to transport materials
- 6-port gas chromatograph valve
- A standard vacuum pump
- Liquid bath with a Grant Optima GR150 temperature controller
- Polyscience immersion coolers
- A personal computer to record data

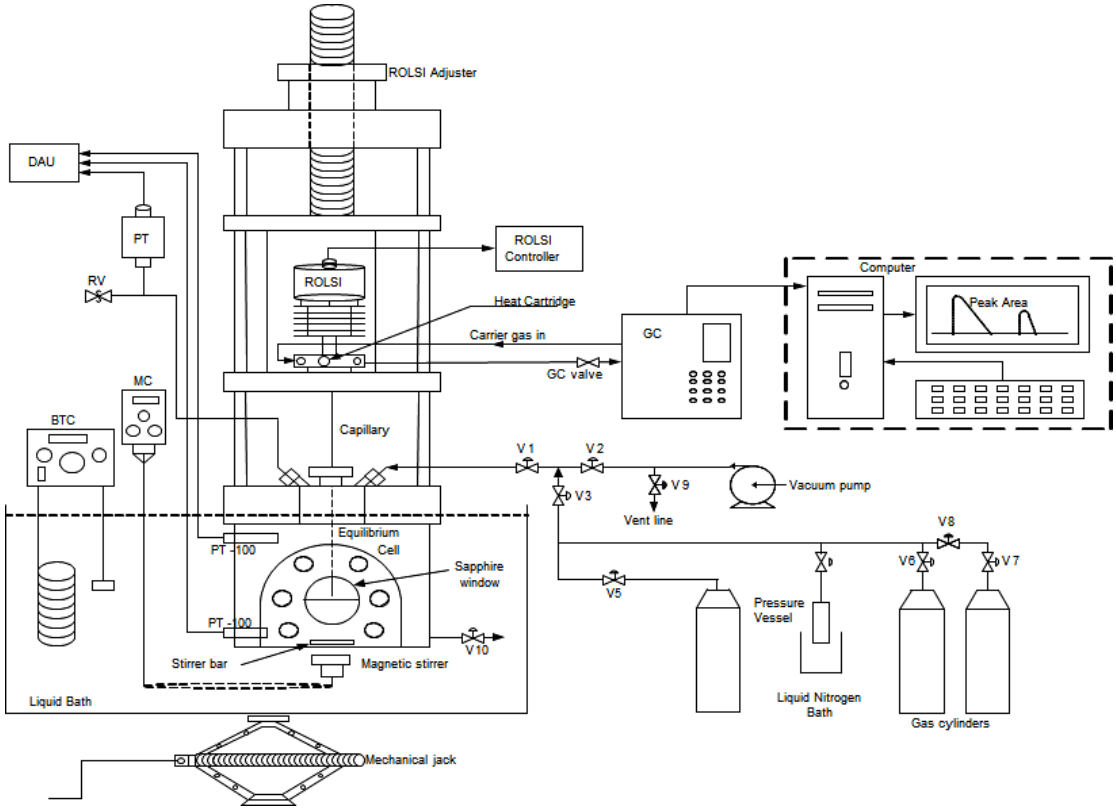

(BTC – bath temperature controller, DAU – data acquisition unit, GC - gas chromatograph, MC – mechanical circulatory, PT – pressure transducer, RV – relief valve, Vi – valve).

Figure 5.1: Schematic diagram of the static-analytic VLE apparatus.

5.1. Equilibrium Cell

The equilibrium cell is constructed from machined 316 stainless steel with a volume of 60 cm^3. The cell is tube-like and oriented vertically, with an internal diameter of 30 mm and a height of 85 mm. Two sapphire windows, each with a diameter of 33 mm and a thickness of 14 mm, allow the observation of the fluid behaviour in the cell. The window flanges, as well as the top and bottom flanges of the cell, are tightened with bolts and sealed with Viton O-rings. Two separate wells, one in the top and one in the bottom flange of the cell, allow temperature measurements to be taken with Pt-100 probes.

A small magnet used for stirring is enclosed inside the cell. The chain drive system, with the variable speed drive (VSD), turns a magnet directly underneath the equilibrium cell to ensure effective mixing inside it. A Heidolph Model RZR 2021 mechanical stirrer is used to turn the magnet. The stirrer has two gear-speed settings which range from 40 to 400 rpm and 200 to 2000 rpm.

There is a small line and valve at the bottom of the cell to drain the liquid contents from the cell. Two small 1/16″ lines are connected to the top flange, where the one line is connected to the pressure transducer. The other line is connected to the feed cylinders and the vacuum pump. At the top of the cell is a small inlet for the capillary tube of the ROLSI™. The inlet is sealed with a series of O-rings, allowing the capillary tube to move up and down.

The ROLSI™ and its capillary tube are connected to a steel plate with two lines flowing to and from the 6-port gas chromatograph (GC) valve. A heating cartridge is also fitted inside the steel plate to ensure that the sample from the cell is over-heated and does not condense to form any blockages in the lines. Again 1/16″ lines are used to transport the sample to and from the GC. The ROLSI™ and the steel plate can be moved up and down, allowing sampling in the liquid phase and the vapour phase with the capillary, depending on the liquid level in the cell.

The 1/16″ inlet line, used to measure the pressure, is connected to a 1/8″ line that connects to a Swagelok pressure relief valve set at 30 bar and the pressure transducer.

The lines connected to the GC and the pressure transducer are wrapped with heating wire, controlled by a variable voltage transformer. Pt-100 probes are used to measure the temperature of the lines, the steel plate around the ROLSI™, the heating block for the pressure transducer and the heating block of the 6-port valve. The lines are heated to above the boiling point of the materials to prevent condensation inside the lines. The lines are insulated with fibreglass wool to minimize heat loss from the lines. The insulation wool is wrapped in aluminium foil to aid insulation and to protect operators from burns.

The cell is loaded by either injecting liquid (the heavier component) or by using a constant volume press to create a high-pressure difference between the press and the cell. TFE is loaded by freezing and then liquefying the TFE to create a high-pressure difference based on the high vapour pressure of TFE at room temperature.

5.2. Liquid Bath

The temperature of the equilibrium cell is controlled by lowering the cell into a liquid bath. The dimensions of the bath are 40 x 30 x 23 cm, giving a volume of about 28 litres. The

walls of the bath are packed with insulation to prevent heat loss to the environment. Different liquids were used to control the bath temperatures at specific operating conditions: ethylene glycol was used for the test system and water was used in the bath for the HFP and OFCB system, operating between 20 and 80 °C. The ethylene glycol is too volatile at the higher end of the temperature range to ensure effective heat transfer to the equilibrium cell. Dynalene HC50®, produced by Dynalene Inc., was used for the other systems operating at lower temperatures.

Two temperature controllers were available, depending on the required temperature. The Grant Optima GR150 immersion circulator has an operating range of between -50 and 50 °C and the operating range of the second controller is between 0 and 100 °C. In addition to the circulation provided by the immersion temperature controllers, a separate circulation pump provided by Labfix was used to ensure proper circulation in the bath around the equilibrium cell. The circulation pumps minimize deviations in the temperature around the equilibrium cell. No extra temperature control is necessary in the liquid bath as the accuracy of the temperature is not as important as the stability of the temperature control.

As the temperature controllers can only heat the liquid, immersion cooling units were used to cool the liquid down to below room temperature. A Polyscience immersion cooling unit, with a temperature range of -45 to 40 °C, was used. The bath, which is open to the atmosphere at the top, was covered with polystyrene to minimize heat loss through the liquid surface. The bath was finally covered with polycarbonate sheeting to prevent heat loss.

5.3. TFE Handling

Due to the possible self-decomposition and auto-polymerization of TFE, special equipment and loading methods had to be used. The unique methods used to load and handle the TFE mitigate the risks surrounding TFE. However, even with special care, explosions are still possible.

All TFE cylinders are filled up to only 1.8 bar (abs) to ensure safe transport and storage.

One way of mitigating the risks of working with pure TFE at high pressures is to work with a very small quantity at a time. A small quantity of TFE has less explosive power than a larger

quantity. The equilibrium cell windows are protected by a polycarbonate shield to mitigate the danger of shrapnel should an explosion occur.

Figure 5.2 shows a diagram of the extra equipment used to load the TFE for experimental work. This equipment was assembled by Necsa. The 1-litre vessel is used to measure a set quantity of TFE from the loading cylinder. This set quantity of TFE is then frozen in a 10-cm^3 pressure vessel, by lowering it into a liquid nitrogen bath. This small cylinder conforms to normal standards for a pressure vessel and can operate safely at pressures up to 10 MPa.

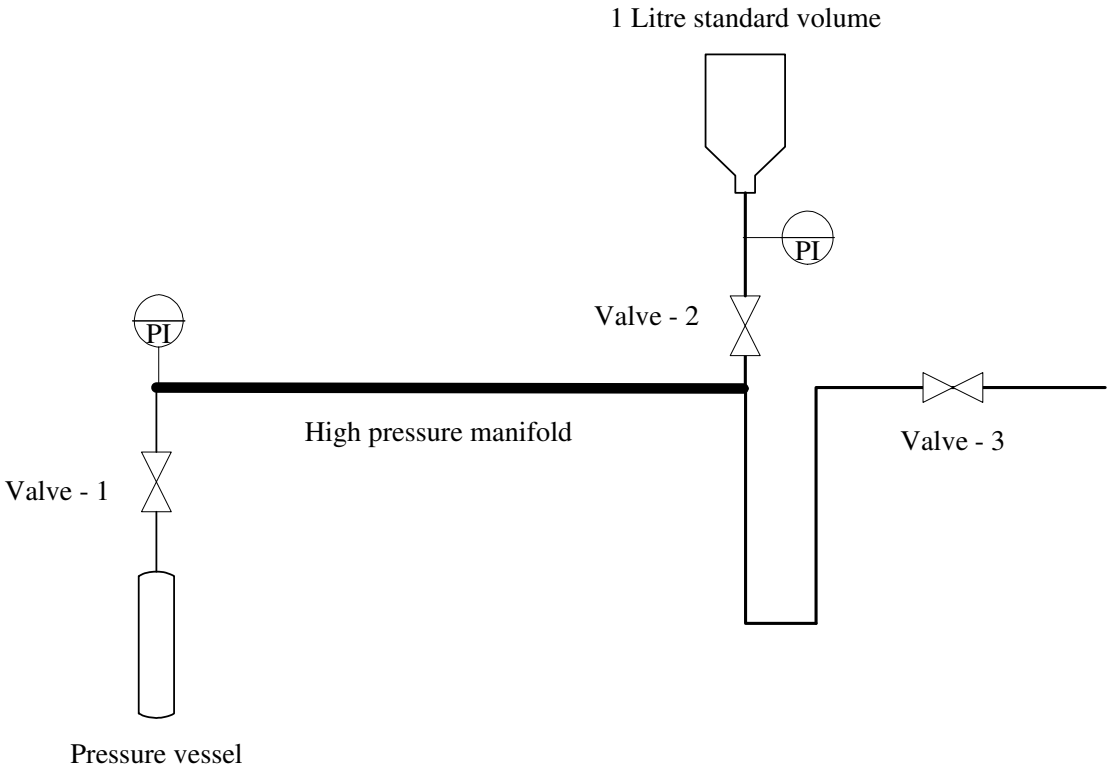

Figure 5.2: Diagram of the equipment used to load TFE safely in the equilibrium cell.

The 1-liter vessel is closed off when the pressure in the vessel no longer falls, i.e. when all the TFE is frozen in the small vessel. To ensure the TFE is pure and free of impurities, the small vessel is opened to the vacuum pump to remove any volatile impurities. From this point, the liquid nitrogen is removed and the small vessel is allowed to heat up to room temperature. The increase in temperature will melt the TFE and create a liquid-vapour interface inside the small vessel. The high vapour-pressure of TFE creates a pressure difference large enough to transfer the TFE to the equilibrium cell.

5.4. Measurement and Control

5.4.1. Temperature

The two platinum resistance thermometer probes (Pt-100 sensors) are situated at the top and bottom flanges of the equilibrium cell and are used to measure the cell temperature. The temperature of the liquid bath is measured and controlled by the immersion circulator. As mentioned earlier, Pt-100 probes were also used to measure the temperature of the lines and heating blocks on the pressure transducer and 6-port valve.

The Pt-100 probes are calibrated against a reference thermometer (CTH – 6500, manufactured by WIKA). The reference thermometer was calibrated by WIKA during production and is certified to have an accuracy ± 0.03 K. WIKA classifies the Pt-100 probes as Class A, with an accuracy of 0.1 K. The calibration is done three times over the temperature range, with two runs from the highest to the lowest temperature and one run from the lowest to the highest temperature to ensure the repeatability of the calibration process. The calibration was done from 243 K to 323 K.

ACS-13A digital indicating controllers, supplied by Shinko, are used to control the temperatures of the heating wire and the heating cartridges of the system. The temperatures measured by the Pt-100 probes are used as an input into the controller. The controller will then either allow more current to heat up the heating wire to the higher temperature or will allow the wire to cool down.

5.4.2. Pressure

A 10 MPa WIKA pressure transducer (model P 10) is used for pressure measurements. The pressure transducer is calibrated against a reference transducer (CPT 6000, WIKA) previously calibrated by WIKA. It is certified as being accurate to within 0.025 %. The calibration is done two times over the pressure range, with one run from the highest to the lowest pressure and one run from the lowest to the highest pressure to ensure the repeatability of the calibration process. The heating line to the pressure transducer is heated to prevent condensation in the line. If condensation does occur, a new vapour-liquid equilibrium point could be created in the line, giving a false reading on the pressure transducer (Ramjugernath, 2010a).

5.4.3. Sampling

Samples are taken from the equilibrium cell by the ROLSI™ sampler. The ROLSI™ was designed by the TEP (Thermodynamique des Equilibres des Phases) laboratory of Mines Paristech (Guilbot, Valtz, Legendre and Richon, 2000). A solenoid electromagnet can open and close the opening to the capillary tube in very short bursts. Each time the ROLSI™ is opened, some of the sample, either liquid or vapour, will flow up the capillary tube into the lines flowing to and from the 6-port valve. The pressure difference between the helium in the lines flowing to the GC and the equilibrium cell enables the sample to travel up the capillary. The very small diameter of the capillary tubes limits the ROLSI™ to taking very small samples at a time. The advantage of such small samples is that the equilibrium in the cell will be barely influenced.

The 6-port valve can switch between two flow pattern settings. On the first setting, helium will flow from the GC through the ROLSI™, collecting the sample and then flowing back through the valve to the GC. On the same setting, the lines flowing to the vacuum pump are closed off to the rest of the loop. The second setting closes the GC off from the ROLSI™ loop. The lines flowing to the ROLSI™ are now open to the vacuum pump so that unwanted impurities can be cleaned from the lines.

The opening time of the ROLSI™ is controlled by a Crouzet Timer Top 948 controller. It sends electrical signals to the solenoid valve to open and close it. The controller has time ranges from 0.01 seconds to 9999 hours.

5.4.4. Composition Analysis

The samples are analysed by a Shimadzu G-17A gas chromatograph (SHIMADZU - G-17A). It can be interlinked to operate with a Thermal Conductivity Detector (TCD). Porapak Q columns were used in the experimental work; different columns and operating conditions were used for different systems. The columns were operated between 388 K and 503 K with a helium flow rate of about 30 ml per minute. The TCD was maintained at temperatures between 388 K and 523 K with a current of 50 mA.

The calibrations were done by repeated injections of known amounts of each pure compound, using either a gas-tight or liquid syringe. For the test system (ethane and propanol), the propanol was diluted with methanol to calibrate the low propanol concentration region. The calibrations for each system had to be repeated several times owing to delays and power

failures. The calibrations were redone because the TCD shows a different analysis after a temperature change or power failure.

5.4.5. Data Acquisition

The temperatures measured by the Pt-100 probes, the pressures measured by the WIKA pressure transducer and the GC analysis were all recorded on the same personal computer. The pressure and temperature readings were recorded *via* the computer linked to an Agilent Data Acquisition Unit (34970A) and the Benchlink Data Logger (Agilent Technologies, v3.0.4). Figure 3.3 shows the user interface of the Benchlink Data Logger, recording the temperatures of the Pt-100 probes and the pressure. GC Solution Analysis, v2.30.00, was used to record the composition analysis data. The GC Solution Analysis also serves as an interface to program the temperatures of the injector, column and detector. Figure 5.3 shows the user interface for programming the GC and Figure 5.4 shows the resulting peaks from several samples taken from the equilibrium cell.

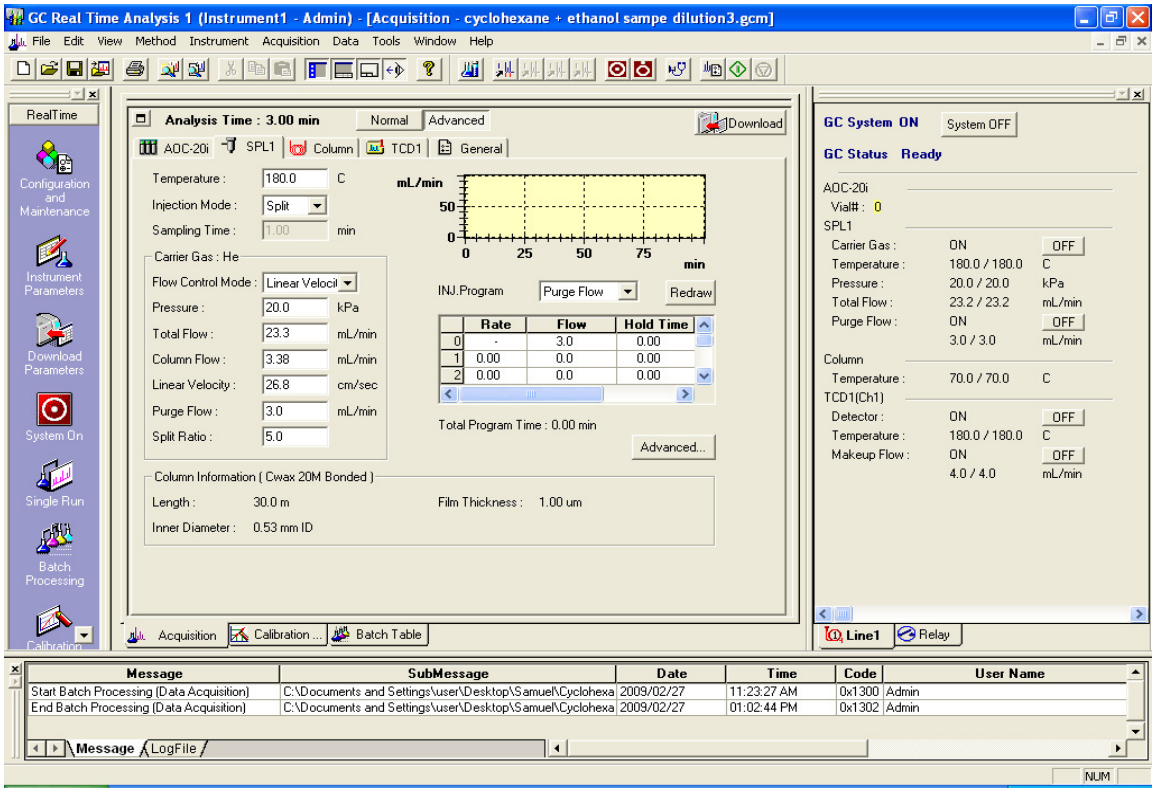

Figure 5.3: The user interface of GC Solution Analysis to program the operating conditions.

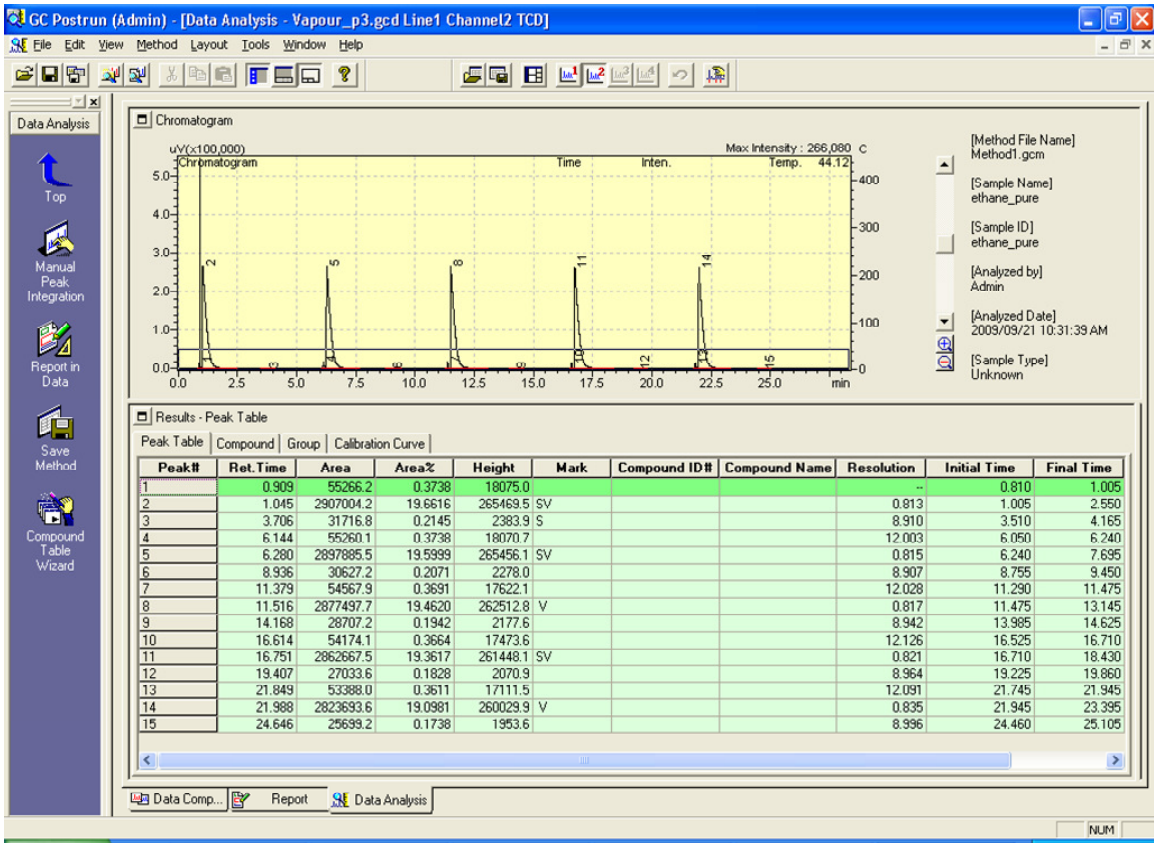

Figure 5.4: A sample analysis from the vapour phase of the ethane – 1-propanol system.

5.5. Experimental Planning

In the experiments, four variables were measured for each point in the VLE curve. As the experiments were isothermal, the temperature for each isotherm was set for each system. The pressure, temperature, liquid phase composition and vapour phase composition were recorded for each VLE point.

The average temperature for the isotherm is calculated from the temperatures of each recorded VLE data point. The data are then used to fit the experimental points to a thermodynamic model.

A test system had to be complete in order to compare the accuracy of the equipment and experimental work to the data available in the literature. A survey was done of the available materials in the laboratory for the test system, as well as the VLE data in the literature on those materials to find a suitable test system. Of the available materials that give high pressures in the range of the fluorocarbon systems, only ethane and propanol fell in the target

ranges set for the test system. In the literature search, several literature sources tested for this specific system at or close to 313 K (Jime'nez-Gallegos, Galicia-Luna, Bouchot, Camacho-Camacho & Elizalde-Solis, 2006; Kodama, Tanaka & Kato, 2001; Suzuki & Sue, 1990).

5.6. Experimental Methods

5.6.1. Preparations

The first step in the experimental work is to do calibrations for the temperature, pressure and composition readings. The calibration method for each variable is described in the previous section. The calibrations should be repeated after the experimental work to ensure that they remain in the same uncertainty range.

The next step before starting a system of isotherms is to ensure that the equilibrium cell and all associated lines are clean and void of any impurities, including air. The cell and lines are left under vacuum for several hours to remove any impurities from the system.

5.6.2. Loading of Heaviest Component

Once the cell is clean and under vacuum, the liquid bath is cooled to just below room temperature. The heaviest component is loaded first. For the test system, propanol liquid is injected straight into the cell with a syringe and for the other systems, either HFP or OFCB is condensed in the cell from the storage cylinders. Just over half of the cell is filled with liquid.

Agitation is started at this point. The speed is set so that enough agitation takes place inside the cell. The variable speed drive is set to operate between 300 and 500 rpm. The cell is opened repeatedly to the vacuum pump to degas the heavy component of any light impurities. The pressure is checked each time when the cell is opened and closed, to see whether it returns to the same pressure. If the pressure is the same within the calibration uncertainty, it is assumed that the heavy component is degassed and void of impurities.

The bath temperature is now set to the temperature specific to each isotherm. The necessary immersion cooling units are switched on to cool down the liquid in the bath. If the pressure and temperature remain constant for about 10 minutes, the pressure and temperature are recorded as well as the vapour-pressure value for the heaviest component.

5.6.3. Loading of the Light Component

The light components are loaded onto the heavy component, increasing the pressure step by step for each VLE point. Ethane and HFP are compressed, in a constant volume press with a pressure indicator, to pressures above that of the equilibrium cell. The cell is loaded by means of this pressure difference. The TFE is frozen in the small pressure vessel with a liquid nitrogen bath and thawed. Once the pressure is higher than that of the equilibrium cell, the TFE is loaded in the cell. Once the lighter component has been loaded into the cell, it is left to reach equilibrium. It is assumed that equilibrium is reached once the temperature and pressure remain constant, within the calibration uncertainty range, for about 10 minutes.

Once equilibrium has been reached, the pressure and temperature are recorded for the equilibrium point. Samples are taken from the liquid and vapour phases and analyzed in the GC. A minimum of 5 repeatable samples are taken from each phase.

5.6.4. Completion of an Isotherm

Next, more of the light component is added to the cell. Should the liquid level in the cell rise too high, some of the liquid is purged through the bottom valve. When the heavy component mole fraction is on the edge of the calibration range, the system is assumed to be completed.

When an isotherm is completed, the cell is emptied into the special building ventilation system that purges the gas into the atmosphere above the buildings. The vacuum pump is switched on and opened to the system to remove any leftover materials.

Chapter 6

Results and Discussions

6. Results and Discussions

6.1. Temperature and Pressure Calibrations

6.1.1. Temperature Calibrations

The temperature calibration for the two Pt-100 probes, situated in the equilibrium cell, was done simultaneously. The Pt-100 probes were placed in a small silicon oil temperature bath that can operate from 243 K to 373 K. Figure 6.1 shows the calibration curve for the probe situated in the bottom flange of the equilibrium cell, numbered 108, which is the same as the display on the Benchlink data logger interface. The residual plot for the standard error in the calibration range is shown in Figure 6.2. The maximum error for the calibration is ± 0.1 K and is assumed to be the uncertainty in further calculations. The linear calibration equation for the temperature probe 108 is:

$$T_{actual} = 0.9982T_{displayed} - 0.7502 \quad (6.1)$$

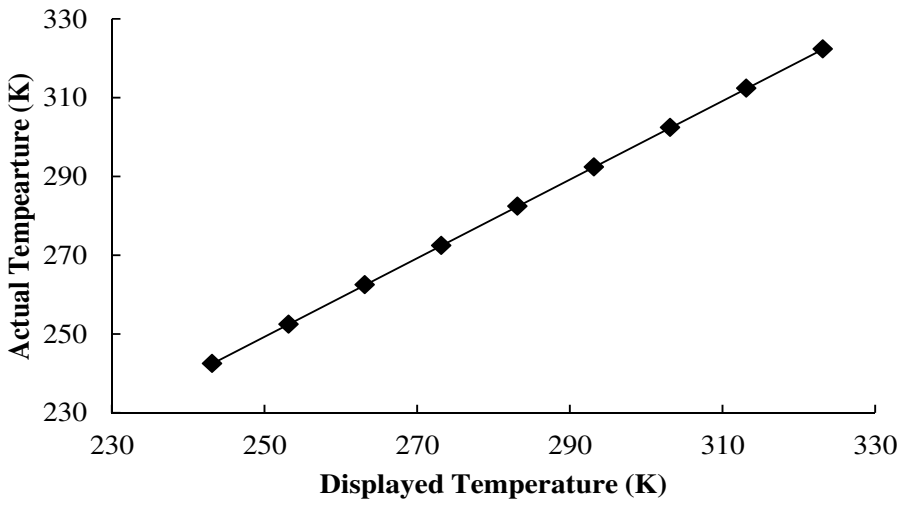

Figure 6.1: Linear temperature calibration for the 108 temperature probe.

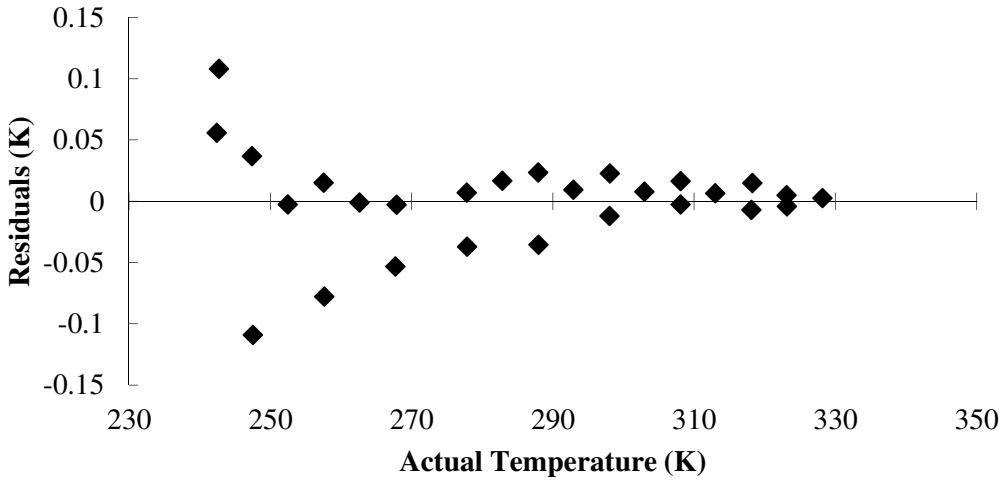

Figure 6.2: Residuals plot for the calibration for probe 108.

Figure 6.3 shows the calibration curve for the probe situated in the top flange of the equilibrium cell, numbered 107, which is the same as the display on the Benchlink data logger interface. The residual plot for the calibration set is shown in Figure 6.4. The maximum error for the calibration is ± 0.1 K. The uncertainty for probe 107 is assumed to be 0.1 K. The linear calibration equation for the 107 temperature probe is:

$$T_{actual} = 0.9986T_{displayed} - 0.5794 \tag{6.2}$$

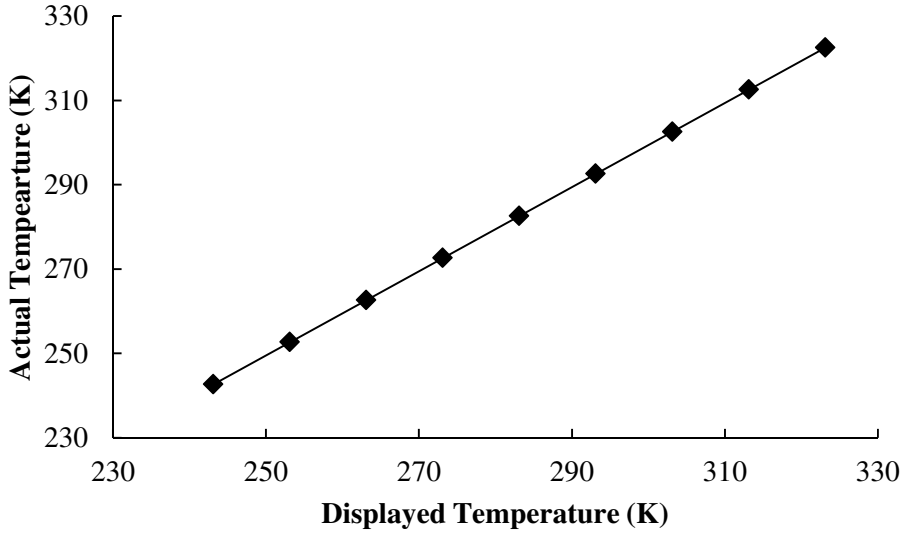

Figure 6.3: Linear temperature calibration for the 107 temperature probe.

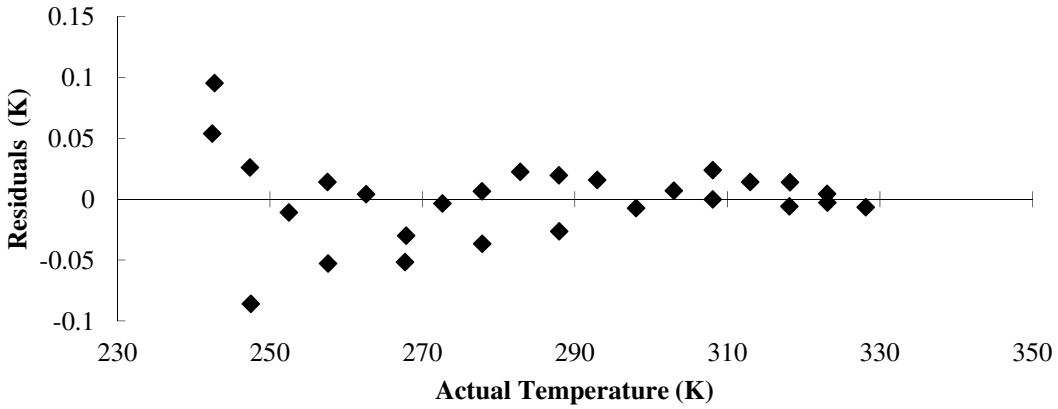

Figure 6.4: The residual plot for the calibration of probe 107.

The temperature calibration was checked at the end of the experimental work, to ensure that the calibrations were still within the uncertainty limits. This was required because of the long duration of the experimental work, several power failures and changes in the experimental configurations. The second set of temperature calibrations was still within the uncertainty limits of the first set of calibrations and was therefore used for all the experimental work.

6.1.2. Pressure Calibrations

The pressure calibration was done in three runs, two in an upward steps and one in a downward step. The pressure ranged from 3 bars to 60 bars. Figure 6.5 shows the calibration curve between the actual pressure and the displayed pressure. All pressures are reported as absolute pressures. The linear calibration equation for the pressure is:

$$P_{actual} = 1.0008P_{displayed} - 0.0648 \quad (6.3)$$

The residual plot between the actual pressure and the calculated pressure is shown in Figure 6.6. The pressure calibrations all fall within the uncertainty range of ± 15 mbars.

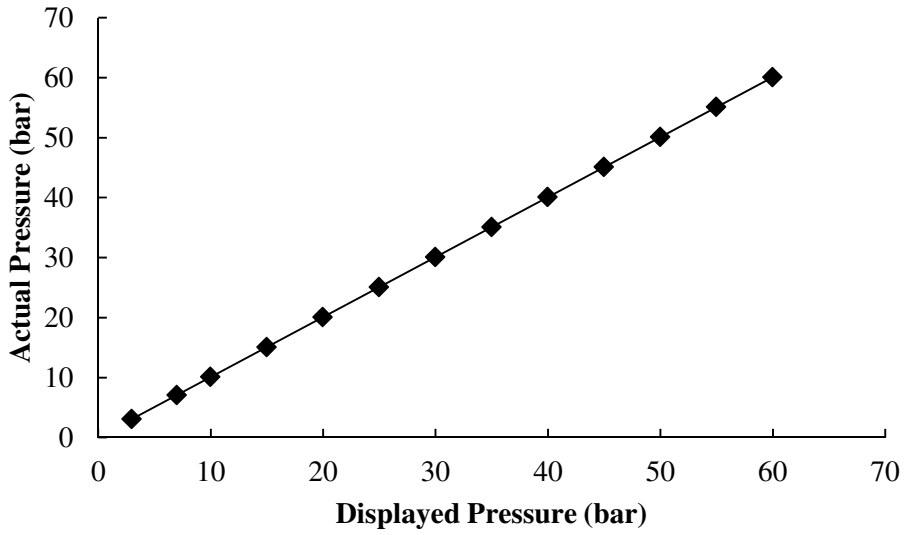

Figure 6.5: Linear pressure calibration for the pressure transducer.

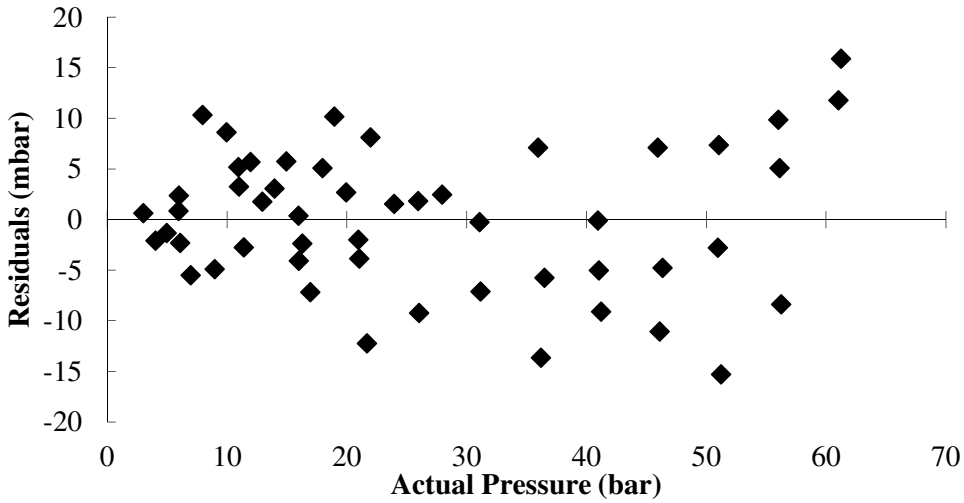

Figure 6.6: Residual plot for the pressure calibration.

A second set of pressure calibrations was done to confirm whether or not the calibration was still within an acceptable uncertainty range. The pressure range for the new set was between 0 and 25 bars. The calibration was not within acceptable limits and a new calibration set was used for the last set of isotherms. Table 6.1 summarizes the calibrations used for each system and isotherm. Figure 6.7 shows a linear equation for the second set of pressure calibrations. The residual plot for the second pressure calibration set is shown in Figure 6.8. Even though the equation changed, the uncertainty remained within 15 mbars. The linear equation for the pressure calibration is:

$$P_{actual} = 1.00084P_{displayed} - 0.00203 \quad (6.4)$$

Table 6.1: A summary of the pressure calibration set used per system.

System	Isotherm	Calibration set 1	Calibration set 2
Test	40	X	
TFE&HFP	-25		X
	-10	X	
	10		X
TFE& OFCB	-25		X
	-10	X	
	10		X
HFP & OFCB	20	X	
	50	X	
	80	X	

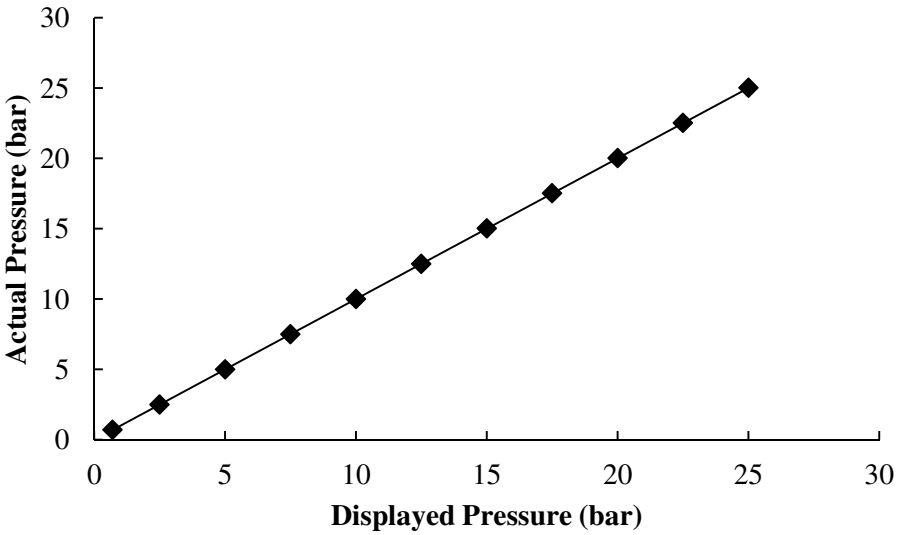

Figure 6.7: Second linear calibration for the pressure transducer.

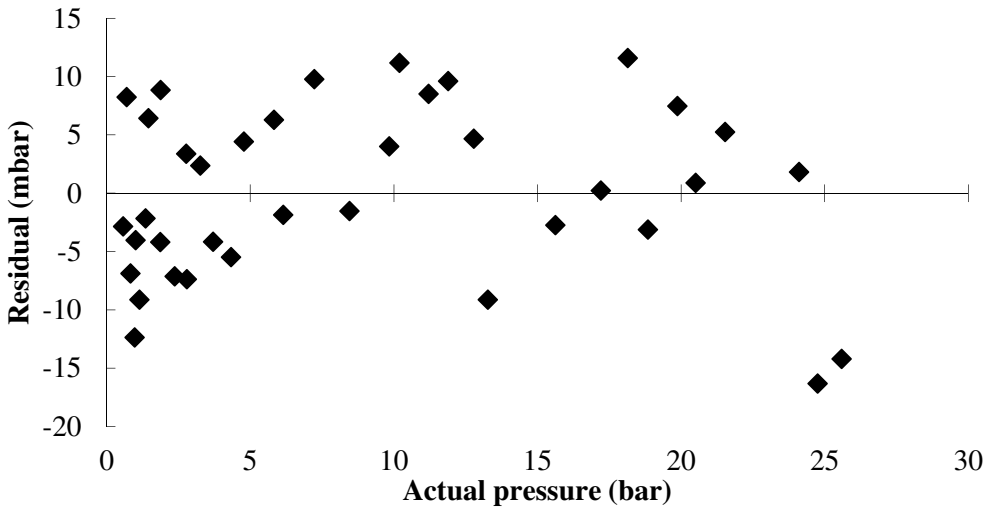

Figure 6.8: Residual plot for the second pressure calibrations.

6.2. Ethane + 1-Propanol Test System

The test system was evaluated at 313.15 K and pressures of up to 54 bars. Operating at higher pressure forced the system into a supercritical mixture, which fell beyond the scope of this investigation.

The operation conditions for the GC were set up to give an optimum separation between the ethane and 1-propanol peaks in the shortest time possible. The following setup was used for the GC:

- The injector was operated at 503 K and 200 kPa. The pressure was set to yield a flow rate of about 30 ml / min through the column.
- A Porapak Q column, 3 m in length and an internal diameter of 1/8", filled with 80/100 mesh, was operated at 503 K.
- The TCD detector was operated at 523 K and a current of 50 mA.

6.2.1 GC Calibrations for the Test System

The ethane calibration was done with repeated injections using a gas-tight syringe, with injection volumes ranging from 0.4 ml up to 2 ml. The mole quantity for each injection is calculated with the ideal gas law:

$$n = \frac{PV}{RT} \tag{6.5}$$

Figure 5.9 shows the calibration curve for the amount of ethane against the peak area of the GC. The best fit was found with a second-order curve. Figure 6.10 shows the residual plot between the actual amount of ethane and the predicted amount of ethane for each injection. The second-order equation for the calibration is:

$$n_{ethane} = 4.2107 \times 10^{-22} \times PeakArea^2 + 1.2008 \times 10^{-14} \times PeakArea + 7.1187 \times 10^{-10} \quad (6.6)$$

The ethane calibration range is between 1.3 x 10^{-8} mole and 8.8 x 10^{-8} mole. The uncertainty in the ethane calibration is about 1 %.

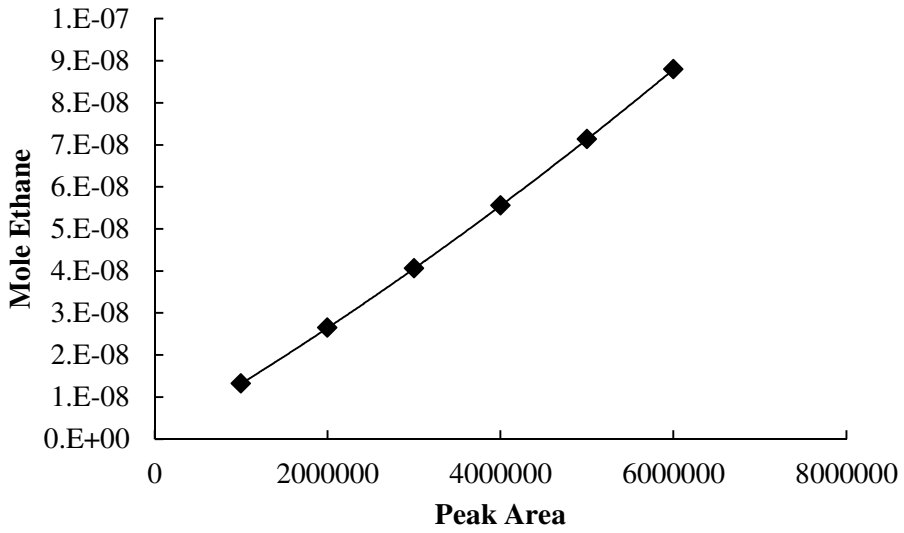

Figure 6.9: Second-order calibration curve for ethane.

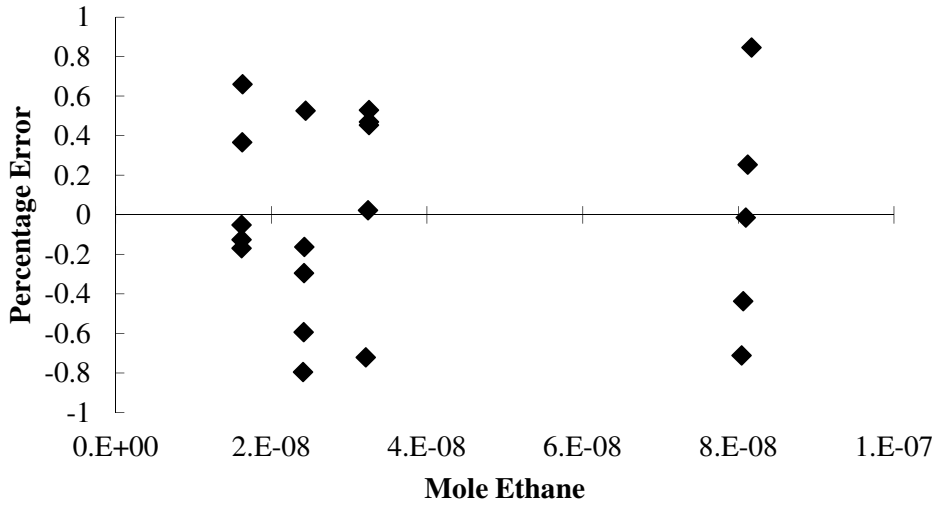

Figure 6.10: Residual plot for the second-order ethane calibration.

Liquid syringes were used for repeated sample injections for the 1-propanol calibrations. Liquid dilutions were made up with methanol for very small quantities of 1-propanol. Methanol separates well inside the GC column, so it is suitable for dilution. The amount of 1-propanol was calculated from the volume of 1-propanol that was injected, as the density for 1-propanol is known. Figure 6.11 shows the linear calibration curve for 1-propanol. The residual plot for the standard error in the calibration is shown in Figure 6.12. The error is large at the lowest concentrations, where mixtures were prepared for the injections. The linear equation that fits the 1-propanol calibrations is:

$$n_{ethane} = 9.1216 \times 10^{-15} \times PeakArea + 2.164 \times 10^{-10} \qquad (6.7)$$

To keep the calibration within acceptable uncertainty limits, the calibration range was limited to 2.5 x 10^{-9} to 1.3 x 10^{-8}.

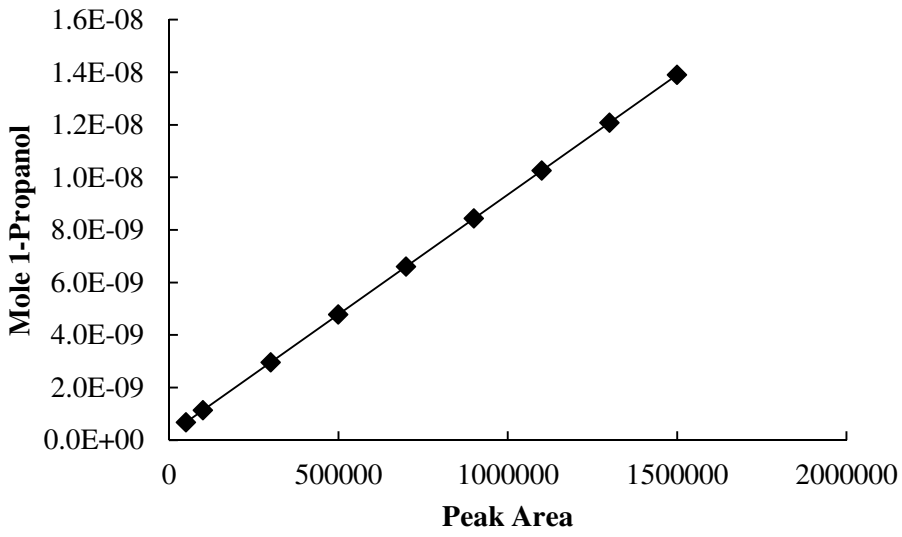

Figure 6.11: Linear GC calibration for 1-propanol.

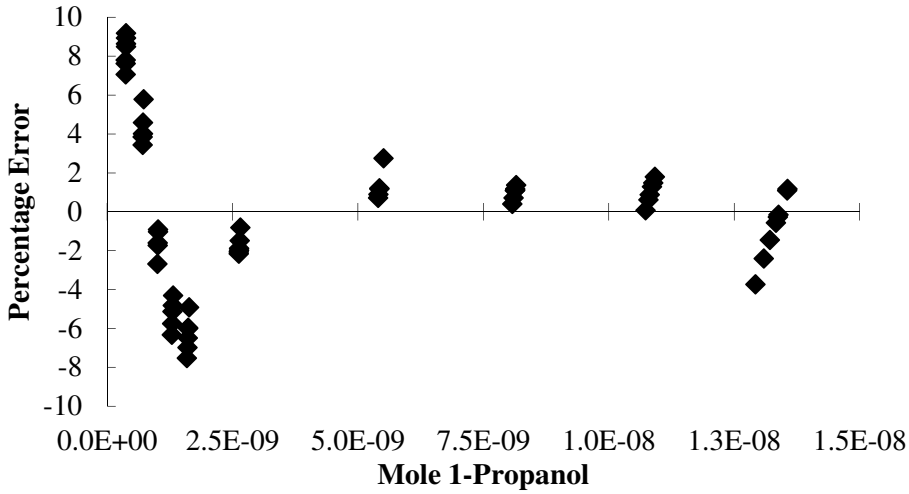

Figure 6.12: Residual plot for the standard errors on the 1-propanol calibrations.

6.2.2. Literature for the Ethane + 1-Propanol System

Two of the literature sources investigated the system at 313 K (Suzuki & Sue, 1990, Komada*et al.*, 2001), whereas Jime'nez-Gallegos *et al.* (2006) tested the system at 318 K. The data presented by Jime'nez-Gallegos *et al.* (2006) can be used for comparison even though it is at a slightly higher temperature, since the literature comparison is used solely to determine how accurately the experimental apparatus predicts the phase behaviour. Figure 6.13 shows the comparison between the literature sources for the liquid phase behaviour and Figure 6.14 shows the vapour phase behaviour as tested by the literature sources. The liquid phase composition for the lightest component in a system is symbolized by x_1.

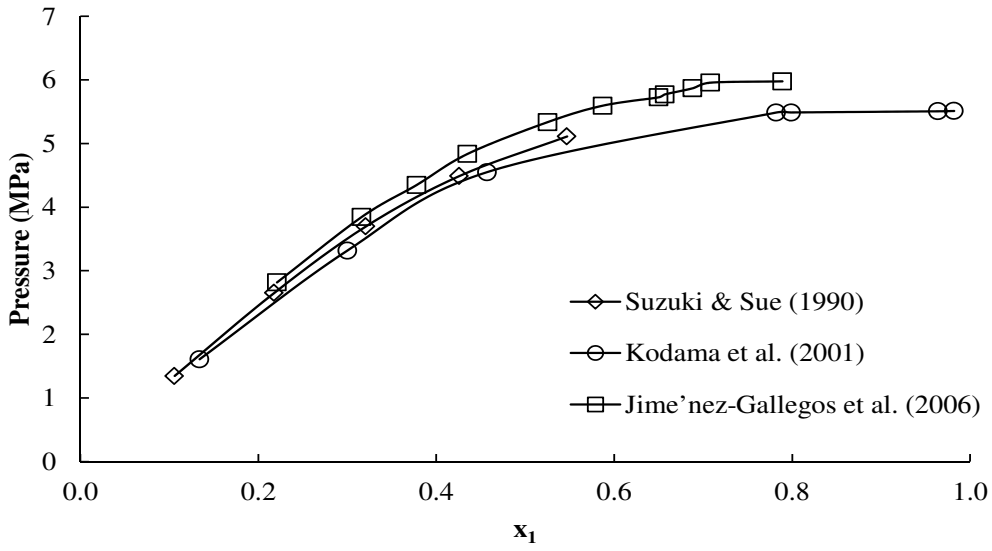

Figure 6.13: P-x diagram comparing the three literature sources for the ethane (1) + 1-propanol (2) system.

The P-x data obtained from the literature, compare fairly well with one another. The isotherm produced by Jime'nez-Gallegos *et al.* (2006) shows the same phase behaviour at slightly higher pressures, which is to be expected as the temperature is slightly higher than that described in the other two literature sources. The P-y data also compares fairly well. Strange behaviour is observed at the top end of curve, which can be attributed to the reaching the supercritical phase. The liquid phase composition for the lightest component in a system is symbolized by x_1.

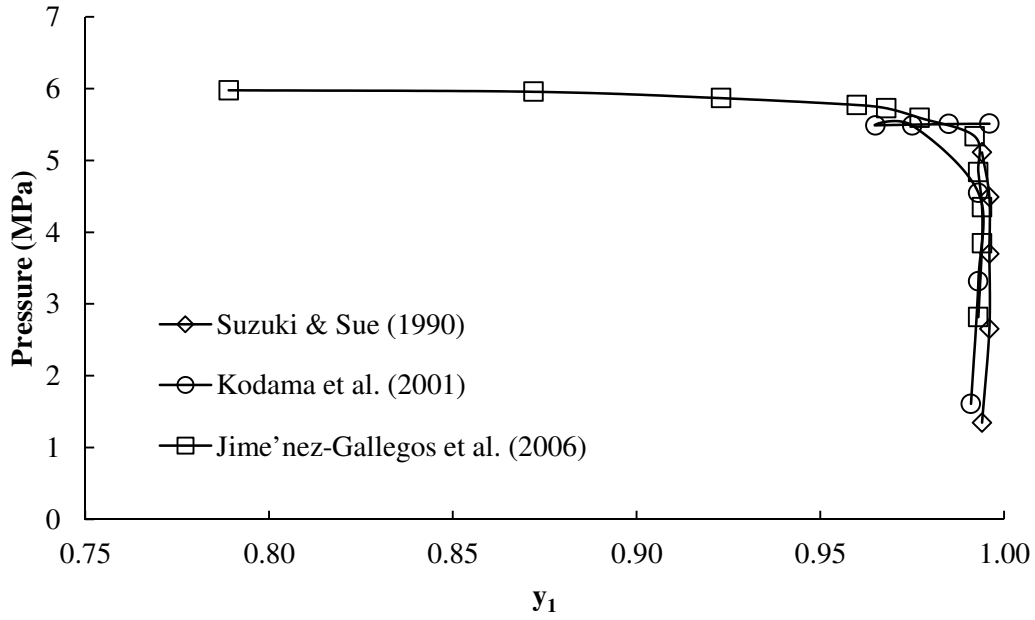

Figure 6.14: P-y diagram comparing the literature sources for the ethane (1) + 1-propanol (2) system.

6.2.3. Experimental Test System Results

The experimental data gathered for the test system are summarized in Table 6.2. Figure 6.15 shows the P-xy diagram for the ethane (1) – 1-propanol (2) system at 313.08 K. Above 5.3 MPa the system moves into a supercritical state, where only one phase exists.

Table 6.2: Experimental data for the ethane – 1-propanol system at 313.08 K.

Pave (MPa)	x_1	y_1
2.871	0.0297	0.9803
3.240	0.0331	0.9817
5.079	0.0546	0.9781
8.000	0.0875	0.9878
12.794	0.1457	0.9903
18.733	0.2197	0.9903

Pave (MPa)	x_1	y_1
22.240	0.2627	0.9901
27.901	0.3550	0.9904
29.051	0.3765	0.9942
30.928	0.4118	0.9949
34.480	0.4987	0.9924
36.652	0.5864	0.9913

The phase behaviour shown by the experimental data compares fairly well with the literature data shown in Figure 6.13 and Figure 6.14. Deviations from the published data in the literature can be explained by the high uncertainties in the 1-propanol calibrations, especially at the very low concentrations of 1-propanol in the vapour phase.

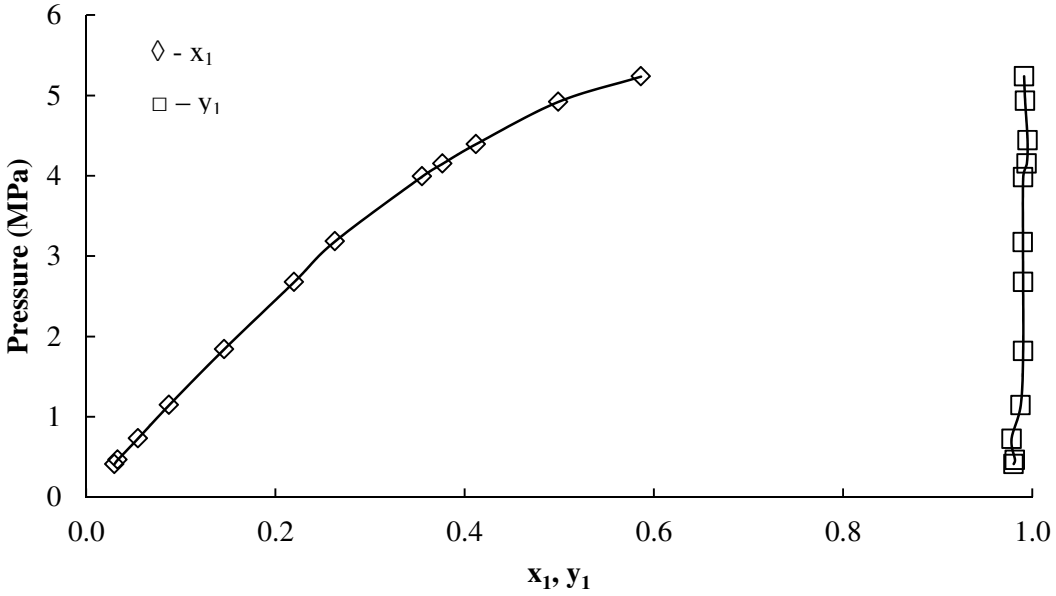

Figure 6.15: P-xy diagram for the experimental data collected at 313.08 K.

6.3. GC Calibrations for TFE, HFP and OFCB

As all three fluorocarbon materials are stored in gas form, the GC calibrations were done with air-tight gas syringes. Due to power failures and changes in the temperatures of the TCD, the calibrations had to be repeated several times. This created several sets of calibrations, which were only used for specific isotherms. The gas volume injections ranged from 0.05 ml up to 1 ml. A 1 ml and a 500 µl syringe were used for the injections. The smaller syringe was used to create a calibration set for the dilute regions in the isotherms. The mole quantity for each injection was again calculated by means of the ideal gas law (Eq. 6.5).

Different GC operating conditions were used for different systems to ensure optimum separation with the column to analyse the peaks. These different sets of operating conditions meant that each system had to have its own calibration sets. The TFE + HFP and TFE + OFCB systems used the following operating conditions:

- A Porapak Q column, filled with 100/120 mesh, with a length of 3 m and an outer diameter of 1/8" was used. The column was kept at a constant temperature of 413 K
- A direct injector was used and kept at a constant temperature of 493 K. The pressure was set at 150 kPa to ensure a helium flow rate of 25 ml/min through the column
- The TCD detector was kept at 423 K, with a current of 50 mA

For the HFP + OFCB system, the GC was operated at the following conditions:

- A Porapak Q column, filled with 80/100 mesh, with a length of 3 m and an outer diameter of 1/8" was used. The column was kept at a constant temperature of 503 K
- A direct injector was used and kept at a constant temperature of 503 K. The pressure was set at 200 kPa to ensure a helium flow rate of 30 ml/min through the column
- The TCD detector was kept at 523 K, with a current of 50 mA

It is important to note that the uncertainties shown below are based on the mole number of the component. The uncertainty for the mole fraction is also shown for each system. The uncertainty in the mole fraction was calculated by adding the uncertainties on the mole number and multiplying it with $(1 - x_1)$. This results in the maximum uncertainty from the determination of the mole fraction (Tshibangu, 2010: 89) shown in section 6.5. This calculation was also used as the basis the calculation of the uncertainty in the relative volatility. According to Tshibangu (2010) the uncertainty for the relative volatility is determined by multiplying the sum of the uncertainty of the comonets with two.

6.3.1. GC Calibrations for the HFP + OFCB System

All three isotherms used the same calibration sets for each component. The data from the repeated injections were fitted to a second-order polynomial. Figure 6.16 shows the second-order calibration curve for the OFCB calibrations. The following equation describes this curve:

$$n_{OFCB} = -2.6406 \times 10^{-20} \times PeakArea^2 + 5.3915 \times 10^{-12} \times PeakArea + 3.668 \times 10^{-7} \quad (6.8)$$

The deviations from the measured data are shown in Figure 6.17. The calibration is for the mole range between 4.2 * 10^{-5} moles and 1.7 * 10^{-6} moles. The uncertainty in the calibration is about 4.5 %. The syringes that were used for these calibrations might not be as accurate at very low volumes and this could explain the higher uncertainty in the lowest calibration regions.

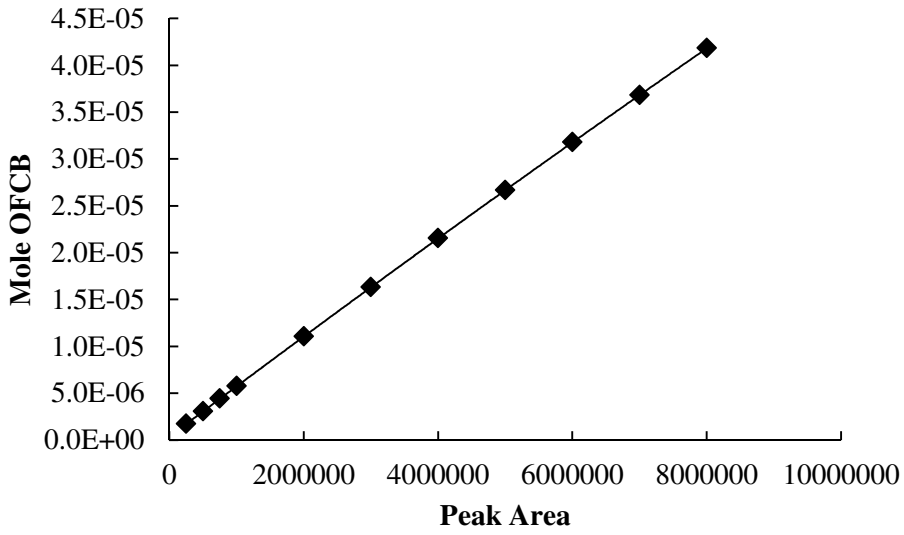

Figure 6.16: Second-order calibration curve for OFCB in the HFP + OFCB system.

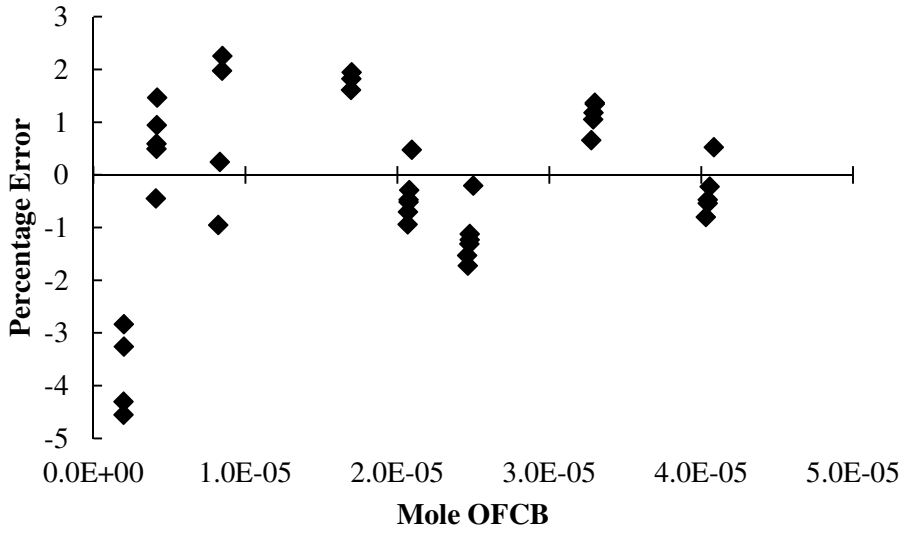

Figure 6.17: Percentage error plot for the OFCB calibration set used in the HFP + OFCB system.

The calibration set for the HFP for this system also fitted best to a second-order polynomial. Figure 6.18 shows the second-order calibration curve for the HFP calibrations. The following equation describes this curve:

$$n_{HFP} = 3.2152 \times 10^{-20} \times PeakArea^2 + 5.8073 \times 10^{-12} \times PeakArea + 3.2762 \times 10^{-7} \quad (6.9)$$

The deviations from the measured data are shown in Figure 6.19. The calibration is for the mole range between 4.2 x 10^{-5} moles and 3.2x 10^{-6} moles. The uncertainty in the calibration is about 2.5 %. As in the previous scenario, the syringes that were used for these calibrations might not have been as accurate at very low volumes. This could explain the high uncertainty in the lowest calibration regions.

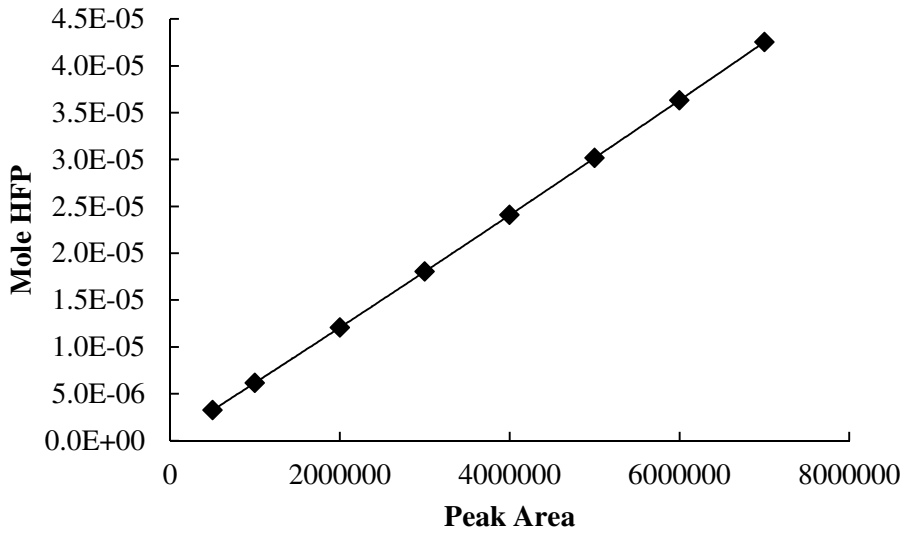

Figure 6.18: Second-order calibration curve for HFP for the HFP + OFCB system.

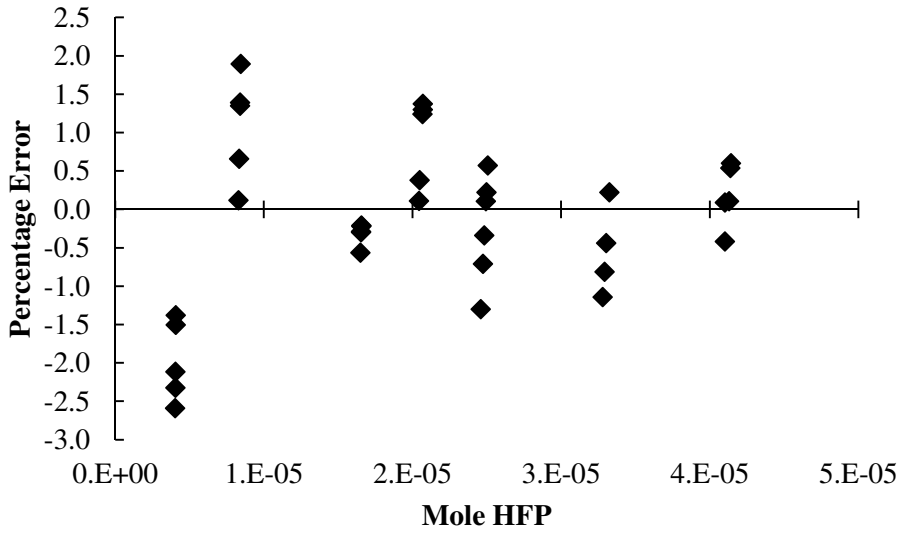

Figure 6.19: Percentage error plot for the calibration of HFP for the HFP + OFCB system.

6.3.2. GC Calibrations for the TFE + HFP System

Each isotherm in this system used its own calibration set. The second-order calibration curves for TFE, the calibration range and the uncertainty for each calibration set are shown in Table 6.3. Similar plots to those of Figure 6.18 and Figure 6.19 can be drawn up for each calibration set.

Table 6.3: GC calibration sets for TFE for the TFE + HFP system.

Calibration System	Calibration Equation	Calibration Range (x 10^5 mole)	Uncertainty (%)
243 K	$n_{TFE} = -5.8679 * 10^{-20} \times PeakArea^2 + 1.2541 \times 10^{-11} \times PeakArea + 2.7602 \times 10^{-7}$	0.65 to 4.3	±1.2
263 K	$n_{TFE} = -2.1474 \times 10^{-19} \times PeakArea^2 + 1.2636 \times 10^{-11} \times PeakArea - 8.5028 \times 10^{-8}$	0.8 to 4	±1.6
263 K Dilute Region	$n_{TFE} = 6.9291 \times 10^{-19} \times PeakArea^2 + 1.1377 \times 10^{-11} \times PeakArea + 1.8876 \times 10^{-7}$	0.2 to 0.81	±2
283 K	$n_{TFE} = -1.264 \times 10^{-19} \times PeakArea^2 + 1.3028 \times 10^{-11} \times PeakArea - 8.1971 \times 10^{-8}$	0.8 to 4	±1
283 K Dilute	$n_{TFE} = -1.1973 \times 10^{-18} \times PeakArea^2 + 1.3281 \times 10^{-11} \times PeakArea - 8.4659 \times 10^{-8}$	0.2 to 0.8	±1

Region

The calibration sets for HFP are shown in Table 6.4. The calibration curve, calibration range and the uncertainty are shown in Table 6.4.

Table 6.4: GC calibration sets for HFP for the TFE + HFP system.

Calibration System	Calibration Equation	Calibration Range (x 10^5 mole)	Uncertainty (%)
243 K and 283 K	$n_{HFP} = 9.3466 \times 10^{-20} \times PeakArea^2 + 8.7715 \times 10^{-12} \times PeakArea + 4.1626 \times 10^{-7}$	0.8 to 4	±1
243 K and 283 K Dilute Region	$n_{HFP} = -2.0143 \times 10^{-20} \times PeakArea^2 + 9.22 \times 10^{-12} \times PeakArea - 2.1762 \times 10^{-8}$	0.2 to 0.9	±1
263 K	$n_{HFP} = 9.1746 \times 10^{-20} \times PeakArea^2 + 8.9353 \times 10^{-12} \times PeakArea + 2.0263 \times 10^{-7}$	0.82 to 4	±1
263 K Dilute Region	$n_{HFP} = 3.2831 \times 10^{-19} \times PeakArea^2 + 8.6284 \times 10^{-12} \times PeakArea + 1.1993 \times 10^{-7}$	0.2 to 0.8	±1

6.3.3. GC Calibrations for the TFE + OFCB System

This system uses the same calibration set for TFE as the TFE + HFP system. The calibration curve equation, calibration range and uncertainties are shown in Table 6.3.

The calibration information for OFCB is shown in Table 6.5. All the calibration curves are fitted to second-order polynomial equations.

Table 6.5: GC calibration sets for OFCB for the TFE + OFCB system.

Calibration System	Calibration Equation	Calibration Range (x 10^5 mole)	Uncertainty (%)
243 K	$n_{OFCB} = 6.2460 \times 10^{-21} \times PeakArea^2 + 8.1253 \times 10^{-12} \times PeakArea + 1.3584 \times 10^{-7}$	0.8 to 4.2	±1.5
243 K Dilute Region	$n_{OFCB} = -4.2868 \times 10^{-19} \times PeakArea^2 + 8.4105 \times 10^{-12} \times PeakArea + 1.1133 \times 10^{-7}$	0.08 to 0.4	±1.1

263 K	$n_{OFCB} = 4.8166 \times 10^{-20} \times PeakArea^2 + 7.6587 \times 10^{-12} \times PeakArea + 1.0065 \times 10^{-7}$	0.8 to 4	±1.8
263 K Dilute Region	$n_{OFCB} = 2.6741 \times 10^{-19} \times PeakArea^2 + 7.8826 \times 10^{-12} \times PeakArea - 2.2094 \times 10^{-8}$	0.2 to 0.81	±1.1
283 K	$n_{OFCB} = 4.3379 \times 10^{-20} \times PeakArea^2 + 7.7652 \times 10^{-12} \times PeakArea + 1.6994 \times 10^{-7}$	0.81 to 4	±0.9
283 K Dilute Region	$n_{OFCB} = 1.6660 \times 10^{-19} \times PeakArea^2 + 7.7802 \times 10^{-12} \times PeakArea + 7.4999 \times 10^{-8}$	0.2 to 0.8	±1.3

6.4. Experimental Vapour-Pressure Data

The vapour-pressures for all three components were measured within the pressure range in which the components would be used in the VLE measurements. The vapour-pressure data are first compared to the data found in the literature. This can be used as an indication of the accuracy of the experimental work. The vapour-pressure data collected from the literature are usually regressed to fit the Antoine equation or a similar data regression equation. The vapour-pressure for the literature data is then calculated from these regression equations at each experimental point and compared. The experimental vapour-pressure data for OFCB are shown in Figure 6.20. These data are compared to the data from Braker and Mossman (1980: 557 – 560), Daubert, Dunner, Sibul and Stebbins (1998) and Yaws (2009), where all show good comparisons to the experimental data. There is a slight deviation, as can be seen in Figure 6.20, at the low-end temperatures. As all three literature sources do correlate to the experimental data, it was decided that the deviation was within an acceptable range and this was used in the modelling described in the next chapter.

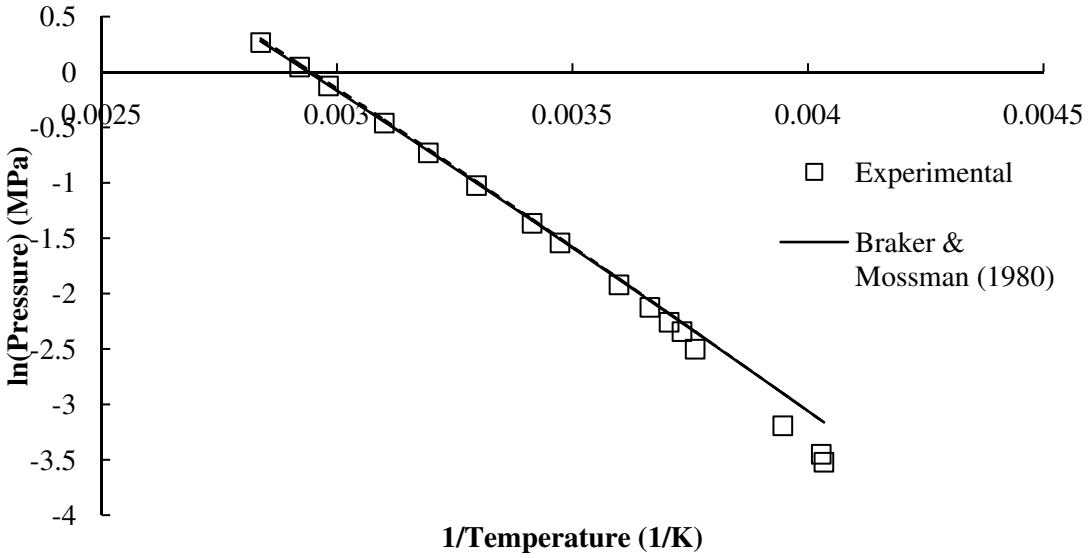

Figure 6.20: Comparison between experimental vapour-pressure data and the data found in the literature for OFCB.

Figure 6.21 compares the experimental vapour-pressure data of HFP to the data published by Whipple (1952) and Coquelet, Ramjugernath, Valtz, Naidoo and Meniai (2010). The experimental data compare well to the data published by Coquelet *et al.* (2010) and have only slight deviations from the data published by Whipple (1952). The experimental vapour-pressure data for TFE are shown and compared to the data by Boublík, Fried and Hála (1975) and Yaws (2009) in Figure 6.22. The experimental data fit well to the data published in the above-mentioned literature sources.

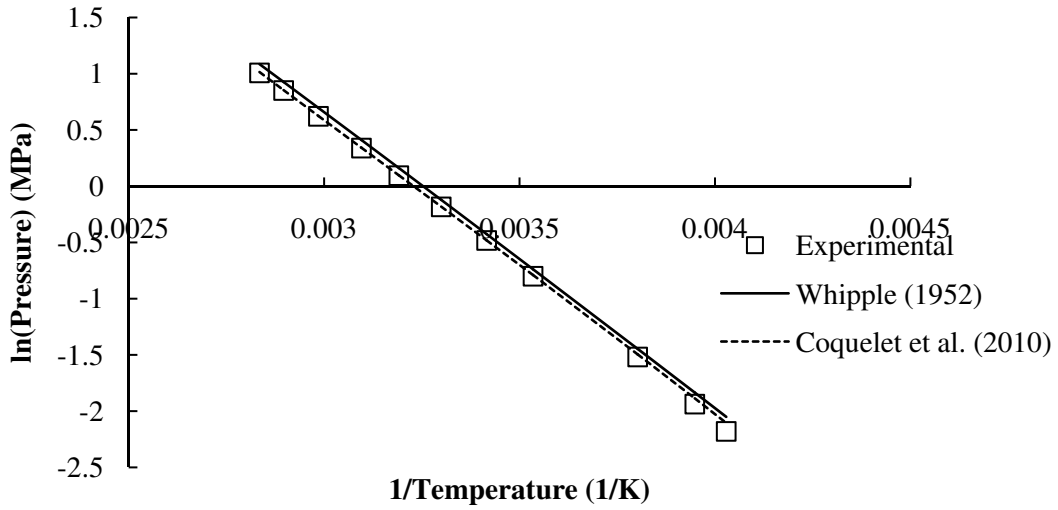

Figure 6.21: Comparison between the experimental vapour-pressure data and the data found in the literature for HFP.

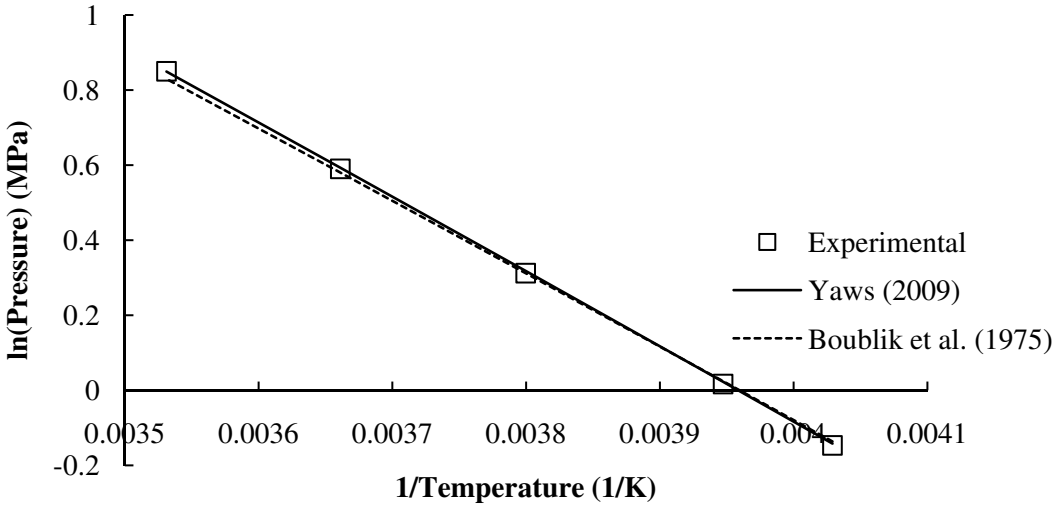

Figure 6.22: Comparison between the experimental vapour pressure data and the data found in the literature for TFE.

Each set of vapour-pressure data was regressed to the Mathias-Copeman Alpha function. The percentage error in the regression is calculated with:

$$P_{error\%} = \frac{P_{exp} - P_{cal}}{P_{exp}} \times 100 \tag{6.10}$$

The deviations from the experimental data and the regressed model are expressed by the *BIAS %* (Eq. 6.11) and the mean relative deviation (*MRD %*) (Eq. 6.12).

$$BIAS\ \% = \frac{100}{n} \times \sum_n \frac{P_{exp} - P_{cal}}{P_{exp}} \tag{6.11}$$

$$MRD\ \% = \frac{100}{n} \times \sum_n \frac{P_{exp} - P_{cal}}{P_{exp}} \tag{6.12}$$

Table 6.6 to Table 6.8 summarize the experimental vapour-pressure values, the regressed values and the percentage error for OFCB, HFP and TFE respectively. The BIAS % and the MRD % for the three components are shown in Table 6.9. The vapour-pressure curve for the experimental values for OFCB, HFP and TFE are shown in Figure 6.23 to Figure 6.25.

Table 6.6: Experimental vapour-pressure data for OFCB compared with the calculated values

T_{exp} (K)	P_{exp} (MPa)	P_{cal} (MPa)	$P_{error\%}$
247.9	0.030	0.030	-0.055
248.3	0.032	0.032	0.059
253.4	0.041	0.041	-0.100
265.9	0.082	0.082	-0.104
267.9	0.096	0.096	0.147
269.9	0.104	0.104	0.117
272.9	0.119	0.119	0.109
277.9	0.146	0.146	0.057
287.9	0.214	0.214	-0.041
292.9	0.255	0.255	-0.073
303.4	0.359	0.359	-0.148
313.1	0.482	0.482	-0.130
322.5	0.630	0.631	-0.047
335.3	0.881	0.881	0.085
342.4	1.045	1.044	0.138
352.4	1.304	1.304	0.040

Table 6.7: Experimental vapour-pressure data for HFP compared with the calculated values

T_{exp} (K)	P_{exp}(MPa)	P_{cal}(MPa)	$P_{error\%}$
248.2	0.113	0.113	-0.013
253.3	0.144	0.144	0.011
263.0	0.219	0.219	0.022
282.9	0.449	0.449	-0.048
292.8	0.617	0.617	0.011
303.1	0.832	0.832	0.005
313.4	1.098	1.098	0.004
323.1	1.403	1.403	0.020
335.0	1.861	1.860	0.029
345.3	2.341	2.341	-0.002
352.8	2.737	2.740	-0.120

Table 6.8: Experimental vapour-pressure data for TFE compared with the calculated values

T_{exp} (K)	P_{exp}(MPa)	P_{cal}(MPa)	$P_{error\%}$
248.2	0.86352	0.864	-0.0020
253.3	1.01695	1.017	0.0034
263.2	1.3665	1.367	-0.0001
273.1	1.8042	1.804	-0.0037
283.2	2.33985	2.340	0.0027

Table 6.9 The BIAS % and the MRD % for the calculated vapour-pressure

	OFCB	HFP	TFE
BIAS p %	0.003	-0.007	0.001
MRD p %	0.091	0.026	0.002

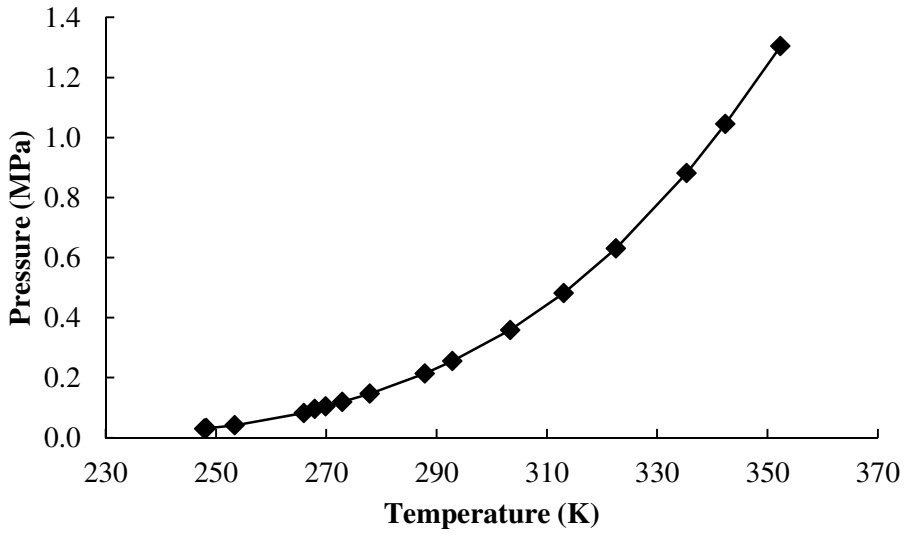

Figure 6.23: Experimental vapour-pressure curve for OFCB.

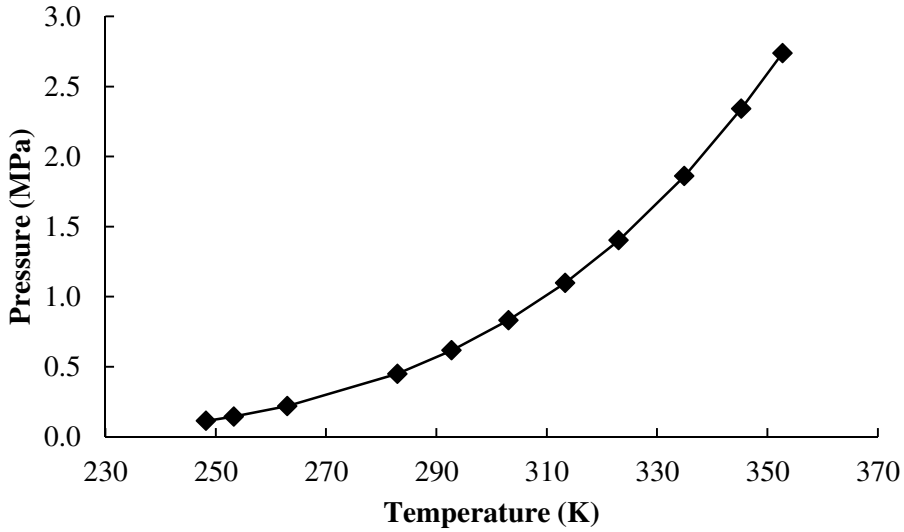

Figure 6.24: Experimental vapour-pressure curve for HFP.

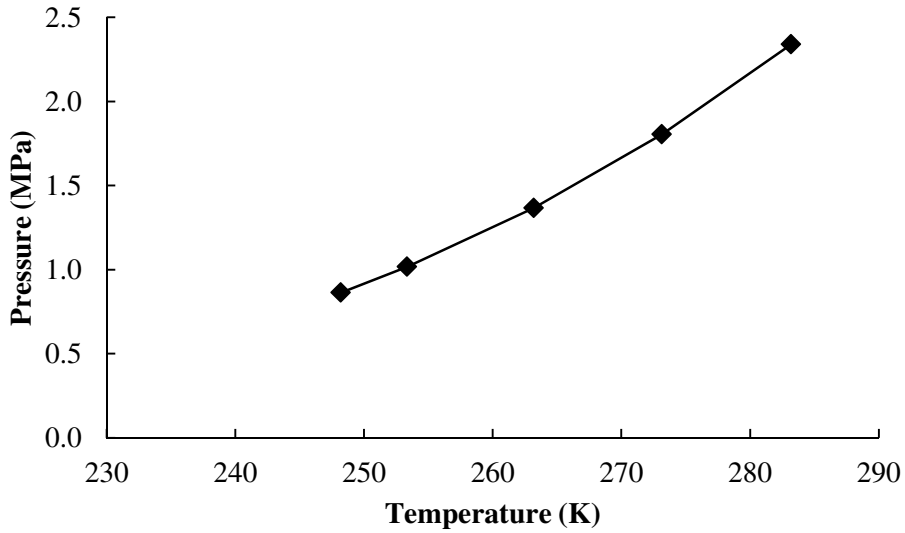

Figure 6.25: Experimental vapour-pressure curve for TFE.

The error percentage between each measured and calculated vapour-pressure point is below about 0.15 %. The MRD % for the vapour-pressures for each component is below 0.1 %. The Mathias-Copeman alpha function therefore gives an accurate description of the experimental vapour-pressure data. The vapour-pressure curves follow the expected trend for each component.

6.5. Vapour-Liquid Equilibrium Experimental Data

Summarized below is the experimental data. This data is then used in the modelling which is shown in Chapter 7. The relative volatility of the experimental data is shown with the suggested model in Chapter 7.

6.5.1. TFE + OFCB System

This system was evaluated at 248.3 K, 263.0 K and 282.9 K. Table 6.7 shows the experimental data collected for the system, as well as the deviation in the samples taken for each phase, for each isotherm. Figure 6.26 to Figure 6.28 show the phase behaviour in the system at each isotherm.

Table 6.7: Experimental data for the TFE (1) + OFCB (2) system for all three isotherms.

P_{exp} (MPa)	$X_{1\ exp}$	dx %	$Y_{1\ exp,}$	dy %
248.3 K				
0.032	0.000		0.000	
0.256	0.318	0.149	0.880	0.042
0.307	0.395	0.128	0.907	0.029
0.349	0.448	0.094	0.923	0.048
0.380	0.481	0.101	0.932	0.031
0.427	0.538	0.117	0.944	0.015
0.477	0.598	0.055	0.955	0.021
0.525	0.653	0.050	0.963	0.034
0.569	0.698	0.034	0.969	0.018
0.615	0.742	0.122	0.974	0.015
0.864	1.000		1.000	
263.0 K				
0.073	0.000		0.000	
0.254	0.154	0.202	0.720	0.068
0.366	0.268	0.163	0.815	0.089
0.450	0.343	0.100	0.851	0.039
0.535	0.417	0.141	0.883	0.039
0.607	0.472	0.093	0.908	0.035
0.699	0.534	0.073	0.923	0.041
0.798	0.617	0.090	0.940	0.021
0.897	0.688	0.078	0.957	0.015
0.994	0.763	0.131	0.968	0.016
1.367	1.000		1.000	
282.9 K				
0.178	0.000		0.000	
0.252	0.052	0.829	0.329	0.257
0.398	0.137	0.357	0.585	0.130
0.594	0.251	0.530	0.741	0.035
0.720	0.320	0.228	0.794	0.052
0.897	0.423	0.146	0.849	0.050
1.065	0.513	0.133	0.882	0.041
1.257	0.603	0.097	0.912	0.044
1.427	0.681	0.074	0.931	0.058
1.645	0.763	0.033	0.951	0.024

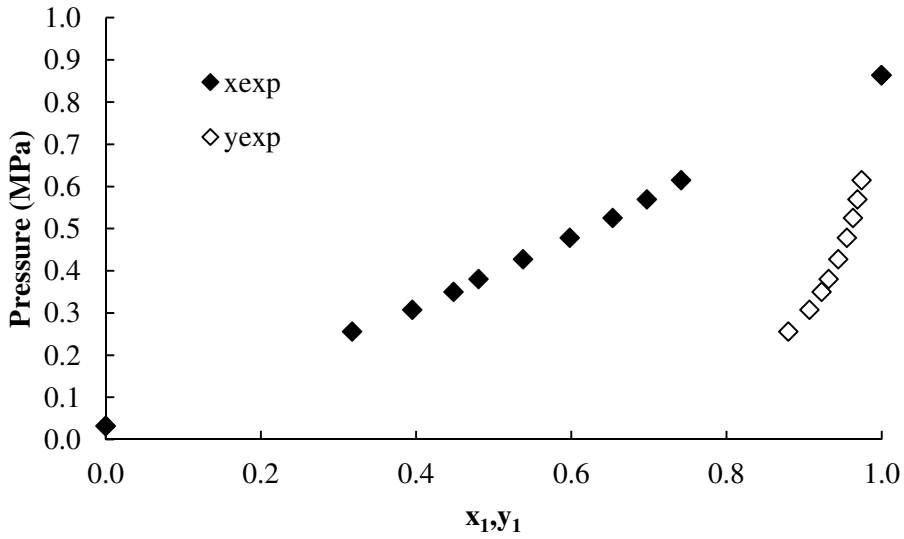

Figure 6.26: Experimental VLE data for the TFE (1) + OFCB (2) system at 248.3 K.

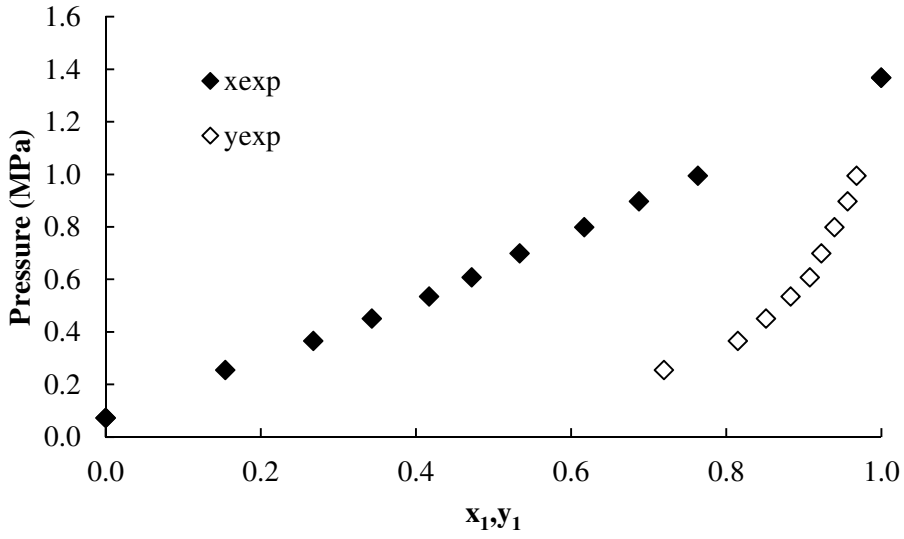

Figure 6.27: Experimental VLE data for the TFE (1) + OFCB (2) system at 263.0 K.

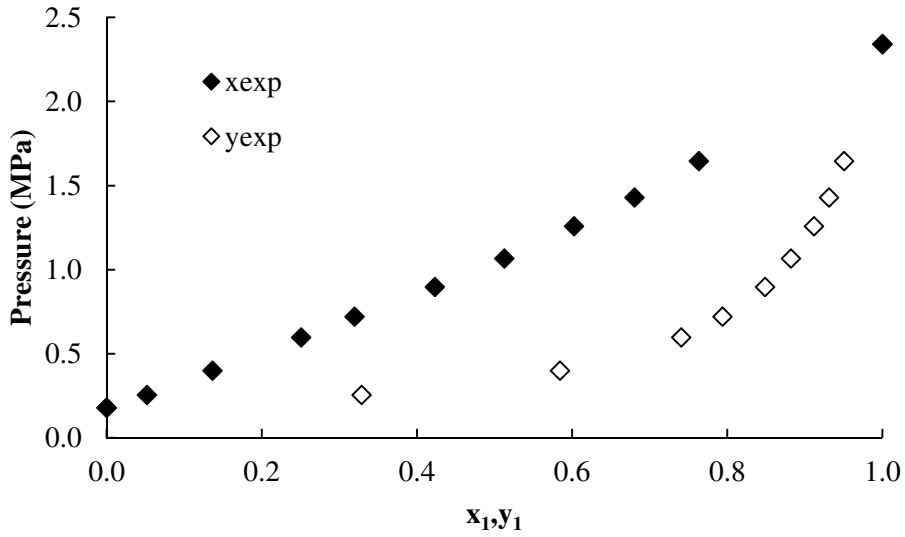

Figure 6.28: Experimental VLE data for the TFE (1) + OFCB (2) system at 282.9 K.

The behaviour for each isotherm is visible from the plots of the experimental VLE data. The bottom end of the VLE plot for the 243 K isotherm is not completed. The apparatus was not able to measure either phase below 0.25 MPa. The maximum uncertainty in the mole fraction was determined as 3.3 % for both pure TFE and pure OFCB.

6.5.2. TFE + HFP System

This system was evaluated at 248.1 K, 263.0K and 282.9 K. Table 6.8 shows the collected experimental data for the system, as well as the deviation in the samples taken for each phase, for each isotherm. The vapour-pressure for the pure components is also shown in Table 6.8. Figure 6.29 to Figure 6.31 show the phase behaviour in the system at each isotherm.

Table 6.8: Experimental data for the TFE (1) + HFP (2) system for all three isotherms.

P_{exp}	$X_{1\ exp}$	dx %	$Y_{1\ exp,1}$	dy %
248.1 K				
0.120	0.000		0.000	
0.258	0.218	0.194	0.620	0.129
0.300	0.270	0.275	0.671	0.091
0.348	0.338	0.125	0.735	0.052
0.394	0.403	0.138	0.782	0.052
0.462	0.492	0.142	0.833	0.078
0.490	0.543	0.154	0.858	0.053
0.537	0.602	0.083	0.884	0.029
0.573	0.648	0.111	0.900	0.070
0.620	0.702	0.095	0.919	0.028
0.694	0.784	0.047	0.953	0.015
0.870	1.000		1.000	

P_{exp}	$X_{1\ exp}$	dx %	$Y_{1\ exp,1}$	dy %
263.0 K				
0.225	0.000		0.000	
0.340	0.120	0.260	0.391	0.179
0.441	0.229	0.161	0.558	0.059
0.546	0.331	0.149	0.679	0.075
0.645	0.422	0.083	0.752	0.040
0.758	0.500	0.291	0.802	0.052
0.808	0.568	0.041	0.825	0.058
0.886	0.627	0.019	0.868	0.020
0.987	0.713	0.048	0.904	0.038
1.075	0.785	0.066	0.931	0.044
1.166	0.857	0.045	0.961	0.020
1.374	1.000		1.000	
282.9 K				
0.456	0.000		0.000	
0.551	0.071	0.250	0.220	0.162
0.671	0.144	0.302	0.381	0.047
0.855	0.263	0.134	0.557	0.079
1.041	0.367	0.128	0.663	0.082
1.166	0.443	0.046	0.720	0.070
1.282	0.507	0.109	0.757	0.089
1.396	0.570	0.098	0.801	0.051
1.509	0.626	0.154	0.837	0.027
1.622	0.677	0.078	0.860	0.042
1.760	0.739	0.042	0.889	0.045
1.874	0.790	0.058	0.913	0.089
1.956	0.832	0.056	0.928	0.056
2.346	1.000		1.000	

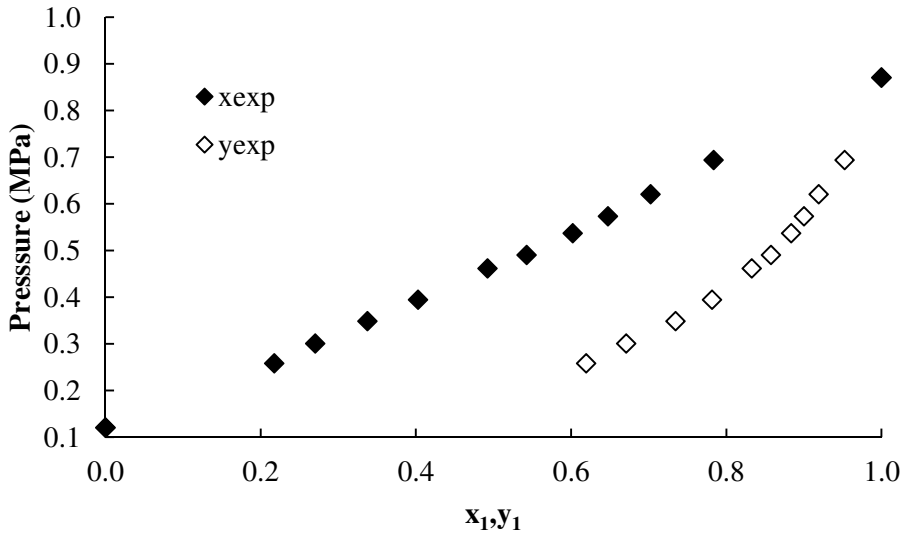

Figure 6.29: Experimental VLE data for the TFE (1) + HFP (2) system at 248.1 K.

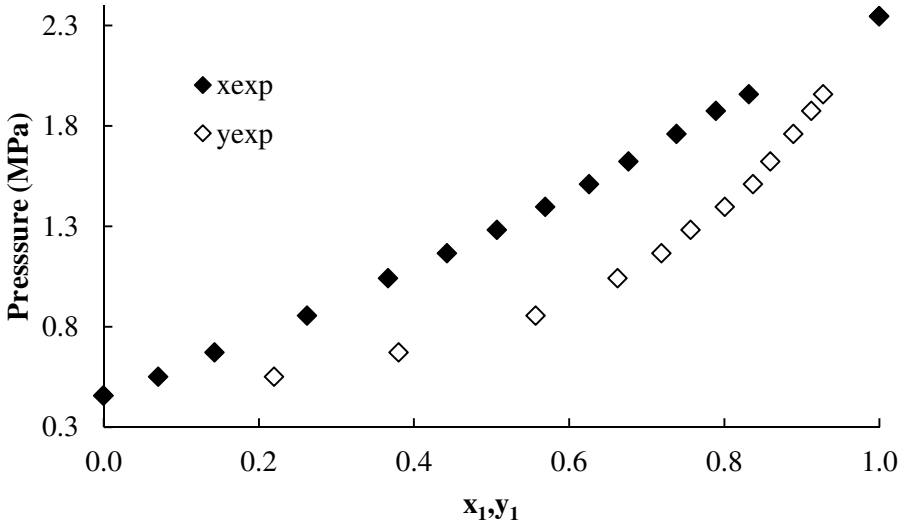

Figure 6.30: Experimental VLE data for the TFE (1) + HFP (2) system at 263.0 K.

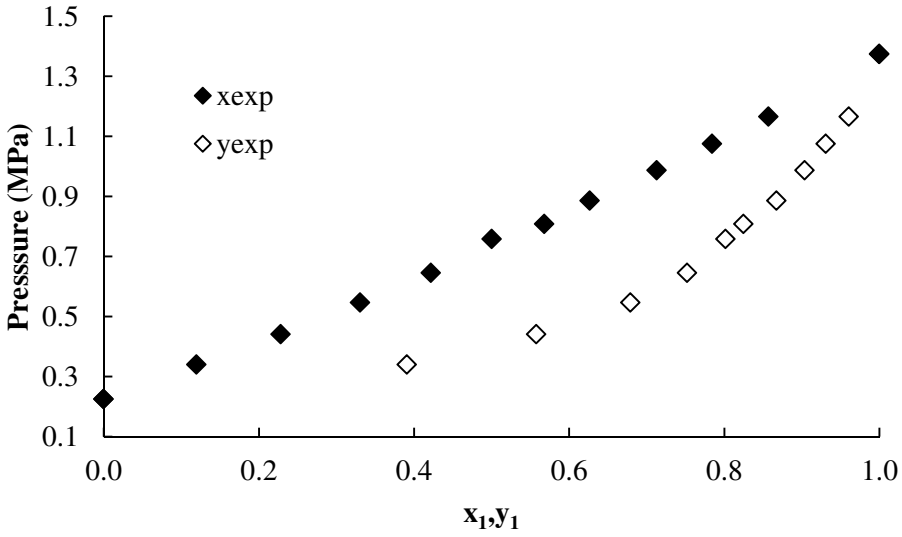

Figure 6.31: Experimental VLE data for the TFE (1) + HFP (2) system at 282.9 K.

Typical VLE behaviour for each isotherm can be seen in the above-mentioned plots. The liquid phase and vapour phase curves tend to become closer to each other as the temperature of the binary system increases. The maximum uncertainty in the mole fraction was determined as 3 % for both pure TFE and pure HFP.

6.5.3. HFP + OFCB System

This system was evaluated at 292.9 K, 323.0 K and 352.7 K. Higher temperatures had to be used as the pressure would have been too low to take samples had the same temperature

ranges been used as those for the other two binary systems. Table 6.9 shows the collected experimental data for the system, as well as the deviation in the samples taken for each phase, for each isotherm. The vapour-pressure for the pure components is also shown in Table 6.9. Figure 6.32 to Figure 6.34 show the experimentally determined phase behaviour in the system for each isotherm.

Table 6.9: Experimental data for the HFP (1) + OFCB (2) system for all three isotherms.

P_{exp}	$X_{1\,exp}$	dx %	$Y_{1\,exp}$	dy %
292.9 K				
0.255	0.000		0.000	
0.286	0.092	0.089	0.177	0.208
0.309	0.152	0.171	0.275	0.121
0.336	0.227	0.230	0.382	0.052
0.368	0.319	0.142	0.491	0.056
0.397	0.399	0.062	0.586	0.100
0.428	0.482	0.129	0.662	0.063
0.447	0.538	0.149	0.709	0.078
0.477	0.612	0.067	0.771	0.114
0.504	0.691	0.047	0.821	0.074
0.528	0.744	0.091	0.859	0.040
0.558	0.838	0.269	0.906	0.017
0.588	0.904	0.010	0.950	0.023
0.617	1.000		1.000	
323.0 K				
0.630	0.000		0.000	
0.713	0.108	0.138	0.179	0.149
0.783	0.204	0.157	0.310	0.505
0.833	0.269	0.145	0.396	0.043
0.921	0.384	0.119	0.524	0.096
0.986	0.469	0.093	0.605	0.069
1.047	0.551	0.173	0.675	0.132
1.089	0.604	0.066	0.720	0.065
1.142	0.671	0.045	0.773	0.055
1.228	0.782	0.071	0.852	0.031
1.313	0.885	0.022	0.922	0.018
1.395	1.000		1.000	
352.7 K				
1.304	0.000		0.000	
1.419	0.091	0.638	0.129	2.231
1.534	0.185	0.358	0.240	0.496
1.722	0.314	0.341	0.403	0.497
1.839	0.396	0.380	0.483	0.346
2.060	0.555	0.334	0.639	0.058
2.258	0.687	0.158	0.752	0.098
2.361	0.766	0.035	0.816	0.145
2.528	0.866	0.062	0.895	0.021
2.609	0.910	0.031	0.930	0.029
2.737	1.000		1.000	

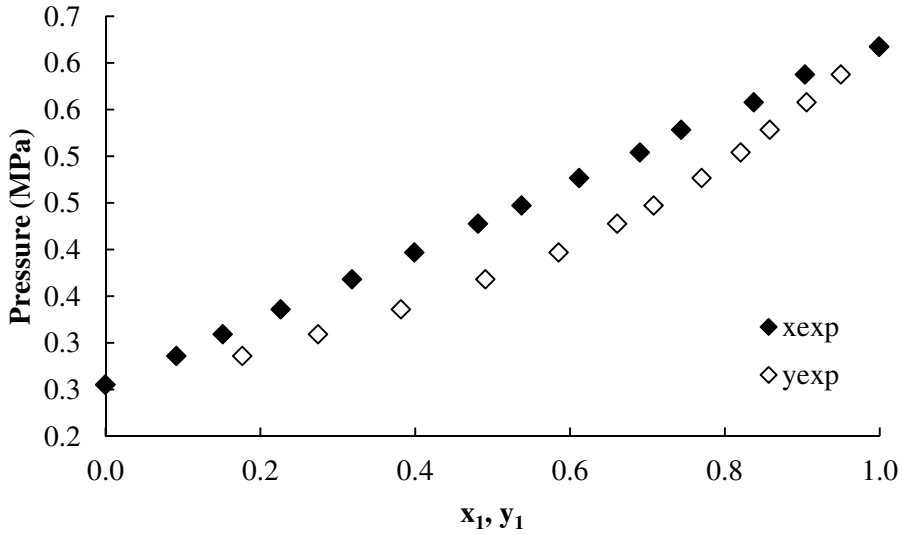

Figure 6.32: Experimental VLE data for the HFP (1) + OFCB (2) system at 292.9 K.

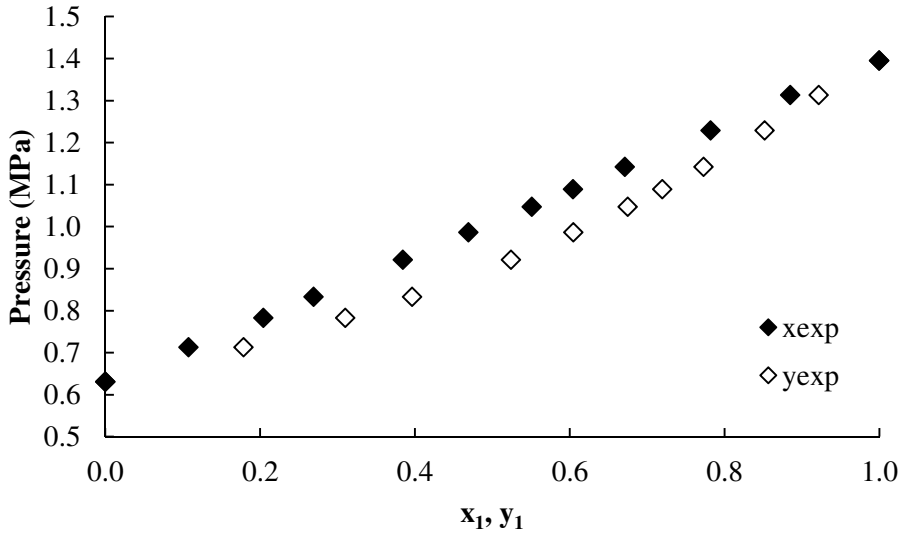

Figure 6.33: Experimental VLE data for the HFP (1) + OFCB (2) system at 323.0K.

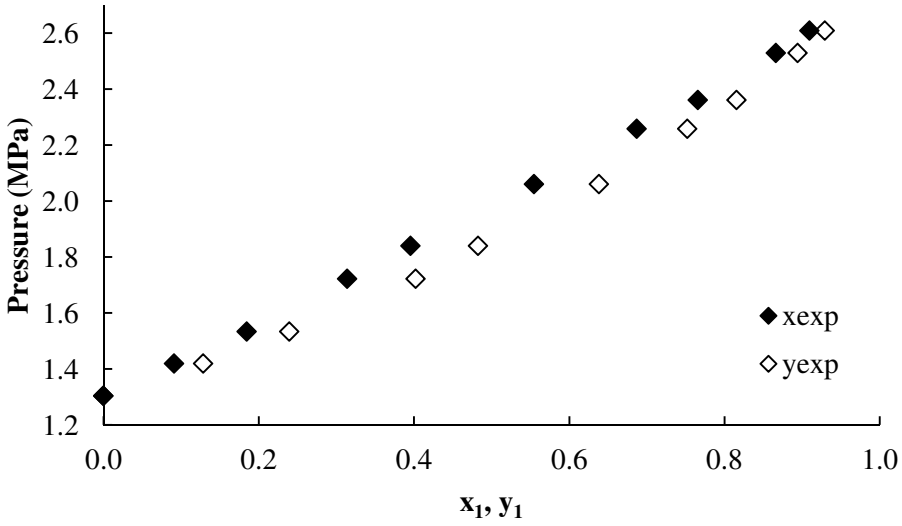

Figure 6.34: Experimental VLE data for the HFP (1) + OFCB (2) system at 352.7 K.

The VLE behaviour is shown in the above plots. The liquid phase and vapour phase compositions are much closer to each other than with the other two systems. The reason for this is that the boiling points of HFP and OFCB are fairly close to each other. The maximum uncertainty in the mole fraction was determined as 5.9 % for both pure HFP and pure OFCB.

Chapter 7

Data Analysis and Modelling

7. Data Analysis and Modelling

The experimental data shown in Chapter 6, were fitted to the Peng-Robinson equation of state (eq. 2.65 to eq. 2.70), utilizing the Mathias-Copeman alpha function (eq. 2.70). The Wong-Sandler mixing rule (eq. 2.88 and eq. 2.89), with the incorporation of the NRTL activity coefficient model (eq. 2.104 to eq. 2.109), was used with the equation of state. Aspen Technologies Inc. was used for the data regression. PR-MC-WS-NRTL refers to the thermodynamic model selected for the data regressions. The selected model has two sets of parameters that need to be adjusted, viz.:

- τ_{ij}, τ_{ji} and α_{ij} for the NRTL local composition model; and
- k_{ij} which is the binary interaction parameter for the Wong-Sandler mixing rules.

The outputs from Aspen for the NRTL parameters are a_{ij} and a_{ji}. α_{ij} is set as a constant value of 0.3 for the model, as suggested by Renon and Prausnitz (1968). To calculate the τ_{ij} and τ_{ji} parameters, both a_{ij} and a_{ji} are multiplied by $(R \times T)$, where R is the ideal gas constant.

7.1. Vapour-Pressure Data Regression

As the Mathias-Copeman alpha function was used in the modelling of the VLE data, the parameters for the equation hadto be calculated. The experimental vapour-pressure data that was collected during the experimental work wasused in the regression for the Mathias-Copeman parameters. The calculated parameters C_1, C_2 and C_3, for the Mathias-Copeman alpha function is shown in Table 7.1. The parameters were fitted to the alpha function by using Aspen Technologies Inc.

Table 7.1: Calculated parameters for the Mathias-Copeman alpha function.

Parameter	OFCB	HFP	TFE
C_1	1.051	0.943	0.546
C_2	-3.145	-1.414	2.316
C_3	15.259	7.843	-10.401

7.2. Vapour-Liquid Equilibrium Data Modelling

Several methods can be used to complete a regression on experimental data. This is done by minizing the error between the experimental data and the calculated model data in each iteration. The experimental data can be determined through various calculations methods. The Aspen Technologies Package used a bubble point calculation, using the temperature and the liquid phase composition as input to start an iteration. Minimization of the mean square error is a common method. The mean square error can be calculated for each variable, such as the temperature, pressure and phase compositions. The maximum likelihood objective function, given in Aspen Technologies, was used to minimize the error in the calculation for x, y, T and P. The maximum likelihood equation is as follows:

$$F = \sum_{n=1}^{NDG} W_n \sum_{i=1}^{NP} \left[\begin{array}{c} \left(\frac{T_{e,i}-T_{m,i}}{\sigma_{T,i}}\right)^2 + \left(\frac{P_{e,i}-P_{m,i}}{\sigma_{P,i}}\right)^2 + \\ \sum_{j=1}^{NC-1}\left(\frac{x_{e,i,j}-x_{m,i,j}}{\sigma_{x,i,j}}\right)^2 + \sum_{j=1}^{NC-1}\left(\frac{y_{e,i,j}-y_{m,i,j}}{\sigma_{y,i,j}}\right)^2 \end{array} \right] \quad (7.1)$$

where

- *NDG* is the number of data groups used in the data regression
- w_n is the weight percentage factor of the data group
- *NP* is the number of data points
- *NC* is the number of components
- *T*, *P* , *x*, *y* are the temperature, pressure, liquid and vapour mole fractions, respectively
- *e* is the estimated data from the model
- *m* is the experimentally measured data
- *i*is the data for data point i
- *j* is the fractional data for component j
- σ is the standard deviation of the specific data (should the standard deviation be 0, the specific data point would not be included in the objective function and the estimated values are set equal to the measured value)

7.2.1. Modelling for the TFE (1) + OFCB (2) System

The experimental and calculated data points for each isotherm are shown in Table 7.2.

Table 7.2: Experimental P-x-y data for TFE (1) + OFCB (2) and correlated model.

Experimental Data			Calculated data with the specified model							
P_{exp} MPa	$x_{1\,exp}$	$y_{1\,exp}$	T_{cal} K	ΔT K	p_{cal} MPa	Δp MPa	$x_{1\,cal}$	Δx_1	$y_{1\,cal}$	Δy_1
				T =	**248.3**	**K**				
0.032	0.000	0.000	248.63	-0.33	0.032	0.000	0.000	0.000	0.000	0.000
0.256	0.318	0.880	248.77	-0.47	0.256	0.000	0.317	0.000	0.895	-0.015
0.307	0.395	0.907	248.11	0.19	0.308	-0.001	0.394	0.002	0.921	-0.014
0.349	0.449	0.923	248.33	-0.03	0.350	-0.001	0.447	0.002	0.933	-0.010
0.380	0.481	0.932	248.75	-0.45	0.380	0.000	0.480	0.001	0.938	-0.006
0.427	0.538	0.944	248.88	-0.58	0.427	0.000	0.538	0.000	0.948	-0.004
0.477	0.598	0.955	249.00	-0.70	0.477	0.001	0.599	-0.001	0.957	-0.002
0.525	0.654	0.963	249.12	-0.82	0.524	0.001	0.654	0.000	0.964	-0.001
0.569	0.698	0.969	249.38	-1.08	0.567	0.002	0.698	-0.001	0.969	0.000
0.615	0.742	0.974	249.65	-1.35	0.612	0.003	0.742	-0.001	0.974	0.000
0.864	1.000	1.000	248.20	0.10	0.864	0.000	1.000	0.000	1.000	0.000
				T =	**262.96**	**K**				
0.073	0.000	0.000	263.00	-0.04	0.073	0.000	0.000	0.000	0.000	0.000
0.254	0.155	0.720	264.39	-1.43	0.253	0.001	0.155	-0.001	0.713	0.007
0.366	0.268	0.815	262.64	0.32	0.366	-0.001	0.267	0.001	0.830	-0.015
0.450	0.344	0.851	262.54	0.42	0.451	-0.001	0.342	0.001	0.870	-0.019
0.535	0.417	0.883	262.55	0.41	0.536	-0.001	0.415	0.002	0.897	-0.014
0.607	0.472	0.908	262.91	0.05	0.607	0.000	0.471	0.001	0.912	-0.004
0.699	0.534	0.923	263.68	-0.72	0.697	0.002	0.535	-0.001	0.925	-0.002
0.798	0.617	0.940	263.55	-0.59	0.797	0.001	0.617	0.000	0.942	-0.002
0.897	0.688	0.957	263.78	-0.82	0.894	0.003	0.688	-0.001	0.954	0.002
0.994	0.763	0.968	263.54	-0.58	0.991	0.003	0.764	0.000	0.967	0.001
1.367	1.000	1.000	263.18	-0.22	1.366	0.001	1.000	0.000	1.000	0.000
				T =	**282.89**	**K**				
0.178	0.000	0.000	282.94	-0.05	0.178	0.000	0.000	0.000	0.000	0.000
0.252	0.052	0.329	282.12	0.77	0.253	-0.001	0.052	0.000	0.332	-0.003
0.398	0.137	0.585	283.00	-0.11	0.397	0.000	0.137	0.000	0.576	0.009
0.594	0.251	0.741	283.16	-0.27	0.594	0.001	0.251	0.000	0.731	0.009
0.720	0.320	0.794	283.28	-0.39	0.718	0.001	0.320	-0.001	0.787	0.007
0.897	0.423	0.849	282.70	0.19	0.897	-0.001	0.423	0.000	0.847	0.002
1.065	0.513	0.882	282.58	0.31	1.067	-0.002	0.512	0.001	0.883	0.000
1.257	0.603	0.912	282.74	0.15	1.258	-0.001	0.603	0.000	0.911	0.001
1.427	0.681	0.931	282.70	0.19	1.428	-0.001	0.680	0.000	0.932	0.000
1.645	0.763	0.951	283.15	-0.26	1.643	0.002	0.763	0.000	0.951	0.000
2.340	1.000	1.000	283.16	-0.27	2.338	0.002	1.000	0.000	1.000	0.000

Table 7.2 also shows the error between the experimental value and the value calculated by the correlated model. The error is calculated as follows:

$$\Delta U = U_{exp} - U_{cal} \tag{6.2}$$

where $U = T$, P, x_1 and y_1. Figure 7.1 shows the calculated model with the experimental data points for the TFE (1) + OFCB (2) system.

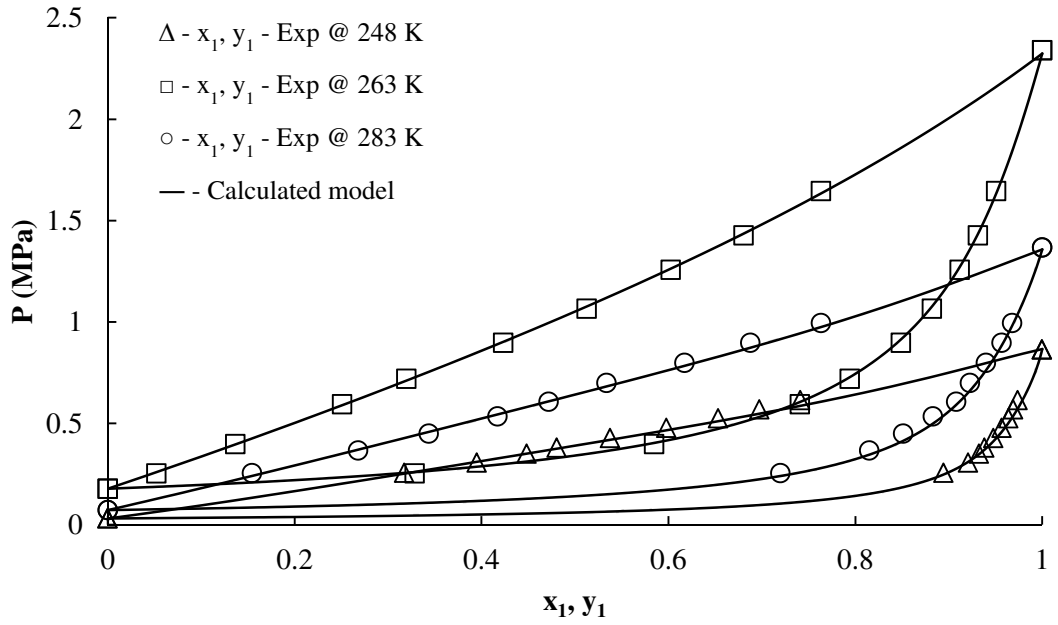

Figure 7.1: The regressed model, with the experimental data, for the TFE (1) + OFCB (2) system.

The correlated parameters for the model are shown in Table 7.3. The BIAS % and the MRD % between the experimental data and the calculated model are shown in Table 7.4. The MRD % for the temperatures and vapour phase composition at the 248.3 K and the 262.96 K isotherms are both relatively large. The deviations for the 282.92 K isotherm are fairly good and the model describes the isotherm fairly well. Even though the deviations are larger for the other two systems, it can still be assumed that itdescribes the system accuratelysincethe MRD % is still below 0.6 %.

Table 7.3: Adjusted binary interaction parameters for the PR-MC-WS-NRTL for the system TFE (1) + OFCB (2).

T (K)	τ_{12}	τ_{21}	k_{12}
248.3	8580	-443	-0.5294
262.96	5384	-1600	-0.0950
282.92	2333	-1585	0.0805

Table 7.4: Relative deviations, BIAS % and MRD %, based on the experimental data fitted to PR-MC-WS-NRTL.

T (K)	BIAST %	MRD T %	BIASP %	MRD P %	BIASx_1 %	MRD x_1 %	BIASy_1 %	MRD y_1 %
248.30	-0.202	0.223	0.087	0.171	0.087	0.158	-0.623	0.630
262.96	-0.110	0.193	0.072	0.215	0.048	0.204	-0.572	0.878
282.92	0.018	0.094	-0.010	0.105	0.000	0.073	0.343	0.565

The temperature evolution for the parameters is important in the design of separation processes. Figure 7.2 and Figure 7.3 show the temperature evolution for the NRTL local composition model parameters and the binary interaction parameters respectively. Second-order curves are used to describe the temperature evolution for all three parameters.

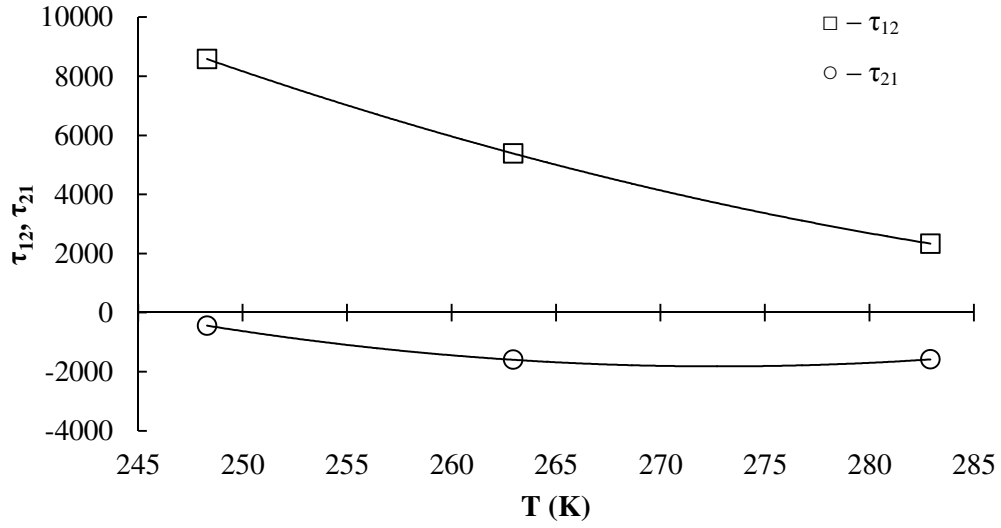

Figure 7.2: The temperature evolution for the NRTL local composition model parameters for all three isotherms for the TFE (1) + OFCB (2) system.

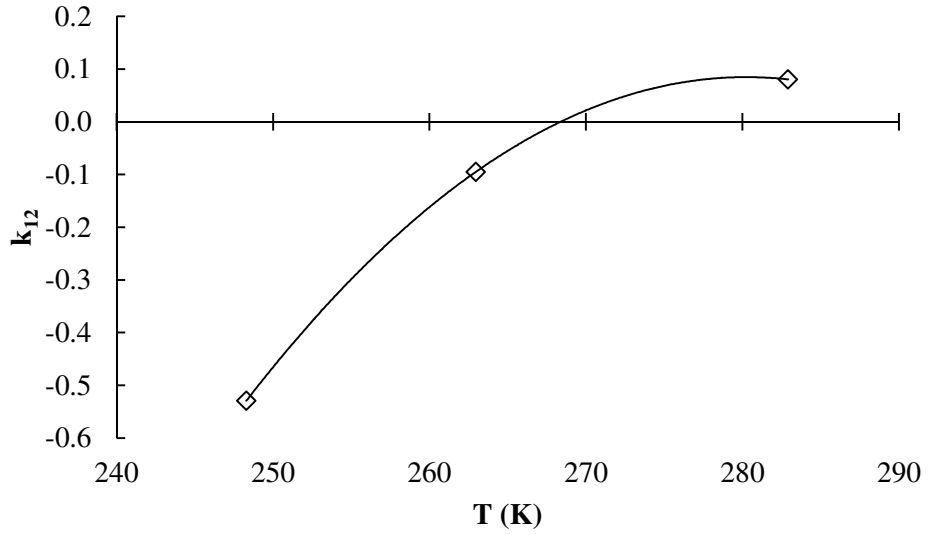

Figure 7.3: The temperature evolution for the binary interaction parameters of the Wong-Sandler mixing rules for the TFE (1) + OFCB (2) system.

The relative volatility, α_{12}, is calculated for the experimental data and then fitted to the model. The plot of these values against the liquid phase composition is shown in Figure 7.4.

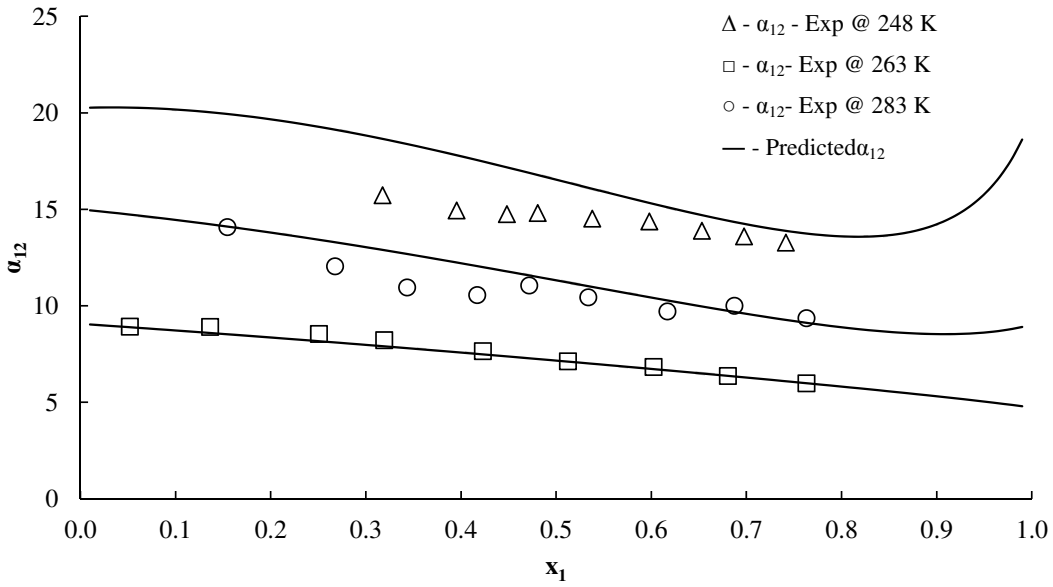

Figure 7.4: Relative volatility (α_{12}) for the TFE (1) + OFCB (2) system, experimental data and model-calculated data.

The uncertainty of the relative volatility for this system was calculated to be ±7,2%. The relative volatility predicted by the model shows fairly largedeviations for the isotherm at 248.3 K. The limitations ofthe apparatus prevented any measurements below 0.25 MPa.

This system reached 0.25 MPa at a vapour phase composition of about 0.5. This only allowed half of the system to be measured. As the model is only fitted to half of a measured isotherm, one mayassume that this contributes to the error in the fit of the model. Due to this inaccurate description of the model, large variations are seen in the relative volatility of the isotherm. There is also some variation in the relative volatility for the isotherm at 262.96 K, where the relative volatility is predicted fairly well for the isotherm at 282.92 K.

7.2.2. Modelling for the TFE (1) + HFP (2) System

The experimental and calculated data points for each isotherm are shown in Table 7.5. Table 7.5 also shows the error between the experimental value and the value calculated by the correlated model. The standard error between the correlated model and the experimental data is calculated by Equation 7.2. Figure 7.5 shows the calculated model with the experimental data points for the TFE (1) + HFP (2) system.

The correlated parameters for the model are shown in Table 7.6. The BIAS % and the MRD % between the experimental data and the calculated model are shown in Table 7.7. The MRD % for the temperatures and vapour phase composition at the 248.14 K and the 263.01 K isotherms are both relatively large. The deviations for the 282.89 K isotherm are fairly good and the model describes the isotherm fairly well. Even though the deviations are larger for the other two systems, it can still be assumed that theydescribe the system accurately.

Table 7.5: Experimental P-x-y data for TFE (1) + HFP (2) at 248.14, 263.01 and 282.89 K and correlated data to the PRWS with MC and NRTL model.

Experimental Data			Calculated data with the specified model							
P_{exp} (MPa)	$x_{1\,exp}$	$y_{1\,exp}$	T_{cal} (K)	ΔT (K)	P_{cal} (MPa)	ΔP (MPa)	$x_{1\,cal}$	Δx_1	$y_{1\,cal}$	Δy_1
					T =248.14 K					
0.1202	0.000	0.000	249.38	-1.24	0.1199	0.0003	0.000	0.0000	0.000	0.0000
0.2581	0.218	0.620	248.12	0.02	0.2582	0.0000	0.218	0.0001	0.629	-0.0088
0.3004	0.270	0.671	248.54	-0.40	0.3002	0.0003	0.270	0.0000	0.688	-0.0167
0.3484	0.338	0.735	248.46	-0.32	0.3482	0.0002	0.337	0.0000	0.748	-0.0133
0.3944	0.403	0.782	248.32	-0.18	0.3943	0.0001	0.403	0.0002	0.794	-0.0117
0.4616	0.492	0.833	248.41	-0.27	0.4614	0.0003	0.492	0.0001	0.841	-0.0081
0.4899	0.543	0.858	247.93	0.21	0.4903	-0.0005	0.542	0.0009	0.864	-0.0067
0.5365	0.602	0.884	248.06	0.08	0.5368	-0.0002	0.602	0.0002	0.887	-0.0033
0.5734	0.648	0.900	248.20	-0.06	0.5734	0.0000	0.648	0.0001	0.903	-0.0028
0.6200	0.703	0.919	248.42	-0.28	0.6195	0.0005	0.703	0.0000	0.920	-0.0010
0.6936	0.784	0.953	248.73	-0.59	0.6915	0.0021	0.784	-0.0006	0.944	0.0081
0.8702	1.000	1.000	248.41	-0.27	0.8695	0.0007	1.000	0.0000	1.000	0.0000
					T = 263.01 K					
0.2246	0.000	0.000	263.68	-0.67	0.2242	0.0004	0.0000	0.0000	0.0000	0.0000
0.3402	0.120	0.391	263.46	-0.45	0.3397	0.0004	0.1200	0.0000	0.3958	-0.0044
0.4408	0.229	0.558	262.77	0.24	0.4412	-0.0004	0.2284	0.0002	0.5827	-0.0249
0.5459	0.331	0.679	262.74	0.27	0.5465	-0.0006	0.3304	0.0003	0.6922	-0.0129
0.6453	0.422	0.752	262.86	0.15	0.6458	-0.0005	0.4219	0.0004	0.7619	-0.0097
0.7576	0.500	0.802	263.94	-0.93	0.7552	0.0024	0.5014	-0.0010	0.8066	-0.0048
0.8078	0.568	0.825	263.02	-0.01	0.8083	-0.0004	0.5668	0.0013	0.8428	-0.0177
0.8863	0.627	0.868	263.36	-0.35	0.8852	0.0010	0.6270	-0.0002	0.8693	-0.0016
0.9866	0.713	0.904	263.28	-0.27	0.9857	0.0009	0.7131	-0.0001	0.9046	-0.0005
1.0755	0.785	0.931	263.26	-0.25	1.0745	0.0009	0.7848	0.0000	0.9312	0.0000
1.1661	0.857	0.961	263.11	-0.10	1.1648	0.0013	0.8574	-0.0002	0.9564	0.0045
1.3741	1.000	1.000	263.33	-0.32	1.3726	0.0015	1.0000	0.0000	1.0000	0.0000
					T = 282.89 K					
0.4561	0.000	0.000	283.20	-0.31	0.4557	0.0004	0.0000	0.0000	0.0000	0.0000
0.5510	0.071	0.220	282.80	0.09	0.5511	-0.0001	0.0707	0.0000	0.2165	0.0035
0.6710	0.144	0.381	283.23	-0.34	0.6702	0.0008	0.1437	-0.0001	0.3753	0.0055
0.8547	0.263	0.557	282.80	0.09	0.8550	-0.0003	0.2628	0.0000	0.5567	0.0004
1.0414	0.367	0.663	283.03	-0.14	1.0408	0.0006	0.3672	-0.0001	0.6643	-0.0012
1.1659	0.443	0.720	282.69	0.20	1.1669	-0.0010	0.4427	0.0004	0.7260	-0.0064
1.2821	0.507	0.757	282.68	0.21	1.2835	-0.0014	0.5065	0.0008	0.7690	-0.0119
1.3965	0.570	0.801	282.63	0.26	1.3982	-0.0017	0.5687	0.0008	0.8058	-0.0047
1.5094	0.626	0.838	282.70	0.19	1.5105	-0.0011	0.6262	0.0001	0.8359	0.0016
1.6220	0.677	0.860	283.00	-0.11	1.6213	0.0007	0.6770	-0.0001	0.8599	-0.0003
1.7599	0.739	0.889	283.26	-0.37	1.7570	0.0029	0.7389	-0.0002	0.8876	0.0018
1.8736	0.790	0.913	283.38	-0.49	1.8692	0.0043	0.7900	-0.0002	0.9097	0.0030
1.9564	0.832	0.928	283.24	-0.35	1.9536	0.0028	0.8322	0.0000	0.9279	-0.0001
2.3465	1.000	1.000	283.25	-0.36	2.3431	0.0034	1.0000	0.0000	1.0000	0.0000

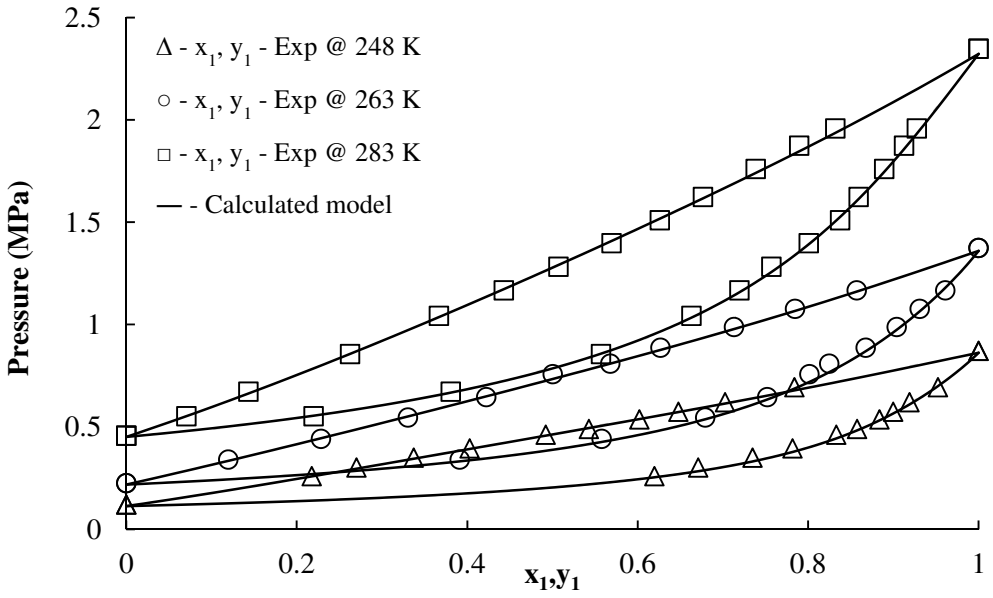

Figure 7.5: The correlated model, with the experimental data, for each isotherm for the TFE (1) + HFP (2) system.

Table 7.6: Adjusted binary interaction parameters for PR-MC-WS-NRTL for the system TFE (1) + HFP (2).

	Parameter		
T (K)	**τ_{12}**	**τ_{21}**	**k_{12}**
248.14	6104	-595	-0.4273
263.01	4456	-1327	-0.1765
282.89	5092	-2311	-0.0321

Table 7.7: Relative deviations, BIAS % and MRD %, based on the experimental data fitted to PR-MC-WS-NRTL

T (K)	**BIAS T %**	**MRD T %**	**BIASP %**	**MRD P %**	**BAIS x_1 %**	**MRD x_1 %**	**BIAS y_1 %**	**MRD y_1 %**
248.14	-0.110	0.132	0.067	0.094	0.023	0.042	-0.892	1.061
263.01	-0.086	0.128	0.067	0.120	0.019	0.079	-1.130	1.223
282.89	-0.036	0.089	0.039	0.104	0.021	0.052	0.047	0.593

Figure 7.6 and Figure 7.7 show the temperature evolution for the NRTL local composition model parameters and the binary interaction parameters, respectively, for the TFE (1) + HFP (2) system. Second-order curves are used to describe the temperature evolution for all three parameters.

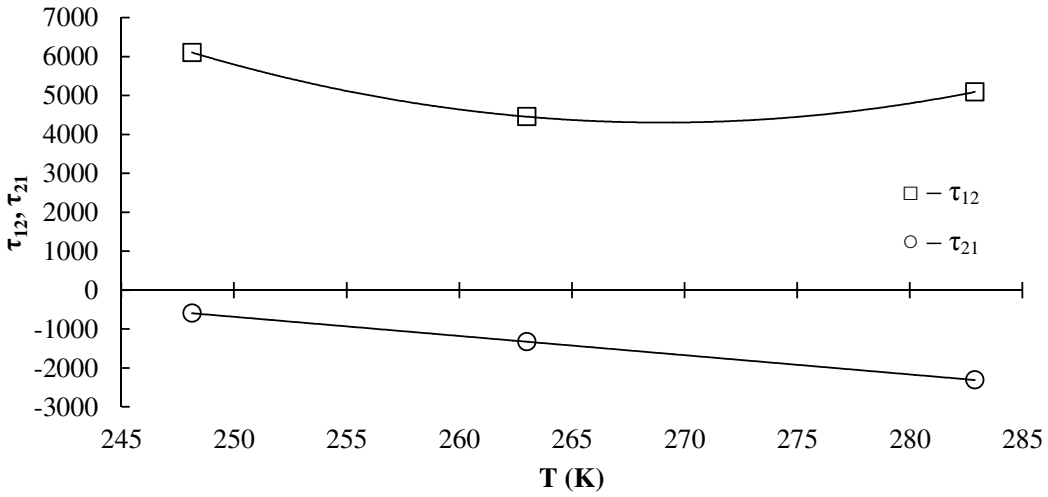

Figure 7.6: The temperature evolution for the NRTL local composition model parameters for all three isotherms for the TFE (1) + HFP (2) system.

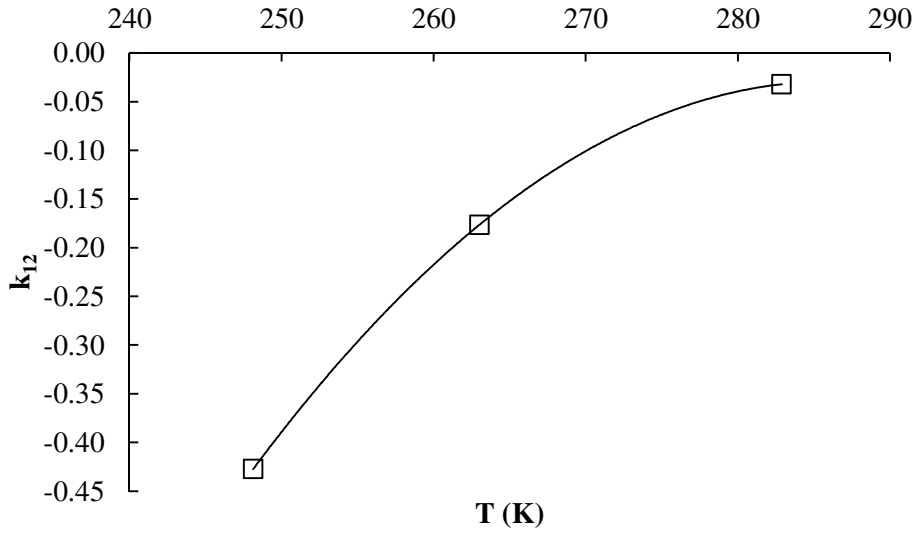

Figure 7.7: The temperature evolution for the binary interaction parameters of the Wong-Sandler mixing rules for the TFE (1) + HFP (2) system.

The uncertainty of the relative volatility for this system was calculated to be ± 6 %. The relative volatility ofthe TFE (1) + HFP (2) system is shown in Figure 7.9. The experimental data areshown with the predicted relative volatility of the selectedmodel. Similarly to that of the TFE (1) + OFCB (2) system, the lowest isotherm at 248.14 K again shows large deviations. The isotherm at 263.01 K shows some deviations but the deviations are less than the deviationof the lowest isotherm. The highest isotherm gives a fairly accurate description of the relative volatility. Any outliers couldpossibly be inaccurate experimental points.

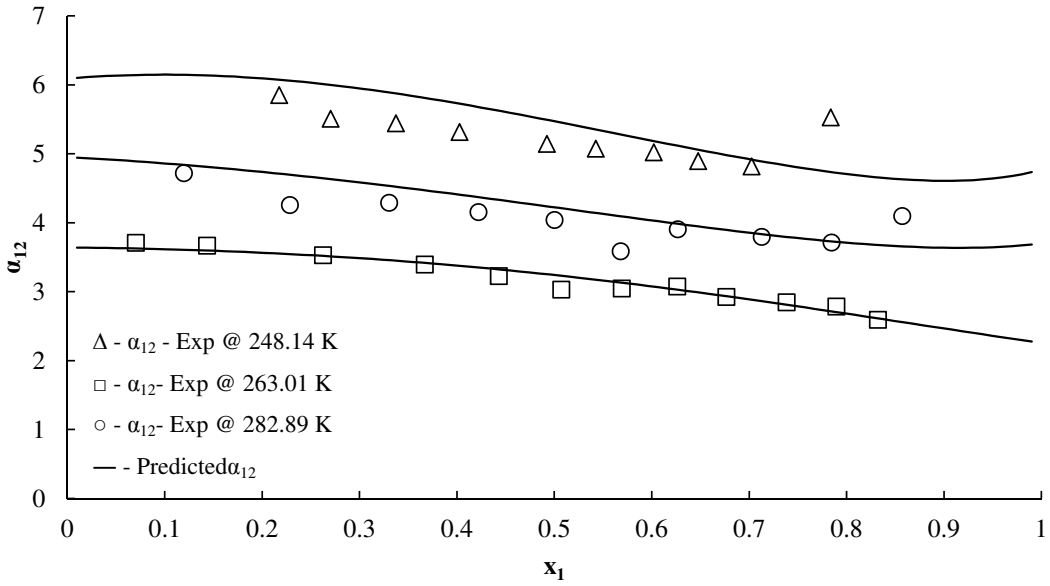

Figure 7.8: Relative volatility (α12) for the TFE (1) + HFP (2) system with experimental data and the relative volatility predicted by the model.

7.2.3. Modelling for the HFP (1) + OFCB (2) System

The experimental and calculated data points for each isotherm are shown in Table 7.8. Table 7.8 also shows the error between the experimental value and the value calculated by the correlated model. The standard error between the correlated model and the experimental data is calculated by Equation 7.2. Figure 7.9 shows the calculated model with the experimental data points for the HFP (1) + OFCB (2) system.

Table 7.8: Experimental P-x-y data for HFP (1) + OFCB (2) and correlated data to PR-MC-WS-NRTL.

Experimental Data			Calculated data with the specified model							
P_{exp} (MPa)	$x_{1\,exp}$	$y_{1\,exp}$	T_{cal} (K)	Δ T (K)	P_{cal}(MPa)	Δ P (MPa)	$x_{1\,cal}$	Δ x_1	$y_{1\,cal}$	Δ y_1
					T = 292.89 K					
0.255	0.000	0.000	292.64	0.25	0.255	-0.0002	0.000	0.0000	0.000	0.0000
0.286	0.092	0.177	292.74	0.15	0.286	-0.0001	0.092	0.0000	0.177	0.0001
0.309	0.152	0.275	292.99	-0.10	0.309	0.0001	0.152	0.0000	0.276	-0.0012
0.336	0.227	0.382	293.01	-0.12	0.336	0.0001	0.227	0.0000	0.385	-0.0031
0.368	0.319	0.491	292.92	-0.03	0.368	0.0000	0.319	0.0000	0.500	-0.0086
0.397	0.399	0.586	292.87	0.02	0.397	0.0000	0.399	0.0000	0.586	0.0000
0.428	0.482	0.662	292.88	0.01	0.428	0.0000	0.481	0.0000	0.662	-0.0007
0.447	0.538	0.709	292.80	0.09	0.447	-0.0001	0.538	0.0001	0.710	-0.0010
0.477	0.612	0.771	292.91	-0.02	0.477	0.0001	0.612	-0.0001	0.766	0.0041
0.504	0.691	0.821	292.82	0.07	0.504	-0.0001	0.691	0.0000	0.821	0.0002
0.528	0.744	0.859	293.07	-0.18	0.528	0.0003	0.744	-0.0001	0.855	0.0035
0.558	0.838	0.906	292.79	0.10	0.558	-0.0002	0.838	0.0001	0.912	-0.0056
0.588	0.904	0.950	293.08	-0.19	0.587	0.0004	0.904	0.0000	0.949	0.0018
0.617	1.000	1.000	292.82	0.07	0.618	-0.0001	1.000	0.0000	1.000	0.0000
					T = 323.02 K					
0.630	0.000	0.000	322.47	0.55	0.632	-0.0013	0.000	0.0000	0.000	0.0000
0.713	0.108	0.179	322.96	0.06	0.713	-0.0002	0.108	0.0000	0.179	0.0002
0.783	0.204	0.310	323.00	0.02	0.783	-0.0001	0.204	0.0000	0.314	-0.0045
0.833	0.269	0.396	323.09	-0.07	0.833	0.0002	0.269	0.0000	0.396	0.0009
0.921	0.384	0.524	323.10	-0.08	0.920	0.0003	0.384	-0.0001	0.521	0.0026
0.986	0.469	0.605	323.07	-0.05	0.986	0.0002	0.469	-0.0001	0.603	0.0017
1.047	0.551	0.675	322.97	0.05	1.047	-0.0002	0.551	0.0000	0.675	0.0003
1.089	0.604	0.720	322.96	0.06	1.089	-0.0003	0.604	0.0000	0.719	0.0012
1.142	0.671	0.773	322.96	0.06	1.142	-0.0002	0.671	0.0000	0.771	0.0023
1.228	0.782	0.852	322.93	0.09	1.229	-0.0004	0.782	0.0000	0.852	-0.0001
1.313	0.885	0.922	323.04	-0.02	1.313	0.0000	0.885	0.0000	0.923	-0.0014
1.395	1.000	1.000	322.91	0.11	1.396	-0.0006	1.000	0.0000	1.000	0.0000
					T = 352.71 K					
1.304	0.000	0.000	352.50	0.21	1.305	-0.0012	0.000	0.0000	0.000	0.0000
1.419	0.091	0.129	352.64	0.07	1.419	-0.0006	0.091	0.0000	0.135	-0.0059
1.534	0.185	0.240	352.57	0.14	1.535	-0.0013	0.185	0.0001	0.258	-0.0183
1.722	0.315	0.403	352.94	-0.23	1.721	0.0018	0.315	0.0000	0.409	-0.0064
1.839	0.396	0.483	353.01	-0.30	1.837	0.0026	0.396	-0.0001	0.493	-0.0106
2.060	0.555	0.639	352.84	-0.13	2.059	0.0013	0.555	-0.0001	0.642	-0.0028
2.258	0.687	0.752	352.84	-0.13	2.257	0.0014	0.687	0.0000	0.752	0.0007
2.361	0.766	0.816	352.52	0.19	2.363	-0.0021	0.766	0.0000	0.815	0.0014
2.528	0.867	0.895	352.65	0.06	2.529	-0.0005	0.867	0.0000	0.893	0.0015
2.609	0.910	0.930	352.79	-0.08	2.607	0.0016	0.910	0.0000	0.927	0.0026
2.737	1.000	1.000	352.52	0.19	2.740	-0.0027	1.000	0.0000	1.000	0.0000

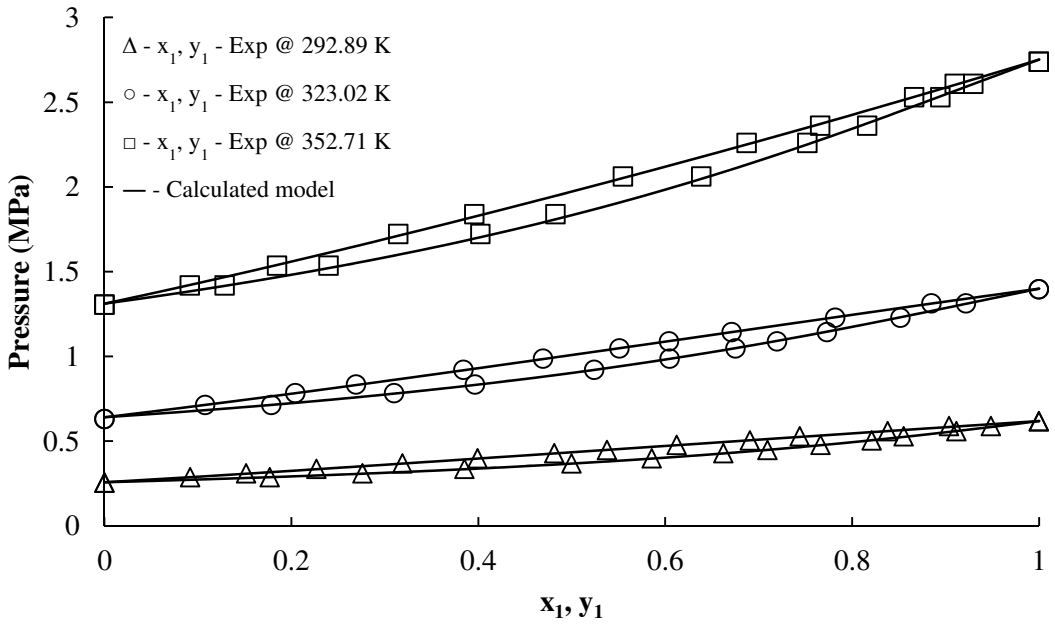

Figure 7.9: The correlated model, with the experimental data, for each isotherm for the HFP (1) + OFCB (2) system.

The correlated parameters for the model are shown in Table 7.9. The BIAS % and the MRD % between the experimental data and the calculated model are shown in Table 7.10. The BIAS % and the MRD % are used to describe the accuracy of the model compared to the experimental data.

Table 7.9: Adjusted binary interaction parameters for PR-MC-WS-NRTL for the system HFP (1) + OFCB (2).

	Parameter		
***T* (K)**	τ_{12}	τ_{21}	k_{12}
292.89	3590	-1191	-0.1823
323.02	4285	-1383	-0.1682
352.71	4016	-2735	0.0274

Table 7.10: Relative deviations, BIAS % and MRD %, based on the experimental data fitted to PR-MC-WS-NRTL

***T* (K)**	**BIAS*T*** **%**	**MRD *T*** **%**	**BIAS*P*** **%**	**MRD *P*** **%**	**BAISx_1** **%**	**MRD x_1** **%**	**BIASy_1** **%**	**MRD y_1** **%**
292.89	0.0025	0.034	-0.002	0.033	0.001	0.008	-0.220	0.424
323.02	0.0203	0.031	-0.025	0.039	-0.001	0.007	0.002	0.325
352.71	-0.0003	0.045	0.000	0.078	0.007	0.021	-1.744	1.902

Figure 7.10 and Figure 7.11 show the temperature evolution for the NRTL local composition model parameters and the binary interaction parameters respectively, for the HFP (1) + OFCB (2) system. Second-order curves are used to describe the temperature evolution for all three parameters.

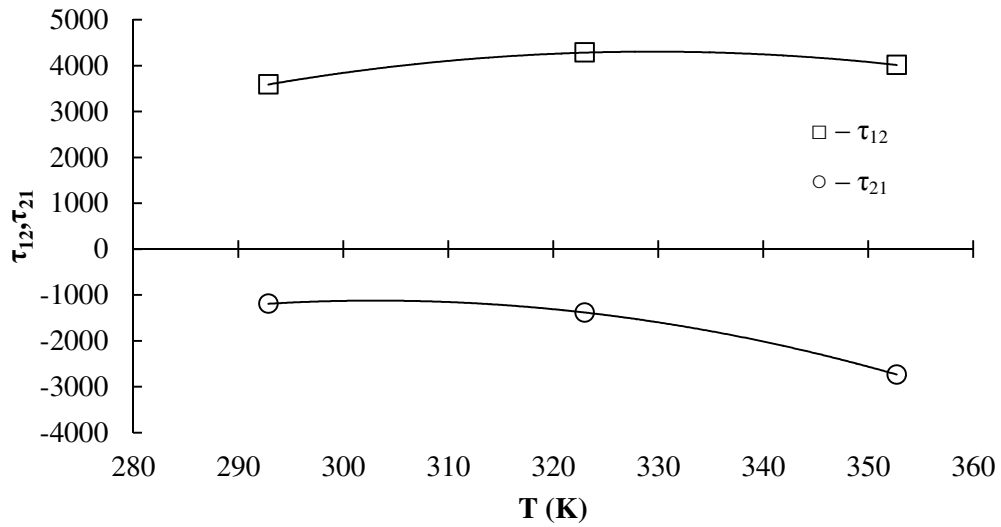

Figure 7.10: The temperature evolution for the NRTL local composition model parameters for all three isotherms for the HFP (1) + OFCB (2) system.

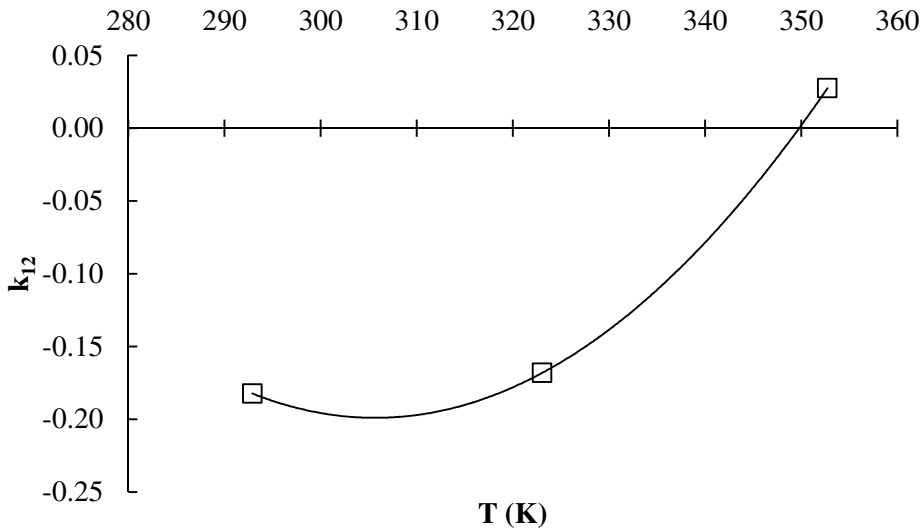

Figure 7.11: The temperature evolution for the binary interaction parameters of the Wong-Sandler mixing rules for the HFP (1) + OFCB (2) system.

The relative volatility ofthe HFP (1) + OFCB (2) system is shown in Figure 7.12. The uncertainty of the relative volatility for this system was calculated to be ± 14 %.

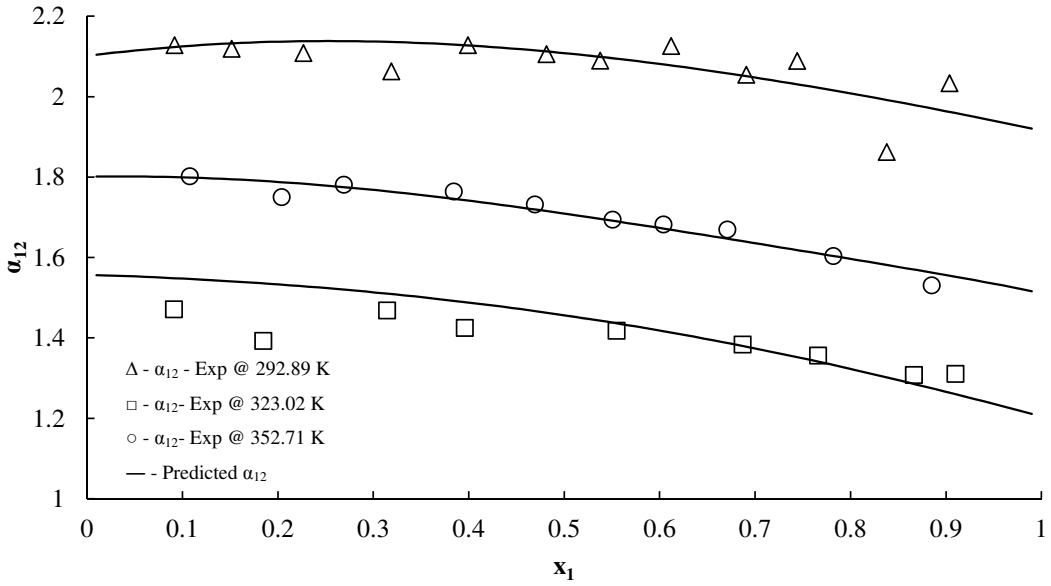

Figure 7.12: Relative volatility (α_{12}) ofthe HFP (1) + OFCB (2) system with experimental data and the relative volatility predicted by the model.

7.3. Thermodynamic Consistency Test

The Point Test, suggested by Smith and Van Ness (2001) was used to test consistency in the calculated model. The point test is summarized in Chapter 2.11. The error between each experimental vapour phase point and the corresponding calculated vapour phase point is calculatedfor each system. The average absolute error is then calculated for each system and is used to confirm the thermodynamic consistency of the experimental data.

7.3.1. Consistency test for the TFE (1) + OFCB (2) system

The calculated error for each point in each isotherm is shown in Figure 7.13. The average absolute error for each isotherm is summarized in Table 7.11. The average absolute error for each isotherm falls within the limit of 0.01 and is therefore thermodynamically consistent.

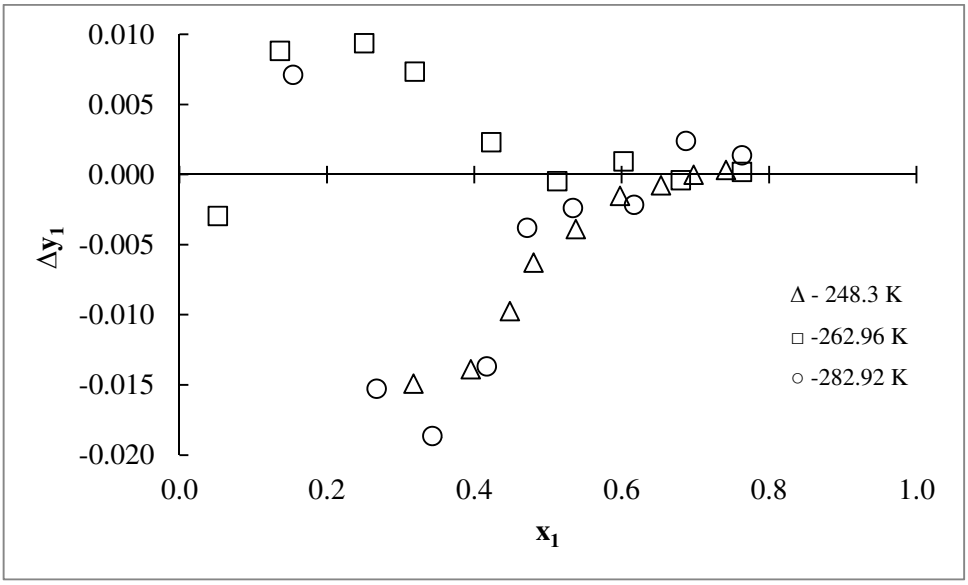

Figure 7.13: The deviations in the vapour phase composition calculations for each isotherm for the TFE (1) + OFCB (2) system.

Table 7.11: Average absolute error for each isotherm in the TFE(1) + OFCB (2) system for the point test.

T (K)	Average |Δy|
248.3	0.006
262.96	0.007
282.92	0.004

The system passes the thermodynamic consistency test sincethe absolute average deviation is below the 0.01 % criterion. The model and data can therefore be used in solving future design problems.

7.3.2. Consistency Test for the TFE (1) + HFP (2) System

The calculated error for each point in each isotherm is shown in Figure 7.14. The average absolute error for each isotherm is summarized in Table 7.12.

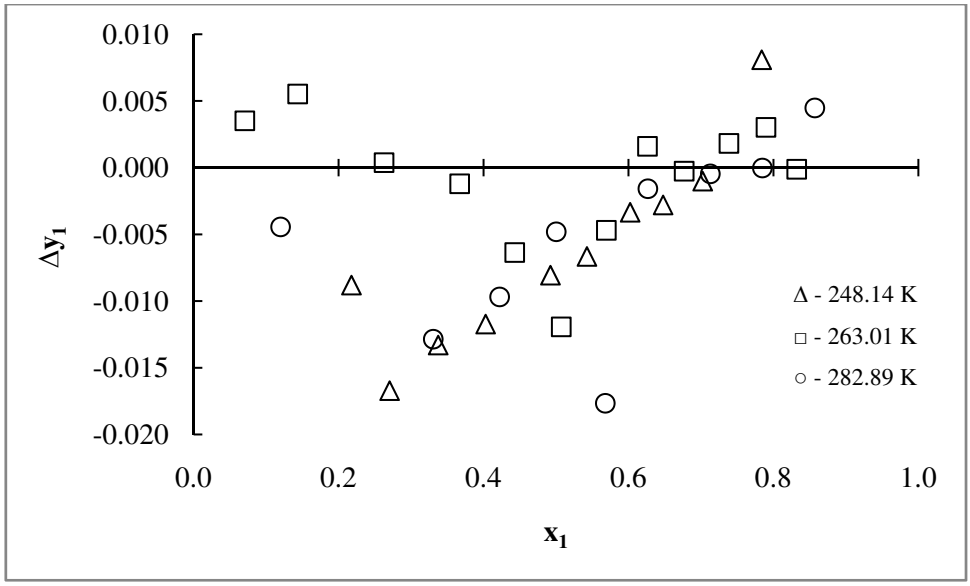

Figure 7.14: The deviations in the vapour phase composition calculations for each isotherm.

Table 7.12: Average absolute error for each isotherm in the TFE(1) + HFP (2) system for the point test.

T (K)	Average |Δy|
248.14	0.008
263.01	0.008
282.89	0.003

The average absolute error for each isotherm falls within the limit of 0.01 and is therefore thermodynamically consistent. The model can be used in future calculations.

7.3.3. Consistency Test for the HFP (1) + OFCB (2) System

The calculated error for each point in each isotherm is shown in Figure 7.15. The average absolute error for each isotherm is summarized in Table 7.13.

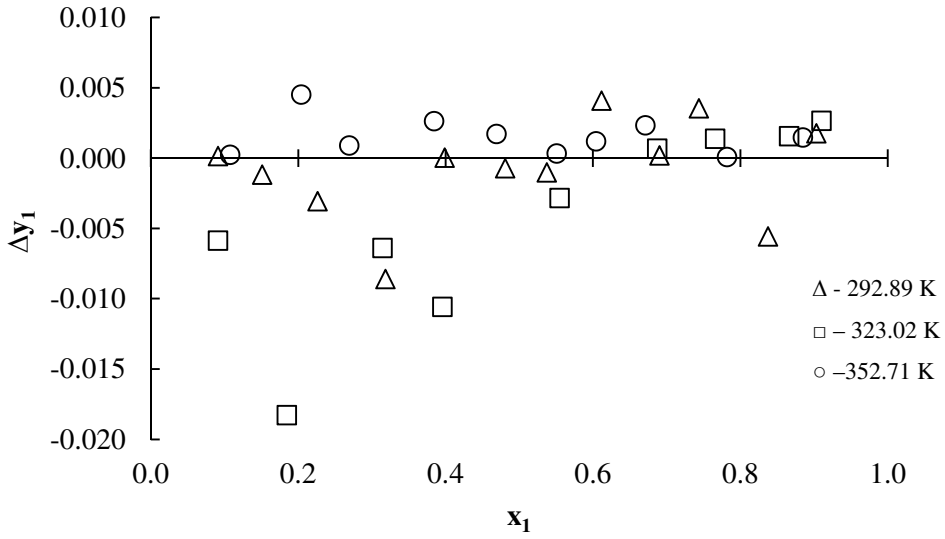

Figure 7.15: The deviations in the vapour phase composition calculations for each isotherm.

Table 7.13: Average absolute error for each isotherm in the HFP(1) + OFCB (2) system for the point test.

T (K)	Average |Δy|
292.89	0.002
323.02	0.002
352.71	0.006

The isotherm at 323.02 K has a clear outlier at a liquid composition of 0.2. This is most probablydue to a bad experimental point. The average absolute error for each isotherm still falls within the limit of 0.01 and is therefore thermodynamically consistent.

Chapter 8

Batch Distillation Column Design

8. Batch Distillation Column Design

The column design and optimisation werecompleted with the aidof Aspen Batch Distillation, a module which is part of the Aspen Plus 7.1 packages. This module allows the design of batch distillation columns. The properties of the components are then predicted with the Aspen Properties Plus module, which allowsthemore accurate prediction of component properties foruse in design calculations. The parameters of the thermodynamic models described in the previous chapters were used in the calculations of the batch distillation column. Unlike the parameters shown in the previous chapter, a temperature dependency for the model parameters wasincluded and isshown in Table 8.1. Equation 8.1 is used to fit the NTRL activity coefficient model to the experimental data:

$$\tau_{ij} = a_{ij} + {}^{b_{ij}}/_{T} + e_{ij} \ln T + f_{ij} T \qquad (8.1)$$

The parameters fitted tothe NTRL model in Chapter 7only used a_{ij} for fitting the VLE data. A temperature dependency for calculations with the fitted parameters gives a more accurate prediction, so temperature dependent parameters such asb_{ij} and f_{ij} were used to fit the experimental data to the NRTL model. c_{ij} was kept constant at 0.3 similarly to the data fitted in Chapter 7. Aspen Batch Distillation utilizes arigorous method for the simulation of the columns that aresetup for the configuration described in this chapter.

Table 8.1: The temperature dependent parameters for the thermodynamic models used in the batch distillation column.

	a_{ij}	a_{ji}	b_{ij}	b_{ji}	f_{ij}	f_{ji}
τ_{12}	10.71	-3.807	-2336	830.2	-	-
τ_{13}	-1.039	1.920			9.0115E-03	-0.05979
τ_{23}	2.463	-1.076	-360.7	104.9	-	-

The main purpose of the column is to produce TFE with a purity of at least 99.999 %. The column must also be able to produce pure HFP. Another constraint for the column is that it mustrecover as much as possible of the components, with an initialrecovery target of at least 80 % of the charged TFE. Another constraint onthe design is that the time required for the distillation must be kept to a minimum.

The average mixture consists of 60 % TFE, 30 % HFP and 10 % OFCB on a mass basis. The column design is based on this initial mixture. The initial charge to the still pot is about 1 kg, as only a single cylinder is distilled at a time and, as mentioned earlier, a cylinder mayonly be loaded to 1.8 bar. Table 8.2 shows the composition of the gas on a mole basis.

Table 8.2: Mole composition of the initial mixture charge to the column.

	Moles charged	**Mole fraction**
TFE	0.00639	0.7059
HFP	0.00216	0.2353
OFCB	0.00054	0.0588

The column is designed by keeping the reflux ratio and the heat duty to the still pot constant. The other design variables selectedfor the design arethe still pot geometry, a constant pressure drop across the column, a constant liquid holdup on the stages and assuming the column starts at a total reflux condition. The time required to complete the distillation should be kept to a minimum as should the number of equilibrium stages in the column.

The specific heat duty to the still pot was selectedas 175 W. When working with such small quantities, this is more than enough to ensure sufficiently high boil-up rates. The Research and Development: Applied ChemistryDivision at Necsa planned to purchase a JulaboFP89-ME Ultra-Low Refrigerated Circulator (www.julabo.de). This unit can deliver a heat duty of 200 W at -80 °C. Using this as themaximum that can be delivered to the still pot and

adjusting for possible heat losses, the heat duty was selectedas 175 W. The temperature will have to change constantly to achieve a constant heat duty in the still pot. The Julabo unit includes a programmable temperature controller and this can be used to control the temperature in the still pot to achieve the constant heat duty.

The liquid holdup on the stages was estimated at 3 % of the initial charge to the pot, which is about 0.0003 kmol per equilibrium stage.

The optimum column design is when the target purity and recovery of TFE areachieved in the shortest time possible. The design target is to find the optimal number of equilibrium stages that will achieve the above-mentioned targets. Once this optimal design has beenfound, one can investigate whether the column would alsobe able to separate HFP. The optimal design can be adjusted to produce pure HFP, without sacrificing too much of the original TFE targets.

8.1. Initial Design for TFE Separation

The first step in the design process was to investigate the effect of increasing the reflux ratio and increasing the number of equilibrium stages inthe distillation process. The design looked at using between 2 and 7 equilibrium stages in the proposed column. A quick investigation showed that more than 7 equilibrium stages wouldnot significantly increase the purity of the productand require a far longer time to complete the distillation. Increasing the reflux ratio too high wouldincrease the heat duties required in the condenser as well as increasing the diameter of the distillation column. Figure 8.1 shows the time required to recover about 80 % TFE at various reflux ratios for a column with threeequilibrium stages. Figure 8.1 indicates that the time required to recover about 80 % TFE increases as the reflux ratio increases. Figure 8.2 shows the increase inthe TFE purity with an increasing reflux ratio for a column with three equilibrium stages. The TFE purity reaches a maximum when the reflux ratio increases above 2. Figure 8.1 indicatesthat this occurs at about 0.5 hours. Similar graphs can be drawnfor the other configurations with a higher numberof equilibrium stages. Figure 8.3 and Figure 8.4 give a summary of the time required to achieve a 99.999 % purity of TFE and a recovery of 80 % at various reflux ratios and equilibrium stages.

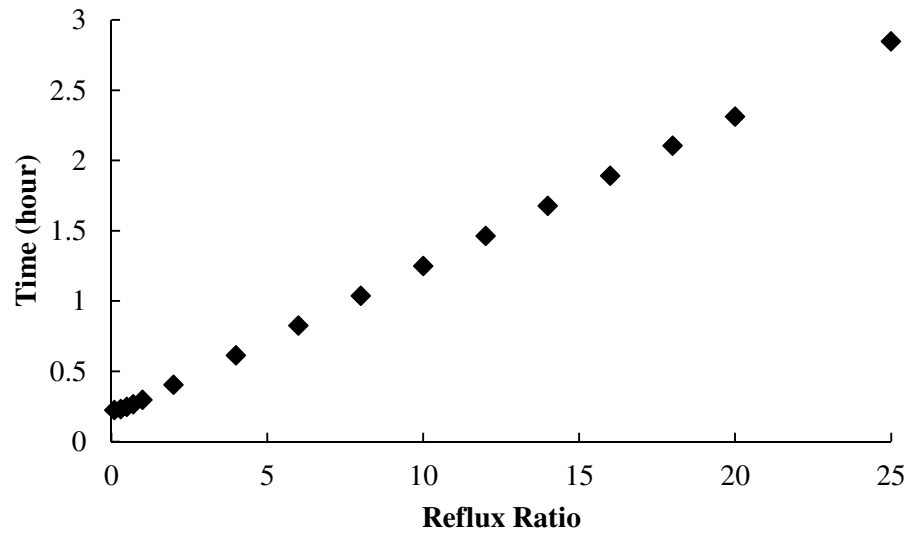

Figure 8.1: The time increases as the reflux ratio increases for a column with threestages.

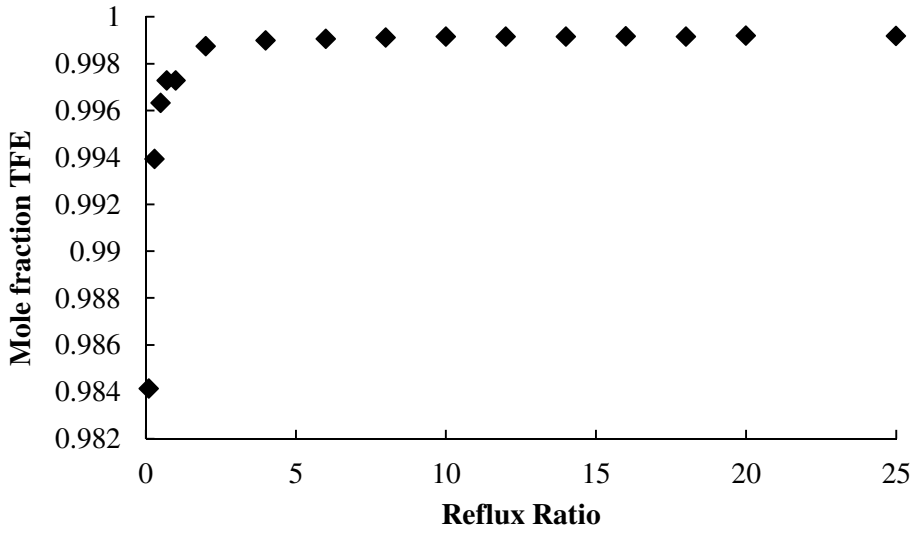

Figure 8.2: A quick increase in the TFE purity can be seen as the reflux ratio increases.

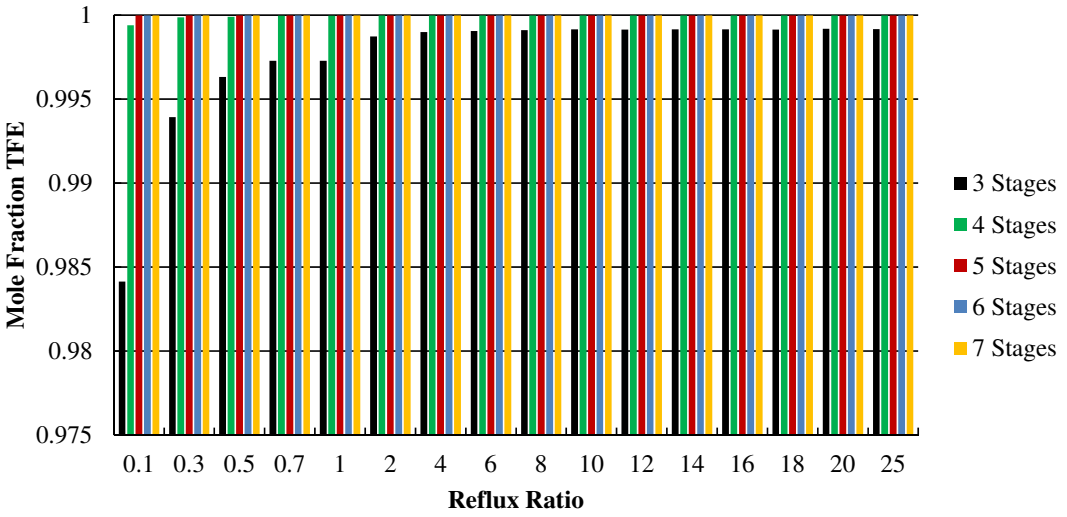

Figure 8.3: High purity TFE is produced by more than fourstages at all reflux ratios.

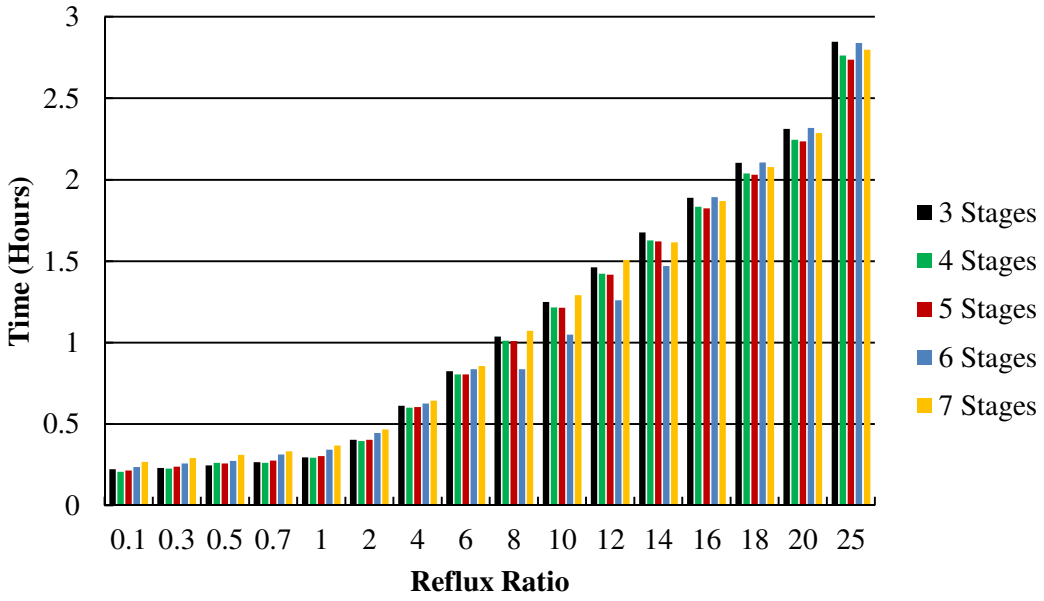

Figure 8.4: Long distillation periods are required at reflux ratios above eight.

To find the optimum design configuration for the column, the data shown in Figure 8.3 and Figure 8.4 must be analyzedtogether. It is clear from these figures that reflux ratios above 8 should be avoided, as they produce no significant increase in the purity but considerably increase thetime required for the distillation. Reflux ratios below 0.7 show worse separation than the other reflux ratios and should be avoided too. The ideal reflux ratio is in the region of 1 to 8.

A similar comparison can be made to select the right numberof equilibrium stages. Four and five stage separation columns require less time than the other configurations. The five-stage configurationrequiresslightly lessdistillation timeto reach high purity TFE and an 80 % recovery. Five equilibrium stages were selected for further design options.

The simulation, put together in Aspen Batch Distillation, was run until the still pot had almost no TFE left for various reflux ratios with fiveequilibrium stages. The time required,the TFE distillate composition, the amount of distillate and the recovery of TFE for some of these simulations are shown in Table 8.3. It is apparent that a recovery of more than 80 % can be achieved with any one of these configurations. While still adhering to the 99.999 % purity constraint, the recovery of TFE can be pushed up to almost 90 % if a reflux ratio of 4 is used for the column operation.

Table 8.3: A summary of the recovery of TFE at various reflux ratios for a five-stage column

Reflux Ratio = 2				**Reflux Ratio = 3**				**Reflux Ratio = 4**			
Time (Hours)	Mole fraction TFE	Distillate Holdup kmol	% TFE recovered	Time (Hours)	Mole fraction TFE	Distillate Holdup kmol	% TFE recovered	Time (Hours)	Mole fraction TFE	Distillate Holdup kmol	% TFE recovered
0.00	0	0.0000	0.00	0	0.000000	0.0000	0.00	0	0.000000	0.0000	0.00
0.03	1.000000	0.0011	16.96	0.04	1.000000	0.0010	15.09	0.05	1.000000	0.0009	13.72
0.06	0.999999	0.0015	23.58	0.08	0.999999	0.0014	21.47	0.09	0.999999	0.0013	20.06
0.09	0.999999	0.0019	29.36	0.12	0.999999	0.0017	27.26	0.14	0.999999	0.0017	25.92
0.13	0.999998	0.0022	34.55	0.16	0.999998	0.0021	32.71	0.19	0.999998	0.0020	31.50
0.16	0.999998	0.0025	39.55	0.20	0.999998	0.0024	38.00	0.23	0.999998	0.0024	37.03
0.19	0.999998	0.0028	44.57	0.23	0.999997	0.0028	43.43	0.28	0.999997	0.0027	42.68
0.22	0.999997	0.0032	49.86	0.27	0.999997	0.0031	48.98	0.33	0.999997	0.0031	48.36
0.25	0.999997	0.0035	55.16	0.31	0.999997	0.0035	54.46	0.38	0.999996	0.0034	53.96
0.28	0.999996	0.0039	60.36	0.35	0.999996	0.0038	59.83	0.42	0.999996	0.0038	59.48
0.31	0.999996	0.0042	65.41	0.39	0.999996	0.0042	65.09	0.47	0.999995	0.0041	64.93
0.35	0.999995	0.0045	70.30	0.43	0.999995	0.0045	70.23	0.52	0.999995	0.0045	70.25
0.38	0.999995	0.0048	74.98	0.47	0.999995	0.0048	75.20	0.56	0.999994	0.0048	75.40
0.41	0.999995	0.0051	79.42	0.51	0.999994	0.0051	79.91	0.61	0.999994	0.0051	80.34
0.44	0.999994	0.0053	83.63	0.55	0.999994	0.0054	84.43	0.66	0.999993	0.0054	85.12
0.47	0.999994	0.0056	87.70	0.59	0.999993	0.0057	88.84	0.70	0.999993	0.0057	89.84
0.50	0.999976	0.0059	91.67	0.63	0.999918	0.0060	93.26	0.75	0.999715	0.0060	94.62
0.53	0.998920	0.0061	95.72	0.67	0.993736	0.0063	97.49	0.80	0.982562	0.0064	98.30
0.57	0.966106	0.0065	98.44	0.70	0.940549	0.0067	98.57	0.84	0.935586	0.0067	98.58
0.60	0.905019	0.0070	98.59	0.74	0.902640	0.0070	98.60	0.89	0.904125	0.0070	98.59
0.63	0.871072	0.0072	98.60	0.78	0.874731	0.0072	98.60	0.94	0.876634	0.0072	98.58
0.66	0.846280	0.0074	98.60	0.82	0.849640	0.0074	98.59	0.99	0.851309	0.0074	98.59
0.69	0.824573	0.0076	98.60	0.86	0.826961	0.0076	98.60	1.03	0.828201	0.0076	98.59
0.72	0.805369	0.0078	98.60	0.90	0.806590	0.0078	98.60	1.08	0.807220	0.0078	98.58
0.75	0.787526	0.0080	98.59	0.94	0.787530	0.0080	98.60	1.13	0.787465	0.0080	98.59

The final design, based solely on the separation of TFE, will consist of fiveequilibrium stages and be operated at a reflux ratio of 4. Table 8.4 shows the same results for the energy requirements for the still pot and the condenser for this configuration.

Table 8.4: Heat requirements for the still pot and condenser for a five-stage column.

Still Pot				Condenser			
Time (Hours)	**Temperature (°C)**	**Pressure (bar)**	**Heat duty (W)**	**Time (Hours)**	**Temperature (°C)**	**Pressure (bar)**	**Heat duty (W)**
0.00	-67.34	1.11	175	0.00	-81.64	1.01	-1546
0.03	-65.91	1.11	175	0.03	-81.64	1.01	-168
0.06	-65.28	1.11	175	0.06	-81.64	1.01	-153
0.09	-64.63	1.11	175	0.09	-81.64	1.01	-146
0.12	-63.97	1.11	175	0.12	-81.64	1.01	-140
0.15	-63.28	1.11	175	0.15	-81.64	1.01	-135
0.18	-62.55	1.11	175	0.18	-81.64	1.01	-131
0.21	-61.78	1.11	175	0.21	-81.64	1.01	-128
0.24	-60.93	1.11	175	0.24	-81.64	1.01	-128
0.27	-60.00	1.11	175	0.27	-81.64	1.01	-130
0.30	-58.95	1.11	175	0.30	-81.64	1.01	-132
0.33	-57.80	1.11	175	0.33	-81.64	1.01	-132
0.36	-56.53	1.11	175	0.36	-81.64	1.01	-130
0.39	-55.11	1.11	175	0.39	-81.64	1.01	-129
0.42	-53.54	1.11	175	0.42	-81.64	1.01	-127
0.45	-51.76	1.11	175	0.45	-81.64	1.01	-127
0.48	-49.73	1.11	175	0.48	-81.64	1.01	-124
0.51	-47.41	1.11	175	0.51	-81.64	1.01	-123
0.54	-44.74	1.11	175	0.54	-81.64	1.01	-120
0.57	-41.67	1.11	175	0.57	-81.64	1.01	-117
0.60	-38.22	1.11	175	0.60	-81.64	1.01	-114
0.63	-34.46	1.11	175	0.63	-81.64	1.01	-111
0.66	-30.61	1.11	175	0.66	-81.64	1.01	-109
0.68	-27.04	1.11	175	0.68	-81.64	1.01	-109
0.71	-24.21	1.11	175	0.71	-81.63	1.01	-111

The distillate collection is stopped as soon as a TFE purity of 99.999 % is reached. The composition profile and the build-up in the still pot and distillate receiverare displayed in Table 8.5. Figure 8.5 shows the vapour composition profile over the equilibrium stages as the distillation is completed and Figure 8.6 gives the liquid composition profile. Figure 8.7 gives the temperature profile across the distillation column. All the targets for the separation of TFE aremet with this design.Only 43 minutes are needed to complete the distillation and a recovery of almost 90 %is achieved, 10 % more than the original target. Table 8.6 shows the amount and composition of the mixture that is left in the column as soon as the desired TFE

purity has beenreached. The values in Table 8.6 include the liquid holdup on the stages as well as the liquid that is left in the still pot. The mixture now contains 67 % HFP which can now be purified.

Table 8.5: Composition profile in the still pot and distillate receiver.

	Still Pot				Distillate Receiver				
Time (hours)	**HFP**	**OFCB**	**TFE**	**Liquid holdup (kmol)**	**HFP**	**OFCB**	**TFE**	**Liquid holdup (kmol)**	**% TFE recovered**
0.00	0.2662	0.0667	0.6671	0.0081	0	0	0	0.0000	0.00
0.03	0.2918	0.0731	0.6351	0.0074	3.84×10^{-09}	0	1	0.0007	11.24
0.06	0.3028	0.0759	0.6213	0.0071	4.27×10^{-09}	0	1	0.0010	15.48
0.09	0.3140	0.0788	0.6072	0.0069	4.69×10^{-09}	0	1	0.0012	19.47
0.12	0.3255	0.0817	0.5929	0.0066	5.12×10^{-09}	0	1	0.0015	23.29
0.15	0.3372	0.0847	0.5782	0.0064	5.59×10^{-09}	0	1	0.0017	26.90
0.18	0.3494	0.0878	0.5628	0.0062	6.10×10^{-09}	0	1	0.0019	30.44
0.21	0.3623	0.0910	0.5467	0.0059	6.64×10^{-09}	0	1	0.0022	33.93
0.24	0.3763	0.0946	0.5291	0.0057	7.25×10^{-09}	0	1	0.0024	37.45
0.27	0.3914	0.0985	0.5100	0.0055	7.93×10^{-09}	0	1	0.0026	41.02
0.30	0.4082	0.1029	0.4890	0.0052	8.74×10^{-09}	0	1	0.0029	44.63
0.33	0.4263	0.1076	0.4661	0.0050	9.75×10^{-09}	0	1	0.0031	48.25
0.36	0.4458	0.1126	0.4416	0.0048	1.10×10^{-08}	0	1	0.0033	51.82
0.39	0.4668	0.1182	0.4150	0.0046	1.26×10^{-08}	0	1	0.0035	55.34
0.42	0.4895	0.1242	0.3863	0.0043	1.46×10^{-08}	0	1	0.0038	58.84
0.45	0.5139	0.1308	0.3552	0.0041	1.76×10^{-08}	0	1	0.0040	62.30
0.48	0.5403	0.1381	0.3216	0.0039	2.13×10^{-08}	0	1	0.0042	65.74
0.51	0.5684	0.1460	0.2856	0.0037	2.71×10^{-08}	0	1	0.0044	69.12
0.54	0.5981	0.1547	0.2472	0.0035	3.63×10^{-08}	0	1	0.0046	72.44
0.57	0.6287	0.1642	0.2071	0.0033	5.34×10^{-08}	0	1	0.0048	75.68
0.60	0.6594	0.1744	0.1662	0.0031	8.77×10^{-08}	0	1	0.0050	78.84
0.63	0.6889	0.1854	0.1258	0.0029	1.72×10^{-07}	0	1	0.0052	81.91
0.66	0.7154	0.1972	0.0874	0.0027	4.25×10^{-07}	0	1	0.0054	84.93
0.68	0.7362	0.2102	0.0537	0.0025	1.59×10^{-06}	0	0.999998	0.0056	87.92
0.71	0.7477	0.2245	0.0278	0.0023	1.00×10^{-05}	0	0.999990	0.0058	90.91

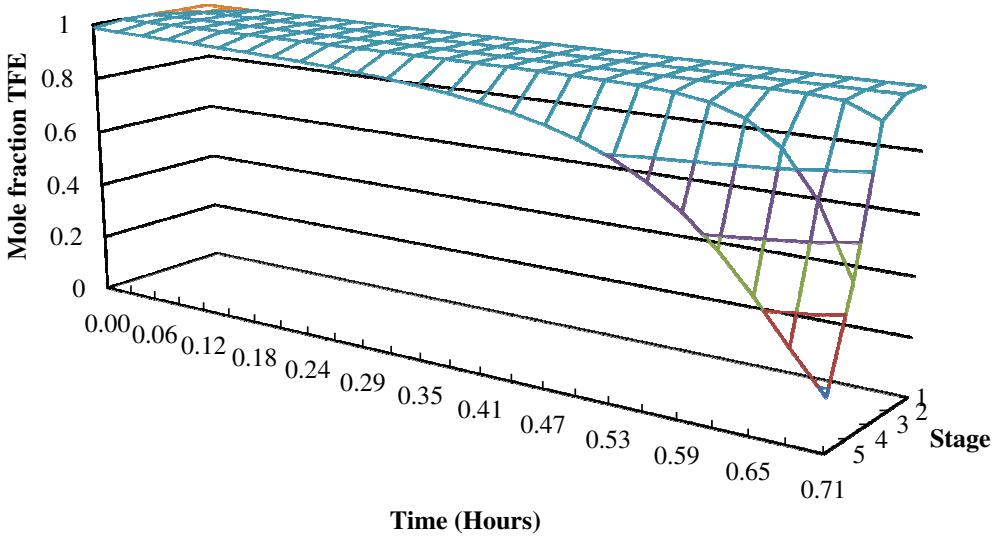

Figure 8.5: The TFE vapour composition over the equilibrium stages.

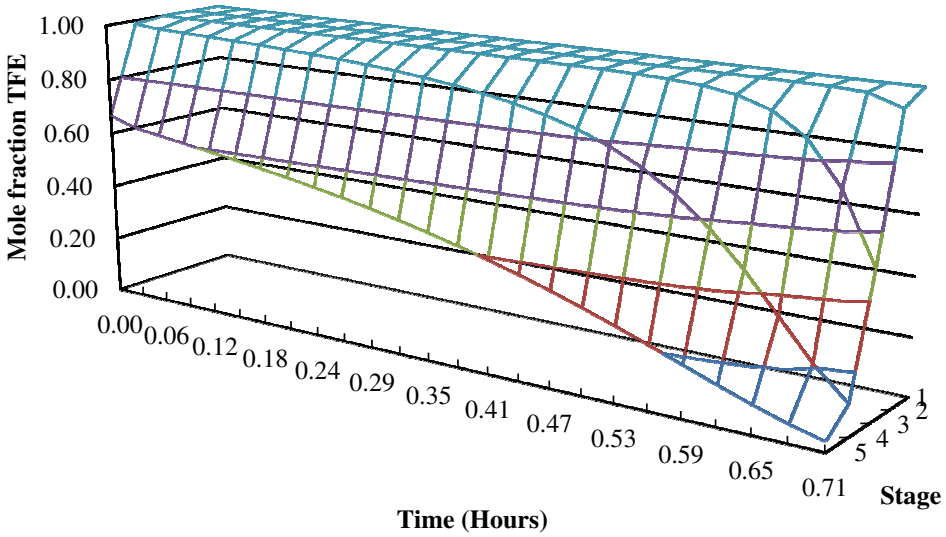

Figure 8.6: The TFE liquid composition over the equilibrium stages.

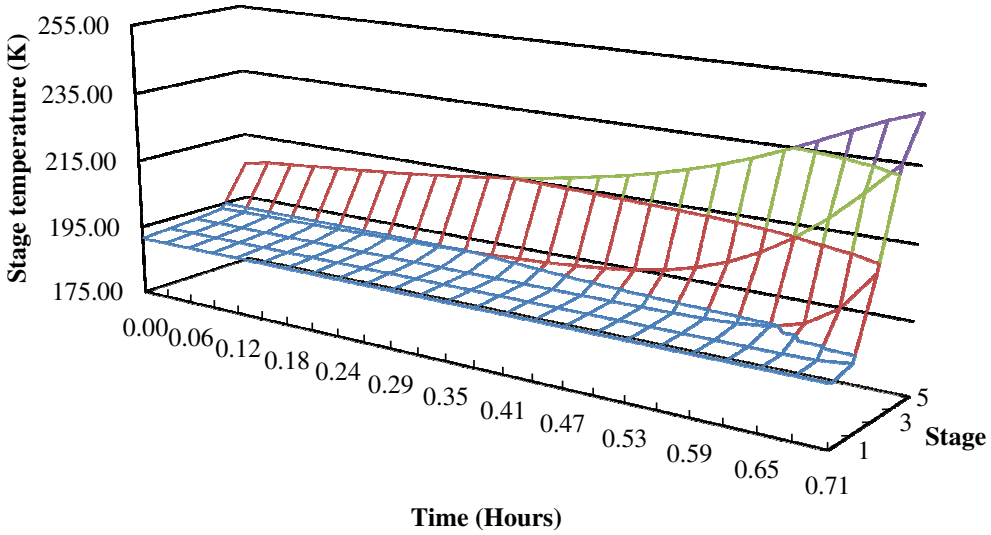

Figure 8.7: The temperature profile of the stages during distillation.

Table 8.6: A summary of the amount of each component that is left after the first main cut.

	OFCB	HFP	TFE
Holdup (kmol)	0.0005	0.0022	0.0005
Mole fraction	0.1693	0.6770	0.1537

8.2. Separation of HFP

The next step of the design process wasto evaluate the possibility of separating HFP with this configuration too. No clear targets for purity or recovery were set for the HFP. To achieve high purity HFP, a fairly large intermediate cut must be made. This cut will not only remove the 10 % TFE that is still left in the column, but will also include a fair amount of HFP. An optimal intermediate cut must be foundin order to produce a high recovery of HFP or a high purity HFP. Producing a product with a high recovery of HFP means that the purity will be fairly low, since a small cut will have to be made. The larger the intermediate cut the higher the purity of the HFP produced, but this will also reducethe overall recovery of HFP.

The intermediate cut will have to be bigger than 0.000491 kmol, as that is the amount of TFE left in the column. Several sizes were investigated for the intermediate cut. After the intermediate cut, the final cut is made for pure HFP. Almost all of the contents in the still pot

are evaporated and the final cut is then analysed along with the intermediate cut. Table 8.7 shows a summary of some of the results found for various sizes of intermediate cuts. The reflux ratio was kept the same as that used in the previous section. The final compositions of each cut are shown in Table 8.7. The highest recovery of HFP is 81.3 % and this was achieved with an intermediate cut of 0.0005 kmol but yielded a final product with a composition of only 95 % HFP. The highest purity of HFP in the final cut was achieved with an intermediate cut size of 0.0008 kmol, thoughthe recovery at this point was only 69.7 %.

Table 8.7: Composition of the intermediate and final cut distillation products.

Intermediate cut size (kmol)	Time (Hours)	Intermediate cut composition			Final cut composition			Accumulated final cut (kmol)
		HFP	OFCB	TFE	HFP	OFCB	TFE	
5.00×10^{-04}	1.20	0.1014	1.11×10^{-04}	0.8984	0.9511	0.0227	0.0262	0.001847
5.50×10^{-04}	1.20	0.1459	2.17×10^{-04}	0.8539	0.9612	0.0233	0.0155	0.001798
6.00×10^{-04}	1.20	0.1960	3.78×10^{-04}	0.8035	0.9673	0.0239	0.0088	0.001748
6.50×10^{-04}	1.20	0.2469	5.85×10^{-04}	0.7525	0.9706	0.0244	0.0050	0.001697
7.00×10^{-04}	1.20	0.2952	8.22×10^{-04}	0.7033	0.9718	0.0253	0.0029	0.001649
7.50×10^{-04}	1.20	0.3392	1.07×10^{-03}	0.6597	0.9726	0.0257	0.0017	0.001597
8.00×10^{-04}	1.20	0.3789	1.32×10^{-03}	0.6198	0.9724	0.0265	0.0011	0.001549
8.50×10^{-04}	1.20	0.4143	1.57×10^{-03}	0.5841	0.9722	0.0271	0.0007	0.001498

Then this configuration was evaluated for a high purity product and a high recovery of HFP. The intermediate cut sizes from the analysis mentioned above wereused. The targets for this evaluation were:

- HFP purity of 99 %
- HFP recovery in the final cut of 80 %

The first distillation step to produce pure TFE was repeated for each run and showed the same results as expected. The composition analysis for the still pot and distillate receivers for the simulation to produce 99 % HFP is shown in Table 8.8. A purity of 99 % HFP was achieved by taking an intermediate cut size of 0.0008 kmol and the whole distillation process took about one hour. The final distillation cut contained only 0.00076 kmol and had an HFP recovery of only 34 %. The still pot contained 0.000302 kmol of HFP and 0.000384 kmol of OFCB, with a negligible amount of TFE. This isan indication that the separation in the column is insufficient to produce high purity HFP at a high recovery.

Table 8.8: A composition analysis on the 99 % pure HFP simulation.

Time (hours)	Still pot composition			Distillate receiver 2			Distillate receiver 3		
	HFP	OFCB	TFE	HFP	OFCB	TFE	HFP	OFCB	TFE
0.75	0.7476	0.2388	1.36E-02	2.96E-03	4.67E-07	0.9970	-	-	-
0.79	0.7289	0.2680	3.06E-03	7.70E-02	7.24E-05	0.9229	-	-	-
0.83	0.6857	0.3140	3.62E-04	3.77E-01	1.32E-03	0.6214	-	-	-
0.87	0.6374	0.3626	3.38E-05	4.14E-01	1.57E-03	0.5841	0.98898	6.16E-03	0.004858
0.91	0.5856	0.4144	4.71E-06	-	-	-	0.99049	6.81E-03	0.002701
0.95	0.5216	0.4784	5.60E-07	-	-	-	0.99057	7.58E-03	0.001851
0.99	0.4414	0.5586	3.23E-08	-	-	-	0.99000	8.61E-03	0.001395

Next a product with an HFP recovery of 80 % was investigated. Table 8.9 summarizes the composition analysis of this simulation. An HFP recovery of 79.97 % was achieved in about 1.2 hours with an HFP purity of 96.12 %. A better recovery is seen in this simulation although the purity of HFP dropped by3 %. The still pot only had 0.00000649 kmol of HFP and OFCB left, which wasless than 1 % of the original mixture. Should the distillation time exceed 1.2 hours on this configuration, the still pot woulddry out and so wouldthe rest of the column, and this should be avoided. Again the separation for this component is not as good as needed. The investigation will have to consider using more equilibrium stages to improve the separation in the column and in this wayincrease the purity and recovery of HFP. More stages will mean there will be more liquid holdup in the column, reducing the total amount of distillable mixture.

Table 8.9: Composition analysis for a simulation recovering 80 % HFP.

Time (hours)	Still pot composition			Distillate receiver 2			Distillate receiver 3		
	HFP	OFCB	TFE	HFP	OFCB	TFE	HFP	OFCB	TFE
0.75	0.7469	0.2412	0.0119	0.0038	0.0000	0.9962	-	-	-
0.80	0.7188	0.2795	0.0017	0.1458	0.0002	0.8540	-	-	-
0.85	0.6611	0.3388	0.0001	-	-	-	0.9229	0.0044	0.07269
0.90	0.6012	0.3988	0.0000	-	-	-	0.9499	0.0054	0.04467
0.95	0.5273	0.4727	0.0000	-	-	-	0.9611	0.0063	0.03258
1.00	0.4298	0.5702	0.0000	-	-	-	0.9668	0.0075	0.02577
1.05	0.3082	0.6918	0.0000	-	-	-	0.9693	0.0092	0.02147
1.10	0.1800	0.8200	0.0000	-	-	-	0.9692	0.0123	0.01851
1.15	0.0788	0.9212	0.0000	-	-	-	0.9649	0.0188	0.01632
1.20	0.0226	0.9774	0.0000	-	-	-	0.9612	0.0233	0.01554

Several simulations for a column with sixstages were completed, similar to the one shown in Table 8.7, to find the optimum intermediate cut that would yield a product with purity close to

99 %. The results ofthese simulations are shown in Table 8.10. It was found that the optimum intermediate cut size wouldbe 0.00063 kmol, which yieldedan HFP product with a purity of 0.989992 and an HFP recovery of 60.32 %. This is an increase of almost 200 % in the recovery of HFP.

Table 8.10: Various intermediate cut sizes for a six-stage column.

Intermediate cut size (kmol)	Final cut HFP purity	Final cut accumulation (kmol)	HFP recovery %
2.00E-04	0.874328	0.001761	71.28
4.00E-04	0.960579	0.001560	69.38
5.00E-04	0.982302	0.001466	66.67
6.00E-04	0.990000	0.001303	59.72
6.20E-04	0.989990	0.001314	60.22
6.30E-04	0.989992	0.001316	60.32
6.40E-04	0.990000	0.001313	60.18

Again the simulation for six stages can be optimized for an HFP recovery of 80 % by selecting the best intermediate cut size. Table 8.11 shows a few intermediate cut sizes for the simulation. The recoveries shown in Table 8.11 are all below 80 % even when the intermediate cut size is almost 0. There is a very small drop in the recovery as the cut size increases but the purity of the product varies more. Table 8.11 shows an optimum setup for a high recovery, with a fairly high purity product at an intermediate cut size of 0.0002 kmol which will yielda product with an HFP purity of 0.8743 and a recovery of 71.28 %.

Table 8.11: HFP recovery for various intermediate cuts.

Intermediate cut size (kmol)	Final cut HFP purity	Final cut accumulation (kmol)	HFP recovery %
9.02E-08	0.786357	0.001963	71.46383
5.00E-05	0.806834	0.001912	71.41975
1.00E-04	0.82824	0.00186	71.32067
2.00E-04	0.874328	0.001761	71.28202
4.00E-04	0.96058	0.00156	69.37522

8.3 Final Column Design for TFE and HFP Purification

A column with six equilibrium stages couldyieldanHFP product with a purity of 99 % anda recovery of 60 %. The still pot counts as an equilibrium stage, but the total condenser does

not, sothe column itself consists of only five equilibrium stages. This change will affect the results obtained for the column design for pure TFE. The increase in the number of equilibrium stages will increase the time required for the TFE distillation as well as the total recovery for TFE, as apurity of 0.99999 is still required. The simulation completed the distillation of TFE and HFP in 1 hour and 7 minutes. The run consisted of three cuts, each going to its own distillate receiver. The first cut was made when the TFE purity approached 0.99999 from above,the second distillate receiver wasfor the intermediate cut, which can be seen as a waste cut. This cut wasmade so that a pure HFP product couldbe recovered. The third distillate receiver received the final cut that consisted mostly of HFP. Figure 8.8 to Figure 8.10 show the composition of the three components in each distillate receiver. Figure 8.11 shows the composition changes in the still pot during distillation. Each receiver will be empty when each cut is made and therefore the initial composition in each receiver is zero in each figure. The secondary and tertiary components in each cut are very small as ultra-high purity components are required. After all three distillation steps, only 13 % of the original mixture is left in the column and still pot. There are54 % HFP and 46 % OFCB (on a mole basis) left in the column.

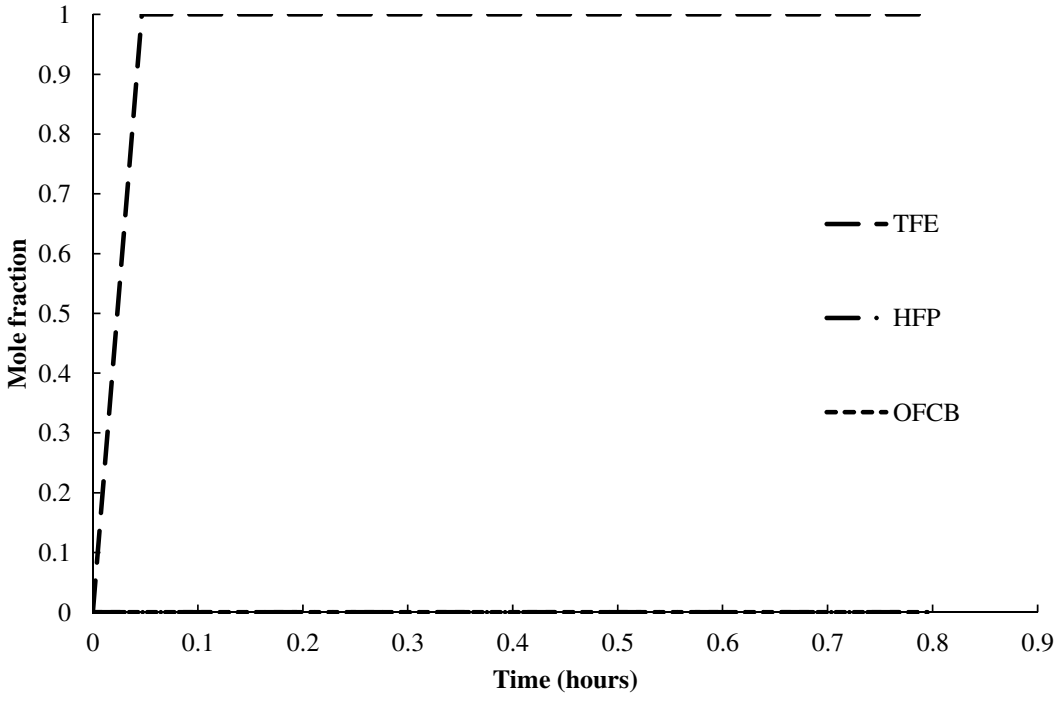

Figure 8.8: Composition profile for distillate receiver one.

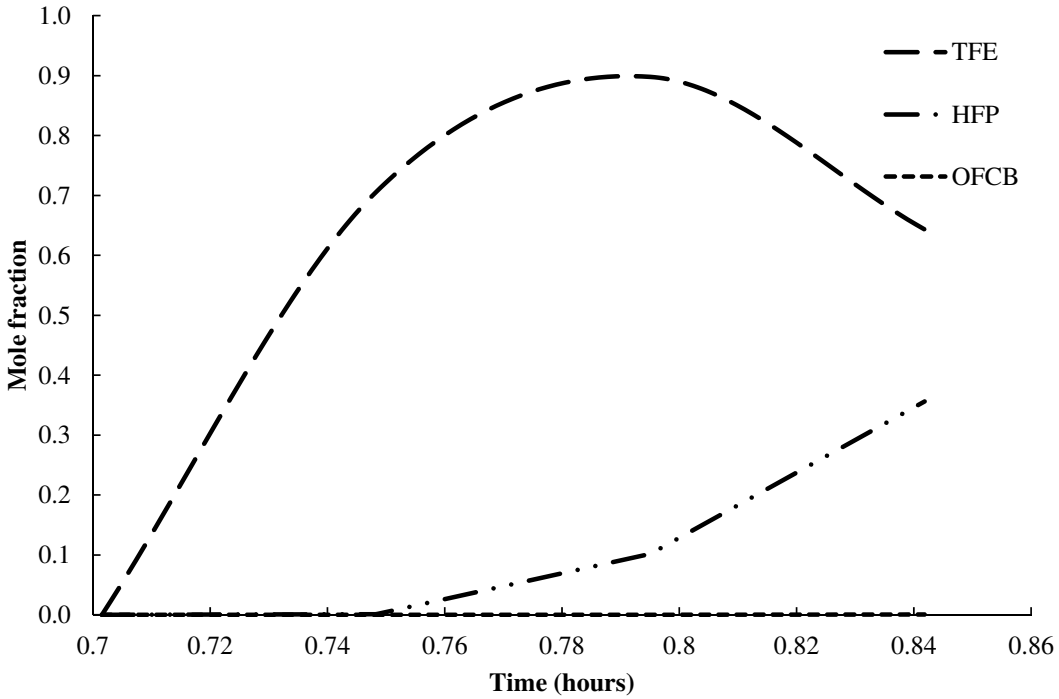

Figure 8.9: Composition profile for the intermediate cut in distillate receiver two.

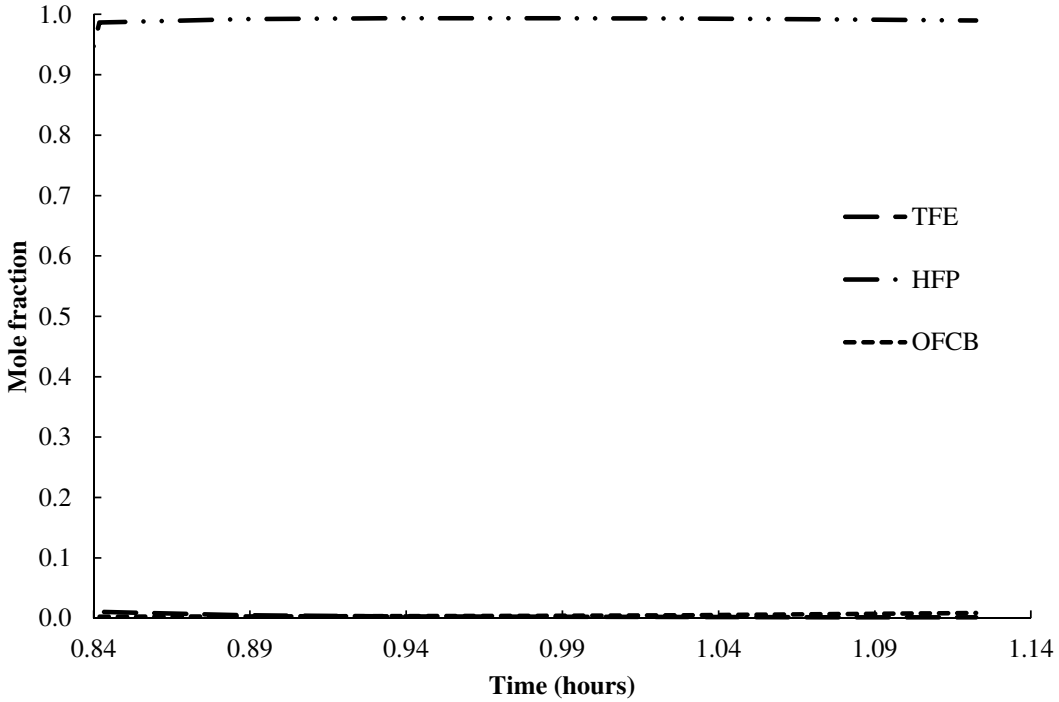

Figure 8.10: Composition profile of the final cut in the third distillate receiver.

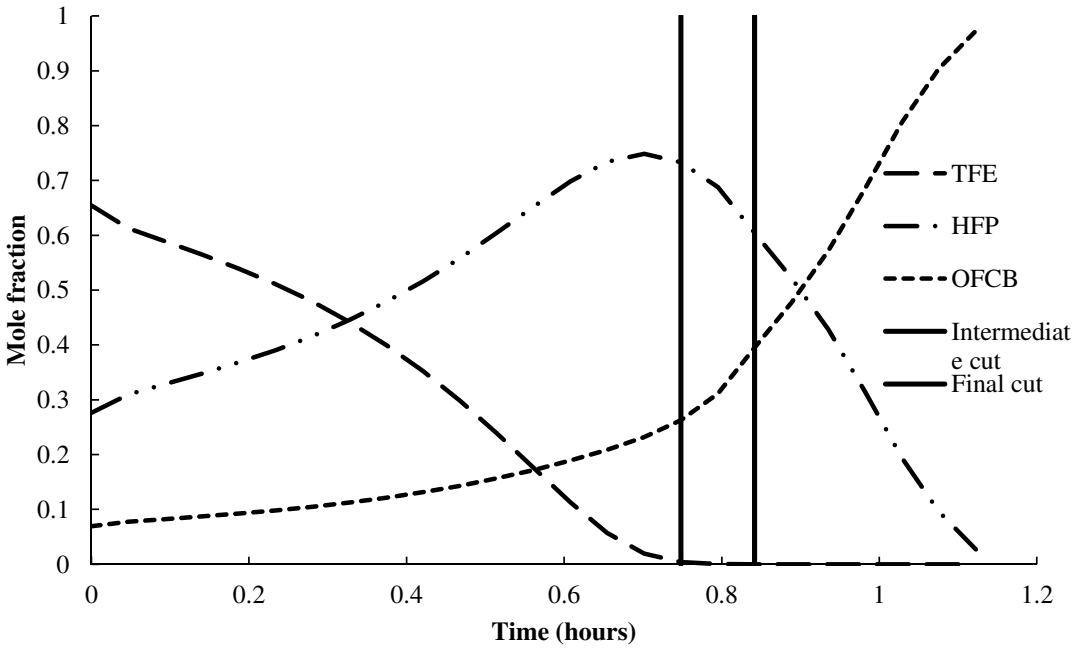

Figure 8.11: The composition in the still pot as the distillation is done.

Figure 8.12 to Figure 8.15 give the liquid composition and the vapour composition for TFE and HFP ateach stage during the distillation. Figure 8.16 gives the temperature profile in the column during the distillation.

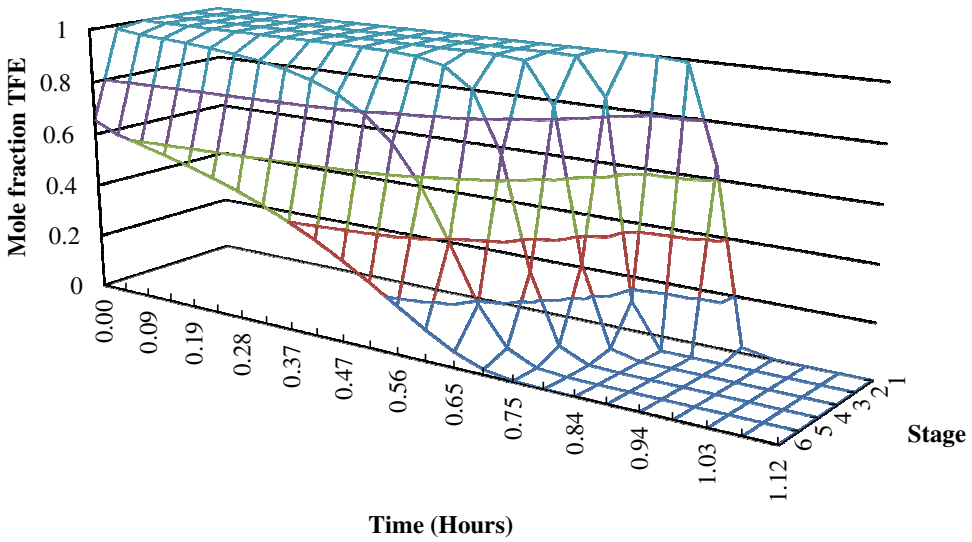

Figure 8.12: Composition profile for liquid TFE in the column.

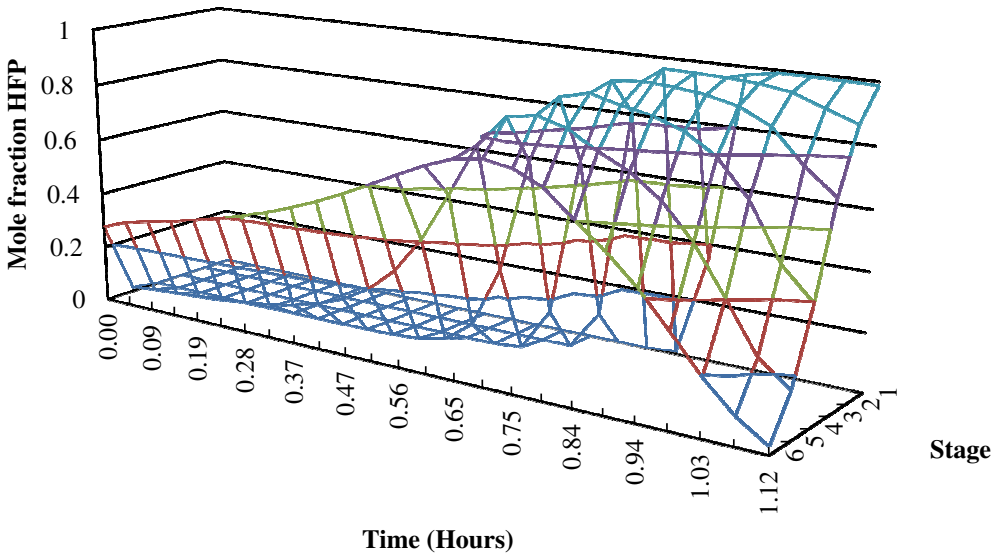

Figure 8.13: Composition profile for liquid HFP in the column.

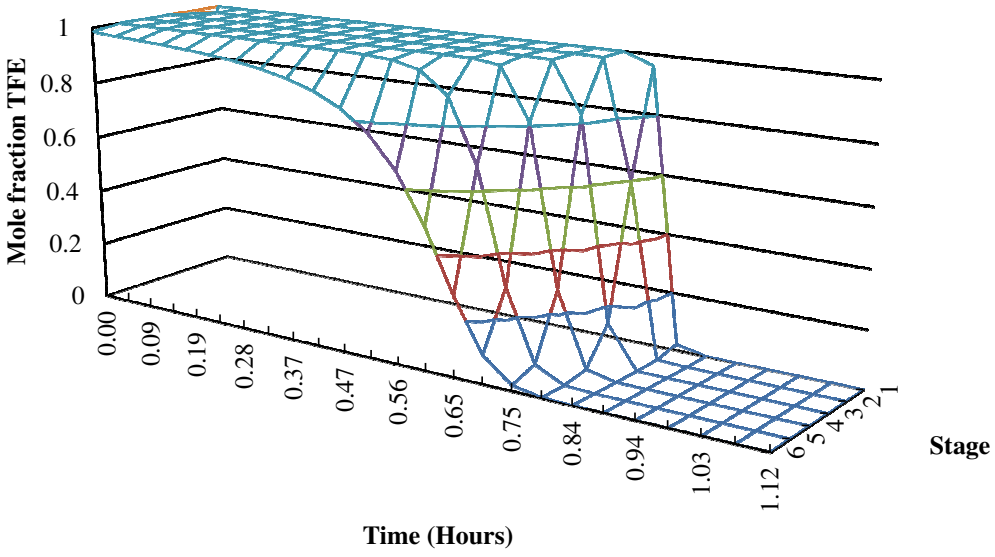

Figure 8.14: Composition profile for TFE vapour in the column.

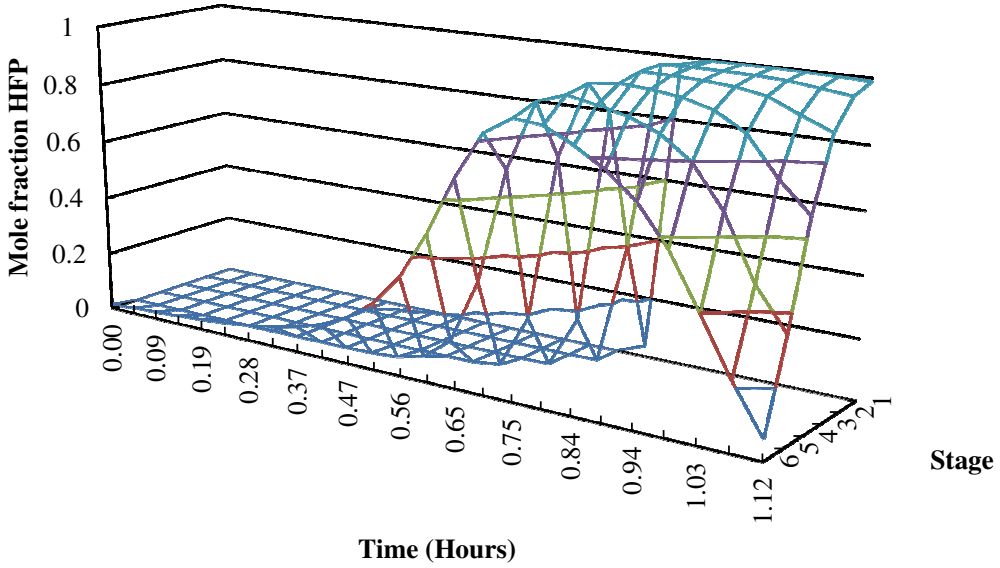

Figure 8.15: Composition profile for HFP vapour in the column.

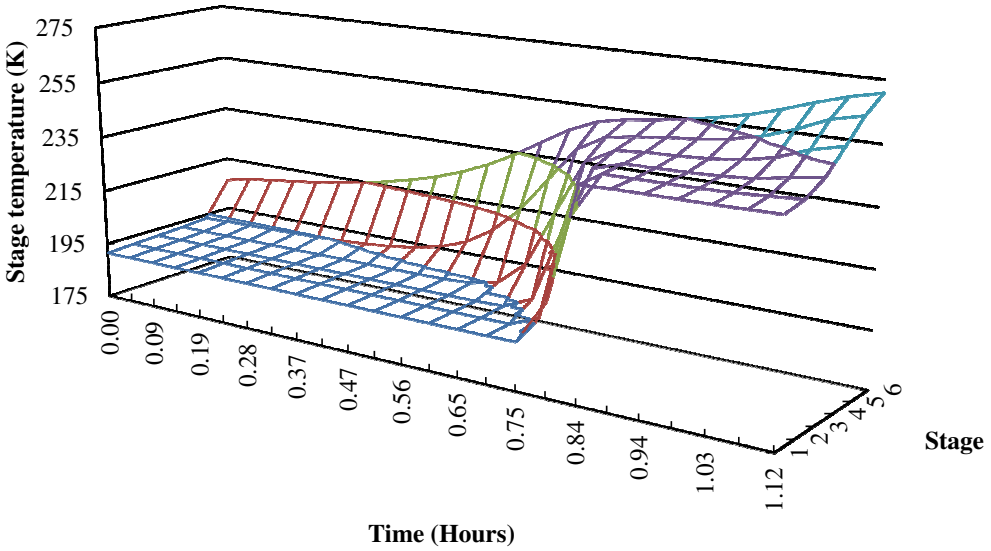

Figure 8.16: Temperature profile through the column.

The heat duties, summarized in Table 8.12, give an indication of the power requirements to run the column. The condenser will be a total condenser, but the distillate product will evaporate and expand into the distillate receivers as the product is drawnoff.

Table 8.12: Heat requirements for a six-stage column.

	Still Pot			Total Condenser		
Time	**Temperature**	**Heat duty**	**Vapour flow rate**	**Temperature**	**Heat duty**	**Liquid flow rate**
(hours)	**(k)**	**(W)**	**(kmol/h)**	**(k)**	**(W)**	**(kmol/h)**
0.000	206.37	175	0.4488	191.5064	-1444	0.2833
0.047	208.27	175	0.0396	191.5064	-155	0.0365
0.094	209.36	175	0.0363	191.5064	-143	0.0337
0.140	210.50	175	0.0335	191.5064	-134	0.0315
0.187	211.73	175	0.0313	191.5064	-127	0.0299
0.234	213.11	175	0.0301	191.5064	-125	0.0294
0.281	214.70	175	0.0298	191.5064	-127	0.0299
0.327	216.61	175	0.0290	191.5064	-128	0.0301
0.374	218.87	175	0.0275	191.5064	-127	0.0299
0.421	221.56	175	0.0255	191.5064	-124	0.0292
0.468	224.89	175	0.0237	191.5065	-122	0.0288
0.514	229.00	175	0.0216	191.5065	-119	0.0280
0.561	234.08	175	0.0199	191.5065	-114	0.0269
0.608	239.95	175	0.0195	191.5065	-110	0.0259
0.655	245.75	175	0.0210	191.5065	-109	0.0256
0.702	249.89	175	0.0236	191.5066	-111	0.0262
0.748	251.93	175	0.0247	191.5464	-127	0.0291
0.795	253.17	175	0.0239	206.607	-281	0.0335
0.842	254.90	175	0.0238	245.5688	-219	0.0261
0.889	256.70	175	0.0221	245.9586	-156	0.0187
0.935	258.92	175	0.0216	245.9981	-148	0.0177
0.982	261.89	175	0.0215	246.0311	-142	0.0170
1.029	265.40	175	0.0217	246.0991	-138	0.0165
1.076	268.51	155	0.0196	246.278	-136	0.0162
1.122	270.87	21	0.0001	246.4634	-41	0.0049

The next step in the design wasto size the column and suggest a final configuration for the column. Firstly the diameter wascalculated with Equation 4.36 to Equation 4.39. To calculate the CAP with Equation 4.36, the value of all three cuts made during the distillation was subtracted from the initial charge to the column. Since the heat duty to the still pot waskept

constant as was the reflux ratio, the boilup rate and distillate rate wouldvary as the distillation continued. Average values for the boilup and distillate rate wereused in the following calculations. The liquid density and vapour density for the calculations are an average value for the column from values predicted by Aspen ateach equilibrium stage. The molecular weight ofthe vapour wasalso taken as an average over time and for each stage of the column. The K_v value was assumed to be 0.3 ft/s (0.09144 m/s) as suggested by Al-Tuwaim and Luyben (1991). Table 8.13 summarizes these values. Table 8.14 shows the results ofthe calculation of the column diameter.

Table 8.13: A summary of the values used for the calculation of the column diameter.

Boilup rate (kmol/h)	**Distillate rate** (kmol/h)	**Liquid density** (kg/m^3)	**Vapour density** (kg/m^3)	**Molecular Weight** (kg/kmol)
0.024611	0.006471	1631	8.701	120.4

Table 8.14: Calculated column diameter.

CAP	0.0007667	kmol/h
V'	2.130E-07	kmol/s
V_m	1.249	m/s
Diameter	28.53	mm

The minimum diameter suggested by the calculations is about 29 mm. If normal piping is used to construct the column, 1¼" piping couldbe used to for the column. This wouldgive a diameter of 31.75 mm which wouldbe acceptable for operation. Next the height of the column must be specified. When working with such a small diameter, it wouldbe more efficient to work with a packed column as installing plates wouldbe difficult to obtain and be expensive for such a small diameter (Sinnott, 2005: 589). This also allows for investigations into different types of column packaging.

The column height can be estimated from the HETP of the possible packings that can be used in the column. One such packing is metal Pall rings, with sizes varying from15 mm to 50 mm. AceChemPack suggests using packing with a size smaller than 25 mm with a column size smaller than 30 mm (www.tower-packing.com). The following calculation uses 1-inch Pall ring packing for determining the column height. Thakore and Bhatt (2007: 453) state that the HETP of Pall ring packing will be between 0.4 and 0.5 m. Hanley and Shethna (2010) showed with experimental results that the HETP for various systems, using various sizes of Pall rings, varies between 0.28 and 0.97 m. The Chemical Engineer's Resources Page (www.cheresources.com) uses 0.46 m for an initial HETP value for 1-inch Pall ring packing. Using 0.4 m as a minimum HETP for 1-inch Pall rings and 0.5 m as a maximum

HETP, theminimum and maximum height of the column can be suggested. The still pot, serving as the reboiler, counts as an equilibrium stage butthe total condenser does not count as an equilibrium stage. The column height must thereforebe designed for five equilibrium stages. The minimum suggested height for the column, using 1-inch Pall ring packing, will be 2 m and the maximum suggested height to achieve the necessary separation requires a 2.5 m column. Taking into consideration the possible design assumptions and incorporating a small safety factor, the column should be 2.5 m tall.

8.4. Variations in Feed Mixture Composition

As the composition of the feed mixture can change for each separate batch due to variations in operating conditions during the pyrolysis of PTFE or due to creating different mixtures with intermediate cuts, the effect of these changes on the column must be investigated. Four mixture compositions were used for this evaluation. Table 8.13 shows the different mixture compositions used for the simulations. Mixtures with high TFE content as well as very low TFE content wereused to see how the column wouldoperate under extreme deviations from the specified user requirements. The target for each simulation was to achieve a TFE product with a purity of 99.999 % with six equilibrium stages in the column. A secondary target of recovering some of the HFP product was also set for the simulations. If it seemed possible or feasible to recover the HFP, an intermediate cut wasmade to deliver a pure HFP product. The time duration for all for simulations was almost the same, taking about an hour to complete the distillation of each batch.

Table 8.13: Different mixture compositions used in the simulation.

	Mixture 1		Mixture 2		Mixture 3		Mixture 3	
	Mass fraction	Mole fraction	Mass fraction	Mole fraction	Mass fraction	Mole fraction	Mass fraction	Mole fraction
TFE	0.80	0.86	0.70	0.80	0.50	0.62	0.33	0.46
HFP	0.15	0.11	0.15	0.11	0.35	0.29	0.33	0.31
OFCB	0.05	0.03	0.15	0.09	0.15	0.09	0.33	0.23

8.4.1. Mixture I

Due to the high TFE content in the mixture, it was not feasible to attempt to recover a high purity HFP product and no intermediate cut was made. The simulation took 58 minutes to complete the full distillation, which recovered 95 % of the original TFE in the feed mixture. The first cut for the TFE product took about 55 minutes and a second cut was made for

anHFP product until the column almost randry. This second product contained 79 % TFE and only about 20 % HFP. Table 8.14 summarizes the results ofthis simulation.

Table 8.14: Results ofthe Aspen simulation forMixture I.

	Composition			Cut size (kmol)	TFE Recovery	HFP Recovery
	TFE	HFP	OFCB			
First Cut	0.99999	9.96E-06	0	0.007601	95	0.01
Second Cut	0.7932	0.2063	4.10E-04	4.66E-04	4.6	9.61

8.4.2. Mixture II

This mixture was used to examine the effect of a higher concentration of OFCB present in the still pot. The main target for a high purity TFE product wasmet and a high recovery rate wasalso achieved. The intermediate cut had a high percentage of TFE present but since the cut wasso small, it wasan acceptable loss. Only about 57 % of the HFP couldbe recovered before the still pot almost ranempty and the product wasonly 79 % pure.

Table 8.15: Results ofthe Aspen simulation forMixture I.

	Composition			Cut size (kmol)	TFE Recovery	HFP Recovery
	TFE	HFP	OFCB			
First Cut	0.99999	9.99E-06	1.81E-09	0.00661	94.45	0.0066
Intermediate Cut	0.95084	0.04907	9.14E-05	3.00E-04	4.08	1.47
Final Cut	0.79320	0.20630	4.10E-04	7.10E-04	1.47	57.70

8.4.3. Mixture III

Mixture III has a lower TFE content and a high HFP content. Again it is possible to achieve the main target for the distillation but the recovery is lower than the previous mixture. With the increase in the HFP in the feed mixture it is now possible to achieve a higher quality HFP product at a high recovery of about 79 %. The distillation was completed with a small intermediate cut and was left until the still pot almost ranempty. With the optimization of the intermediate cut size, a higher purity HFP couldbe collected, but at the expenseof lowering the overall recovery in the final cut.

Table 8.16: Results ofthe Aspen simulation forMixture III.

	Composition			Cut size (kmol)	TFE Recovery	HFP Recovery
	TFE	HFP	OFCB			
First Cut	0.99999	9.99E-06	1.81E-09	0.004577	91.56	0.0020
Intermediate Cut	0.97317	0.02683	5.78E-06	2.89E-04	5.63	0.33
Final Cut	0.07040	0.91796	0.01164	2.00E-03	2.82	78.69

8.4.4. Mixture IV

Mixture IV is an extreme condition where the ratio in the mixture for the three compounds is 1:1:1. It is apparent from these results that the separation of the three gases is fairly easy, and thata high purity TFE product is still drawn off. The recovery of the TFE product is slightly lower than in the other situations. The simulation was not optimized for a high purity HFP product, but it is evident that almost all of the HFP couldbe recovered. Increasing the size of the intermediate cut will not make a big difference tothe purity of the HFP as the OFCB doesnot separate veryeasily from the HFP.

Table 8.17: Results ofthe Aspen simulation forMixture IV.

	Composition			Cut size (kmol)	TFE Recovery	HFP Recovery
	TFE	HFP	OFCB			
First Cut	0.99999	9.99E-06	1.81E-09	0.002807	85.08	0.0013
Intermediate Cut	0.98653	0.01346	5.98E-06	3.00E-04	8.97	0.18
Final Cut	0.06635	0.77885	0.15480	2.80E-03	5.63	99.14

8.5. Still Pot Heat Duties

The heat duty for the still pot was a selected variable during the initial design and simulation process in Aspen Batch Distillation. The choice of the heat duty was based on the maximum capabilities of a chilling unit that might be used in the demonstration plant. As the unit might not be bought or different units might be used, a small study onthe effects of different heat duties for the still pot was done. The biggest change in the column, due to this change, wouldbe the boil-up rate from the still pot. This wouldincrease the time required to complete the distillation and as the vapour and liquid wouldmove more slowlythrough the column, more mass transfer wouldbe possible, resulting in higher purity products.

The following heat duties were investigated:

- 200 W
- 150 W
- 100 W
- 50 W

The simulations for 200 W, 150 W and 100 W had a first cut when the purity of TFE reached 0.99999, an intermediate cut size of 6.3 x 10^{-4} kmol and a final cut was made when the purity of HFP reached 0.99. For the 50 W simulation, the intermediate cut was made smaller,

2.2 x 10^{-5} kmol, and for the HFP product cut the still pot was allowed to run almost empty, to see if a high product purity and a high product recovery could be achieved. A summary of the time required for the distillation, the percentage TFE recovered in the first cut, the purity of the HFP in the final cut as well as the percentage of the recovered HFP in the final cut is shown in Table 8.18.

Table 8.18: Different heat duties used in the column simulation.

Heat Duty (W)	Time (hours)	TFE recovery %	HFP purity	HFP recovery %
200	0.98	92.21	0.99	59.95
150	1.31	92.19	0.99	60.45
100	1.92	92.19	0.99	60.78
50	3.79	91.71	0.78	69.43

A TFE recovery of around 92.2 % was achieved for the first three simulations and a slightly lower recovery of 91.71 % for the last run. This is still close to the other three runs and can be attributed to the simulation making the first cut earlier owingto calculation errors at very high purities. As the heat duty is lowered on the still pot, the recovery of the HFP increases slightly. The intermediate cut size can be increased to increase the purity of the final cut for the fourth run. This will increase the purity but reducethe recovery of HFP.

8.6. Conclusions

The final design for the column should be based on the requirements of the HFP product, as ultra-high pure TFE can be produced for all the options investigated with the simulation. The HFP product specifications can be controlled merely by changing the intermediate cut size. Variations in mixtures should not create problems with the column either, as it is designed to separate HFP as well.

The suggested column should consist of six equilibrium stages, where the total condenser and the still pot both count as an equilibrium stage. The reflux ratio used in the simulations is 4. These gave the best simulation results. The HETP for the Pall ring 1-inch packing selected for the preliminary design is between 0.4 and 0.5 m. The column should have the following physical measurements:

- An internal diameter of 31.75 mm
- A height of 2.5 m
- Still pot diameter 0.125 m
- Still pot height of 0.1 m with a flat bottom and elliptical roof
- A pot volume of 1.483 x 10^{-4} m^3

Lower heat duties on the still pot couldbe considered but this wouldincrease the distillation time.

Chapter 9

Conclusions

9. Conclusions

The project objective was todesign a small batch distillation column to purify tetrafluoroethylene and hexafluoropropylene from a mixture containing tetrafluoro-ethylene, hexafluoropropylene and octafluorocyclobutane.

As no vapour-liquid equilibrium data were available for these chemicals in this mixture, new vapour-liquid equilibrium data were experimentally generated and modelled for use in the design. A static-analytical apparatus was used to gather the experimental data. Three isotherms for each of the three binary systems were investigated for this study.

The data were fitted to the Peng-Robinson equation of state, utilizing the Mathias-Copeman alpha function. The model was used with the Wong-Sandler mixing rules alongside the NRTL alpha function.

The model was fitted with mean relative deviations lower than 1.2 %, indicating an acceptably accurate description of the gathered VLE-data by the model. The experimental data and the model also passed the thermodynamic consistency test for all the systems and isotherms.

The design simulations were completed with the aidof Aspen Batch Distillation, a module of the Aspen Technologies package. The results show that the optimum design for recovering high-purity products, requires six equilibrium stages in the column. The batch column should consist of a still pot, also functioning as a reboiler, a packed column section and a total condenser. The total condenser and the reboiler both count as equilibrium stages. With this design a TFE product purity of 99.999 % is predicted with a recovery of 96 %. An HFP product purity of 99 % is predicted at a recovery of 68 %. The recovery of the HFP product can be increased but at the expense of a significant loss of product purity.

The minimum column diameter required to achieve the flow rates suggested in the simulation is 29 mm. The column diameter was selected on the basis of the standard pipe diameters available in the industry, as 1¼ ″ (or 31.75 mm). Pall ring packing is suggested for use in the column, with an estimated HETP of between 0.4 and 0.5 m and, with fiveequilibrium stages in the column itself, the column has to be at least 2.5 m high. The following dimensions for the still pot were used in the simulations:

- Still pot diameter 0.125 m
- Still pot height of 0.1 m with a flat bottom and elliptical roof

Chapter 10

References

10. References

Abrams, D. and Prausnitz, J.M. (1975) "Statistical thermodynamics of liquid mixtures: A new expression for the excess Gibbs energy of partly or completely miscible systems" *AIChE Journal*, 21 (1), 116 – 128.

AceChemPack Tower Packing Co., Ltd "Packed Column Design" www.tower-packing.com/Dir_column_packing.htm [September 2011].

Ahmar, E.E., Valtz, A., Naidoo, P., Couquelet, C. and Ramjugernath, D. (2011) "Isothermal Vapor-Liquid Equilibrium Data for the Perfluorobutane (R610) + Ethane System at Temperatures from (263 to 353) K", J. Chem. Eng. Data, 56 (5), 1918 – 1924.

Al-Tuwaim, M.S. and Luyben, W.L. (1991) "Multicomponent batch distillation.3. Shortcut design of batch distillation columns" *IEC Res.*, 30 (3), 507 – 516.

Annamalai, K. and Puri, I.K. (2002) *Advanced Thermodynamics Engineering*, CRC Press, Florida, United States of America.

Boston, J.F., Britt, H.I., Jirapongphan, S. and Shah, V.B. (1981) *Foundations of Computer-aided Chemical Process Design*, Engineering Foundations, New York.

Boublík, T.; Fried, V.; Hála, E. (1975) *The Vapour Pressures of Pure Substances.* Elsevier Scientific Publishing Company.

Braker, W. and Mossman, A.L. (1980) *Matheson Gas Data Book*, The Matheson Company Inc, New Jersey.

Chambers of Mines of South Afrrica (2007) "Facts & figures 2007", http://www.bullion.org.za/Publications/Facts&Figures2006/Facts&Figures2007.pdf [January 2009].

Coquelet, C.; Ramjugernath, D.; Valtz, A.; Naidoo, P.; Meniai, A.H. (2010) "Experimental measurement of vapour pressures and densities of pure hexafluoropropylene" *J. Chem. Eng.*, 55 (6), 2093 - 2099.

Danner R.P. and Gess M.A. (1990) "A data base standard for the evaluation of vapour-liquid equilibrium models", Fluid Phase Equilibria, 56 (1), 285 – 301.

Daubert, T.E.; Danner, R.P.; Sibul, H.M.; Stebbins, C.C. (1998) *Physical and Thermodynamic Properties of Pure Chemicals*, Taylor & Francis.

Distefano, G.P. (1968) "Mathematical modelling and numerical integration of multicomponent batch distillation equations" *AIChE J*, 14 (1), 190 – 199.

Diwekar, U.M. and Madhavan, K.P. (1991) "Multicomponent batch distillation column design", *Ind. Eng. Chem. Res*, 30 (4), 713 – 721.

Doherty, M.F. and Malone, M.F (2001) *Conceptual Design of Distillation Systems*,The McGraw-Hill Companies, Inc., New York, United States of America.

Dohrn, R. and Brunner, G (1995) "High-pressure fluid-phase equilibria: experimental methods and systems investigated (1988 – 1993)", Fluid Phase Equilibria, 106 (1 - 2), 213 – 282.

Dong, X., Gong, M., Liu, J. and Wu, J. (2011) "Experimental Measurement of Vapor Pressures and (Vapor + Liquid) Equilibrium for {1,1,1,2-Tetrafluoroethane (R134a) + Propane (R290)} by a Recirculation Apparatus with View Windows", Journal of Chemical Thermodynamics, 43 (3), 505 – 510.

Dong, X., Gong, M., Liu, J. and Wu, J. (2010) "Vapor-Liquid Equilibria for 1,1,2,2-Tetrafluoroethane (R134) + Fluoroethane (R161) at Temperatures between (263.15 and 288.15) K", J. Chem. Eng. Data, 55 (9), 3383 – 3386.

Epsch, R.,Goldmann, G.,Killich, A., Löhr, G. and Staudt, H. (2002) "About the thermodynamic and kinetic fundamentals of the self-decomposition of tetrafluoroethylene - Part I: Thermodynamic computation of the pressure Increase ratio" Chem. Eng. Technol. 25 (3), 277 – 282.

Galindez, H. and Fredenslund, A. (1988) "Simulation of multicomponent batch distillation processes" Comput. Chem. Eng., 12 (4), 281 – 288.

Guilbot, P., Valtz, A., Legendre, H. And Richon, D. (2000) "Rapid on-line sampler-injector – a reliable tool for HT-HP sampling" *Analusis*, 28 (5), 426-431.

Hanley, B. and Shethna, H. (2010) "Improved mass transfer correlations for random and structured packings" 2010 AIChE Spring Meeting, San Antonio, Texas.

Hou, S.-X. and Duan, Y.-Y. (2010) "Vapor-Liquid Equilibrium Measurement and Modeling for the Difluoromethane+ Pentafluoroethane+ Propane Ternary Mixture", Fluid Phase Equilibria, 298 (1), 106 – 112.

Hunadi, R.J. and Baum, K. (1982) "Tetrafluoroethylene: A convenient laboratory preparation" Synthesis, 1982 (6), 454.

Huron, M. and Vidal, J. (1979) "New mixing rules in simple equations of state for representing vapour-liquid eqauilibria of strongly non-ideal mixtures" Fluid Phase Equilibria, 3 (4), 255 – 271.

Jime'nez-Gallegos, R., Galicia-Luna, L.A., Bouchot, C., Camacho-Camacho, L.E. and Elizalde-Solis, O. (2006) "Experimental Determination and Correlation of Phase Equilibria for the Ethane + 1-Propanol and Propane + 1 – Propanol Systems" J. Chem. Eng. Data, 51 (5), 1629 – 1633.

Kim, S.A., Lim, J.S. and Kang, J.W. (2010) "Isothermal Vapor-Liquid Equilibria for the Binary System of Carbon Dioxide (CO_2) + 1,1,1,2,3,3,3-Heptafluoropropane (R-227ea)" J. Chem. Eng. Data, 55 (11), 4999 – 5003.

Kim, S.A., Yoo, K.-P., and Lim, J.S. (2010) "High Pressure Isothermal Vapor-Liquid Equilibria for the Binary System of Carbon Dioxide (CO_2)+1,1,1-Trifluoroethane (R-143a)" Korean Journal of Chemical Engineering, 1 – 5.

Kodama, D., Tanaka, H. and Kato, M. (2001) "High pressure phase equilibrium for ethane + 1-propanol at 314.15 K" J. Chem. Eng. Data, 46 (5), 1280 – 1282.

Krell, E. (1982) *Handbook of Laboratory Distillation,* Elsevier Scientific Publishing Company, Netherlands.

Kyle, B.G. (1999) *Chemical and Process Thermodynamics,* Prentice Hall PTR, New Jersey.

Lisochkin, Y.A. and Poznyak, V.I. (2006) "Explosive-hazard estimates for several fluorine-containing monomers and their mixtures, based on the minimum ignition pressure with a fixed igniter energy" Combustion, Explosion, and Shock Waves, 42 (2), 140 – 143.

Mathias, P.M. and Copeman, T.W. (1983) "Extension of the Peng-Robinson equation of state to complex mixtures: Evaluation of the various forms of the local composition concept", Fluid Phase Equilibria, 13 (1), 91 – 108.

Meadows, E.L. (1963) "Multicomponent Batch Distillation", Chem. Eng. Progr., 58 (9), 96.

Miller, M.M. (2009) "Fluorspar" http://minerals.usgs.gov/minerals/pubs/commodity.../fluorspar/mcs-2009-fluor.pdf [September 2010].

Mujtaba, I.M. (2004) *Batch Distillation Design and Operation*, Imperial College Press, London.

Naidoo, P., Ramjugernath, D. and Raal J.D. (2008) "A New High-Pressure Vapour-Liquid Equilibrium Apparatus" Fluid Phase Equilibria, 269 (1 – 2), 104 – 112.

Orbey, H. and Sandler, S.I. (1998) *Modelling Vapour-Liquid Equilibria, Cubic Equations of State and Their Mixing Rules*, Cambridge University Press, United Kingdom.

Patocka, J. and Bajgar, J. (1998) "Toxicology of Perfluoroisobutene" The ASA Newsletter, 98 – 5 (68).

Peng, D. and Robinson, D.B. (1976) "A new two-constant equation of state", Ind. Eng. Chem., Fund., 15 (1), 59 – 64.

Perry, R.H. and Green, D.W. (1997) *Perry's Chemical Engineers' Handbook, Seventh Edition*, McGraw-Hill Companies, United States of America.

Pitzer, K.S. and Curl, R. F. (1957) "The Volumetric and Thermodynamic Properties of Fluids. III. Emperical Equation for the Second Virial Coefficeint" J. Am. Chem. Soc., 79 (10), 2369 – 2379.

Prausnitz, J.M. (1969) *Molecular Thermodynamics of Fluid Phase Equilibria*, Prentice Hall Inc.

Prausnitz, J.M., Lichtenthaler, R.N. and de Azevedo, E.G. (1999) *Molecular Thermodynamics of Fluid-phase Equilibria*, Prentice Hall PTR, United States of America.

Raal, J D and Mühlbauer, A L, (1994), "The Measurement of High Pressure Vapour-Liquid Equilibria", Dev. Chem. Eng. Mineral Process, Vol. 2, pp. 69-105.

Raal J.D. and Mühlbauer A.L. (1998) *Phase equilibria: Measurement and computation*, Taylor & Francis, Washington DC, United States of America.

Ramjugernath, D (2010a) "False pressure readings due to condensation close to pressure transducer", Personal Communication.

Ramjugernath, D (2010b) "Thermodynamic model for fitting experimental data", Personal Communication.

Ramjugernath, D., Valtz, A., Couquelet, C. and Richon, D. (2009) "Isothermal Vapor-Liquid Equilibruim Data for Hexafluoroethane (R116) + Propane System at Temperatures from (263 to 323) K", J. Chem. Eng. Data, 54 (4), 1292 – 1296.

Rathakrishnan, E. (2006) *Fundamentals of Engineering Thermodynamics,* Second Edition, Prentice-Hall, India.

Redlich, O. and Kister, A.T. (1948) "Algebraic representation of thermodynamic properties and the classification of solutions" Ind. Eng. Chem., 40 (2), 345 – 348.

Redlich, O. and Kwong, J.N.S. (1949) "On the thermodynamics of solutions. V. An equation of state. Fugacities of gaseous solutions", Chem. Rev., 44 (), 233 – 244.

Reid, R. C.; Prausnitz, J. M.; Poling, B. E. (1987) *The Properties of Gases and Liquids, Fourth Edition*, McGraw-Hill Book Company.

Renon, H. and Prausnitz, J.M. (1968) "Local Compositions in Thermodynamic Excess Functions for Liquid Mixtures" AIChE Journal, 14 (1), 135 – 144.

Richon, D (1996) "New experimental developments for phase equilibrium measurements", Fluid Phase Equilibria, 116 (1 – 2), 421 – 428.

Searder, J.D. and Henley, E.J. (2006) *Separation Process Principles*, John Wiley & Sons, Inc., New Jersey, United States of America.

Sinnott, R.K. (2006) *Chemical Engineering Design*, Elsevier Butterworth-Heineman, Oxford.

Smith, J.M., Van Ness, H.C. and Abbott, M.M. (2001) *Introduction to Chemical Engineering Thermodynamics*, The McGraw-Hill Companies, Inc., New York, United States of America.

Soave G. (1972) "Equilibrium constants from modified Redlich-Kwong equation of state", Chem. Eng. Sci., 27 (), 1197 – 1203.

Sundaram, S. and Evans, L.B. (1993) "Shortcut procedure for simulating batch distillation operations", Ind. Eng. Chem. Res., 32 (3), 511 – 518.

Suzuki, K. and Sue, H. (1990) "Isothermal Vapour-Liquid Equilibrium Data for Binary Systems at High Pressures: Carbon Dioxide - Methanol, Carbon Dioxide - Ethanol, Carbon Dioxide – 1-Propanol, Methane – Ethanol, Methane – 1-Propanol, Ethane – Ethanol and Ethane – 1-Propanol Systems" J. Chem. Eng. Data, 35 (1), 63 – 66.

Thakore, S.B. and Bhatt, B.I. (2007) *Introduction to Process Engineering and Design*, Tata McGraw-Hill, New Delhi.

The Chemical Engineer's Resource Page "Packed Column Design" www.cheresources.com [February 2011].

The Royal Society of Chemistry (2009) "Structure Editors Used with ChemSpider", www.chemspider.com [2010, October].

Tshibangu, M.M. (2010) *High Pressure Vapour-Liquid Equilibrium Data of Fluorochemical Systems For Various Temperatures Using A New Static Analytical Apparatus*, MSc Dissertation, University of KwaZulu Natal, South Africa.

Tsonopoulos, C. (1974) "An empirical correlation of second virial coefficients", AIChE Journal, 20 (2), 263 – 272.

Van der Walt, I.J. and Bruinsma, O.S.L. (2006) "Depolymerization of Clean Unfilled PTFE Waste in a Continuous Process" Journal of Applied Polymer Science, 102 (3), 2752 – 2759.

Valtz, A., Courtial, X., Johansson E., Couquelet, C. and Ramjugernath, D. (2011) "Isothermal Vapor-Liquid Equilibrium Data for the Carbon Dioxide (R744)+ Decafluorobutane (R610) System at Temperatures from 263 to 353K", Fluid Phase Equilibria, 304 (1-2), 44 – 51.

Valtz, A., Coquelet, C., Baba-Ahmed, A. and Richon, D. (2002) "Vapor-liquid equilibrium data for the propane + 1,1,1,2,3,3,3-heptafluoropropane (R227ea) system at temperature from 293.16 to 353.18 K and pressure up to 34 MPa" Fluid Phase Equilibria, 202 (1), 29 – 47.

Weir, R.D. and De Loos, Th.W. (2005) *Measurement of the Thermodynamic Properties of Multiple Phases*, Elsevier B.V., The Netherlands.

Whipple, G.H. (1952) "Vapor-liquid equilibria of some fluorinated hydrocarbon systems" Ind. Eng. Chem. 44 (7), 1664-1667

Wilson, G.M. (1964) "Vapour-liquid equilibrium. XI. A new expression for the excess free energy of mixing" J. Am. Chem. Soc., 86 (2), 127 -130.

Wong, D.S.H., Orbey, H. and Sandler, S.I. (1992) "Equations of state mixing rule for non-ideal mixtures using available activity coefficient model parameters that allow extrapolation over large ranges of temperature and pressure" Ind. Eng. Chem. Res., 31 (8), 2033 – 2039.

Yaws, C.L. (2009) *Yaws Handbook of Antoine Coefficients for Vapor Pressure,* 2nd Electronic Edition. Knovel.

Yu. I. Babenko, Ya. A. Lisochkin, and V. I. Poznyak, (1993) "Explosion of tetrafluoroethylene during non-isothermal-polymerization," Comb., Expl., Shock Waves, 29 (5), 603–609.